Politechnika Wrocławska

WYDZIAŁ PODSTAWOWYCH
PROBLEMÓW TECHNIKI

PRACA DOKTORSKA

Anny Magdaleny Melnychenko

pt. „Wytwarzanie i zastosowanie przeźroczystych elektrod w spektroskopii struktur półprzewodnikowych”

napisana pod kierunkiem
prof. dra hab. inż. Roberta Kudrawca

Wrocław 2022

Praca doktorska należąca do programu „Doktorat wdrożeniowy" realizowana była na Wydziale Podstawowych Problemów Techniki na Politechnice Wrocławskiej we współpracy z Instytutem Sieci Badawczej Łukasiewicz PORT – Polski Ośrodek Rozwoju Technologii. Opiekę promotora pomocniczego sprawowała dr inż. Katarzyna Komorowska.

Podziękowania

Do powstania tej pracy przyczyniło się wiele osób, na każdym z jej etapów. Jestem za to ogromnie wdzięczna i pragnę podziękować.

Dziękuję wszystkim, którzy pomogli mi postawić pierwsze kroki w laboratorium, nauczyli mnie tajników obsługi sprzętu specjalistycznego i ratowali przy wszelki awariach.

Dziękuję wszystkim, którzy pomagali mi opracowywać i analizować otrzymane wyniki oraz sugerowali dalsze działanie.

Dziękuję wszystkim, którzy chętnie zagłębiali się w temat mojego doktoratu, by pomóc mi znaleźć rozwiązania aktualnych problemów.

Dziękuję wszystkim, którzy wspierali mnie w pisaniu publikacji poprzez dobre rady, okazywanie wsparcia i podnoszenie na duchu.

Szczególnie gorące podziękowania kieruję w stronę mojego promotora, bez którego ta praca by nie powstała. Za ciekawe pomysły, sugerowanie rozwiązań i wiarę, że to wszystko się uda. Dziękuję za to, że po konsultacjach zawsze wychodziłam zmotywowana z przemyślanym planem dalszych działań.

Dziękuję moim koleżankom i kolegom z uczelni i instytutu za pomoc, wsparcie i naukowe poczucie humoru.

Dziękuję moim rodzicom, dzięki którym miałam możliwość rozpocząć studia i dojść aż do tego etapu.

Dziękuję mojej rodzinie, rodzeństwu i przyjaciołom, którzy dopingowali mnie na tej drodze.

Pracę dedykuję mojemu mężowi, który zaangażował się w nią w stopniu nie mniejszym niż ja sama. Jestem szczególnie wdzięczna za wsparcie na końcowym etapie doktoratu składającym się z odpowiadania na zawiłe pytania recenzentów czasopism, a następnie niecierpliwego wyczekiwania na decyzję edytora. Dziękuję za zrozumienie, uśmiech i przede wszystkim za pomoc w złapaniu balansu między życiem zawodowym a prywatnym.

Spis treści

Streszczenie PL

W rozprawie omówione zostały typy przeźroczystych elektrod oraz metody ich wytwarzania wraz z możliwymi zastosowaniami ze szczególnym naciskiem na pomiary optoelektryczne. Pierwsza z prac opisuje metodę wytwarzania przeźroczystych elektrod wykorzystującą techniki ultraprecyzyjnej depozycji tuszu srebrnego. Naniesione ścieżki w kształcie siatki o szerokości 10 μm zostały wykorzystane do pomiarów bezkontaktowego elektroodbicia fosforku indu – dobrze znanego materiału, w celu optymalizacji układu pomiarowego. Druga praca opisuje technikę otrzymywania przeźroczystych elektrod wykorzystującą ablację laserową do strukturyzacji dowolnych kształtów na powierzchni warstwy polimerowej oraz osadzanie warstwy metalicznej metodą fizycznego odparowania z fazy gazowej. Dzięki wykorzystaniu metody „laser lift-off" otrzymana została elektroda srebrna i miedziana w kształcie siatki oraz przeprowadzone zostały pomiary na krysztale van der Waalsa. Przeprowadzono eksperymenty bezkontaktowego elektroodbicia w zoptymalizowanym układzie, jak również pokazany został nowy układ do pomiaru termoodbicia, gdyż przeźroczysta elektroda znalazła zastosowanie jako grzałka i możliwe było modulowanie widma odbicia próbki za pomocą temperatury. W trzeciej pracy opisano przeźroczystą elektrodę o ciągłej warstwie przewodzącej wykonanej z grafenu. Opisana została synteza oraz transfer grafenu, a następnie pomiary jakie przeprowadzono z wykorzystaniem tej elektrody. Dzięki ciągłości warstwy możliwe było utworzenie kontaktu z próbką na całej jej powierzchni, a tym samym przeprowadzenie pomiarów elektroodbicia w tak zwanym „miękkim kontakcie" tj. przy styku grafenu z badanymi kryształami van der Waalsa. Przy ustawieniu elektrody w minimalnej odległości od próbki (rzędu kilkudziesięciu mikrometrów) przeprowadzono pomiar fotonapięcia powierzchniowego, w którym kluczowe jest „zbieranie" sygnału z całej powierzchni próbki w trakcie jej oświetlania. Wyniki te także zostały uwzględnione w opublikowanej pracy. Natomiast czwarta praca opisuje typowo występujący problem pękania warstwy polimerowej sugerując wykorzystanie niepowtarzalnego wzoru do nietypowych zastosowań np. w kryptografii. Metoda „crack-templated lift-off" nie wymaga użycia lasera w celu strukturyzacji, ponieważ proces ten zachodzi samorzutnie podczas pękania w odpowiednich warunkach. Kolejny etap nanoszenia warswy metalicznej i wywołania wzoru przebiega tak samo jak w przypadku metody „laser lift-off". Jednak w metodzie „crack-templated lift-off" efektem uzyskanym jest przeźroczysta elektroda o nieregularnych kształtach, co poszerza spektrum potencjalnych zastosowań tych elektrod do szyfrowania.

Streszczenie ENG

This thesis discusses the types of transparent electrodes and the methods of manufacturing them, along with possible applications, with particular emphasis on optoelectrical measurements. The first paper describes a method for manufacturing transparent electrodes using ultraprecise silver ink deposition techniques. The deposited 10 μm wide grid-shaped paths were used for contactless electroreflectance measurements of indium phosphide, a well-known material, in order to optimize the measurement setup. The second paper describes a technique for obtaining transparent electrodes using laser ablation to structure arbitrary shapes on the surface of a polymer layer and deposition of a metallic layer by physical vapor deposition. As a result of using the "laser lift-off" method, a silver and copper electrode in the shape of a mesh was obtained, and measurements were carried out on a van der Waals crystal. Contactless electroreflectance experiments were carried out in the optimized system, but also a new system for measuring thermoreflectance was shown, as the electrode found an application as a heater, and it was possible to modulate the sample reflection spectrum with temperature. The third paper describes a transparent electrode with a continuous conductive layer made of graphene. The synthesis and transfer of the graphene is described, followed by the measurements that were carried out using this electrode. Because of the continuity of the layer, it was possible to form a contact with the sample over its entire surface, and thus to carry out electroreflectance measurements in the so-called "soft contact" i.e., at the contact between the graphene and the van der Waals samples under study. With the electrode positioned at a minimum distance from the sample (on the order of tens of micrometers), surface photovoltage measurements were carried out, where it is crucial to collect the signal from the entire surface of the sample as it is illuminated. These results are also included in the published work. The fourth paper, meanwhile, addresses the typically occurring problem of polymer layer cracking by suggesting the use of cracking for unusual applications such as cryptography. The “crack-templated lift-off” method does not require the use of a laser system for structuring, as the process occurs spontaneously during cracking under the right conditions. The next step of applying the metallic layer and developing the pattern is the same as in the "laser lift-off" method. However, in this case, the result obtained is a transparent electrode with irregular shapes, which broadens the spectrum of potential applications of these electrodes for encryption.

1. Cel pracy oraz hipotezy badawcze

Celem pracy jest opracowanie metod wytwarzania przeźroczystych elektrod (TEs z ang. transparent electrodes) kompatybilnych z układem pomiarowym wykorzystywanym na Politechnice Wrocławskiej w pomiarach optoelektrycznych. Stosowane techniki spektroskopii modulacyjnej służą do charakteryzacji materiałów półprzewodnikowych. Badania nad nowymi materiałami cieszą się obecnie dużym zainteresowaniem ze względu na wciąż rosnące zapotrzebowania aplikacyjne urządzeń półprzewodnikowych tj. detektorów światła, diod LED lub laserów. Te urządzenia, zwłaszcza w ostatnich latach, znajdują zastosowanie w takich obszarach jak alternatywne źródła pozyskiwania energii (alternative energy sources), pojazdy autonomiczne (self-driving car) oraz rzeczywistość rozszerzona (augmented reality).

W tej pracy doktorskiej postawiona została hipoteza mówiąca, że poprzez zastosowanie bardziej nowoczesnej przeźroczystej elektrody, stanowiącej okładkę kondensatora umieszczanego w układzie optycznym, możliwe będzie zoptymalizowanie badań spektroskopii elektromodulacyjnej dzięki ulepszonej konstrukcji kondensatora oraz zredukowaniu wartości przykładanego napięcia przy zachowaniu lub nawet zwiększeniu transmisji światła przez elektrodę.

Omówienie struktury pracy

W celu weryfikacji hipotez badawczych przeprowadzono eksperymenty szczegółowo opisane w Rozdziale 2, który dotyczy różnych wariantów spektroskopii struktur półprzewodnikowych z wykorzystaniem wytworzonych przeźroczystych elektrod różnymi technikami opisanymi w Rozdziale 3. Wyniki przedstawiono w opublikowanych artykułach załączonych w Rozdziale 4. Dodatkiem do tego rozdziału są wyniki symulacji nad przeźroczystymi elektrodami przeprowadzone w programie COMSOL Multiphysics, które dodatkowo wprowadzają w tematykę badań. W ostatnim Rozdziale 5 omówiono szczegółowo wdrożenie wyników pracy zarówno w jednostce zatrudniającej (PORT) jak i w jednostce naukowej (PWr).

2. Spektroskopia struktur półprzewodnikowych wykorzystująca przeźroczyste elektrody

W technikach spektroskopowych głównym wynikiem pomiaru jest widmo uzyskane w rezultacie oddziaływania promieniowania na materię. Metody spektroskopii dzielą się na odbiciowe, absorpcyjne i emisyjne [1]. Spośród nich można wyróżnić spektroskopię modulacyjną, która daje możliwości zbadania półprzewodników i ich struktur. Na widmo badane techniką spektroskopii modulacyjnej można wpłynąć modulując różne parametry w próbce: temperaturę, naprężenie i pole elektryczne. Z tego powodu powstały różne odmiany spektroskopii modulacyjnej, które w zależności od rodzaju występującej modulacji dzielą się na: termomodulację, piezomodulację i elektromodulację [2]. Każda z tych technik ma wspólną cechę jaką jest wprowadzenie zaburzenia wpływającego na okresową zmianę odpowiedzi materiału względem wzbudzenia optycznego. Jest to możliwe, ponieważ w metodzie tej mierzona jest zmiana (pochodna) odbicia względem modulowanego parametru. Pozwala to na zredukowanie niekorzystnego tła w widmie, uwydatniając rezonanse oznaczające proste przejścia optyczne w strukturze pasmowej półprzewodnika. Poprzez wykorzystanie fazoczułych technik detekcji możliwe jest dokładne wyodrębnienie małej zmiany sygnału odbicia (ΔR) lub absorpcji rzędu 10^{-4} – 10^{-6} z szerokiego tła. W tym celu stosowany jest nanowoltomierz fazoczuły typu lock-in, który odfiltrowuje małe zmiany sygnału spośród silnego szumu wykorzystując modulację sygnału wejściowego. Poniżej przedstawiony jest przykładowy schemat układu pomiarowego (Rys. 1).

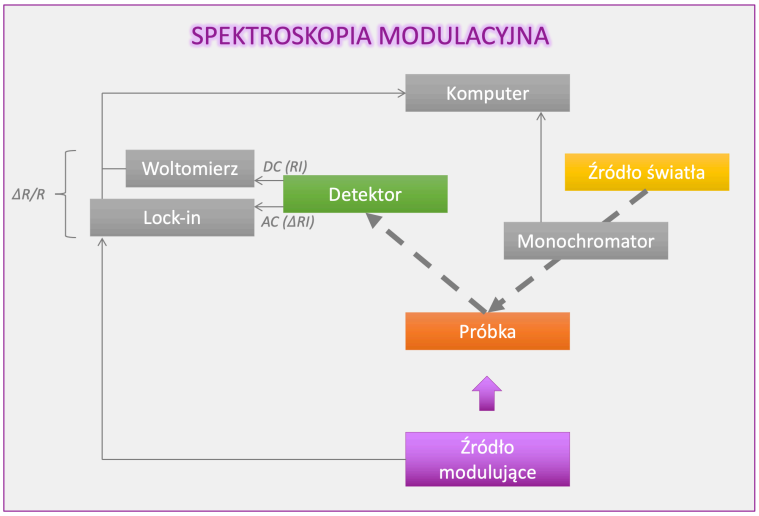

Rysunek 1. Schemat blokowy układu pomiarowego stosowanego w spektroskopii modulacyjnej. *I* – natężenie wiązki padającej, *R* – energetyczny współczynnik odbicia próbki, *ΔR* – zmiana współczynnika odbicia wywołana modulacją, *DC* – sygnał stałoprądowy, *AC* – sygnał zmiennoprądowy.

2.1 Spektroskopia elektromodulacyjna

W spektroskopii elektromodulacyjnej zaburzenia wprowadzane są do badanej próbki przez periodyczną zmianę pola elektrycznego na dwa sposoby: przez oświetlenie wiązką laserową (fotoodbicie), przez wprowadzenie zewnętrznego pola elektrycznego (elektroodbicie oraz bezkontaktowe elektroodbicie) (Rys. 2). Technika ta, nie jest wrażliwa na przejścia skośne i pozwala na precyzyjne wyznaczanie energii przejść prostych, jak również ich przesunięć na skutek zmiany czynników zewnętrznych [3–6].

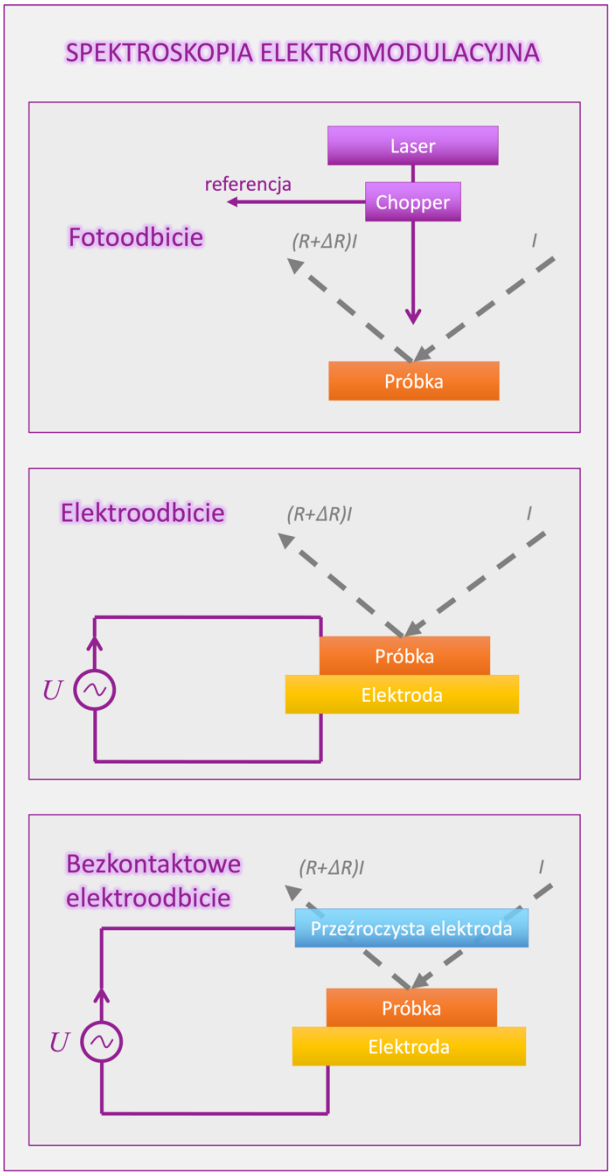

Rysunek 2. Fragment schematu blokowego obejmujący otoczenie próbki w układzie pomiarowym dla poszczególnych technik: elektroodbicia, fotoodbicia i bezkontaktowego elektroodbicia. *I* – natężenie wiązki padającej, *R* – energetyczny współczynnik odbicia próbki, *ΔR* – zmiana współczynnika odbicia wywołana modulacją.

2.1.1 Fotoodbicie

W technice fotoodbicia (PR z ang. photorelfectance) modulacja pola elektrycznego w próbce jest spowodowana wzbudzeniem par elektron-dziura generowanych przez źródło laserowe. Ma ono energię większą od przerwy energetycznej i jest modulowane z określoną częstotliwością. Zaburzenie wprowadzane jest przez periodyczne przerywanie wiązki laserowej za pomocą mechanicznego modulatora wiązki (ang. chopper). W momencie oświetlania próbki wygenerowane nośniki mniejszościowe separują się we wbudowanym polu elektrycznym i są pułapkowane przez stany powierzchniowe co wpływa na redukcję pola. Odwrotna sytuacja ma miejsce, gdy do próbki nie dociera wiązka laserowa. Wtedy zajęcie stanów pułapkowych i tym samym pole elektryczne wraca do stanu początkowego. Technika ta jest nie destrukcyjna dla próbki [7,8].

2.1.2 Elektroodbicie

Spektroskopia elektroodbicia (ER z ang. electroreflectance) zalicza się do metody odbiciowej, ponieważ opisuje ona zmiany w widmie odbicia badanego materiału na skutek wpływu pola elektrycznego na próbkę. Pole elektryczne przy powierzchni jest próbkowane przez modulowaną wiązkę odbitą od powierzchni. W trakcie pomiaru badany jest jedynie obszar przypowierzchniowy, dzięki czemu nie uwzględnia się ruchliwości nośników w całej objętości, a grubość próbki nie ma znaczenia. Technika ta umożliwia skomplikowaną analizę struktury pasmowej materiałów półprzewodnikowych przez interpretację zmian w widmie odbicia. Modulacja zewnętrznym polem elektrycznym odbywa się poprzez kontakty elektryczne naniesione na powierzchnię próbki. Spektroskopia elektroodbicia może być domyślnie podzielona na dwa typy ze względu na sposób wytwarzania modulującego pola elektrycznego przykładanego do próbki: wzdłużny i poprzeczny. W pierwszym przypadku napięcie przykładane jest do przedniej i tylnej powierzchni, w drugim przypadku na jednej powierzchni przykładane jest napięcie do dwóch elektrod. Niezależnie od sposobu przykładania napięcia, w obu przypadkach z zasady konieczne jest nanoszenie elektrod bezpośrednio na powierzchnię próbki, co wyklucza tę technikę w przypadku próbek zbyt małych, o nieregularnej powierzchni lub mniejszej stabilności [9,10].

2.1.3 Bezkontaktowe elektroodbicie

Istnieje również druga odmiana spektroskopii elektroodbicia, a konkretnie jej bezkontaktowy wariant, który jest niedestrukcyjny dla próbki. Nie wymaga on nanoszenia elektrody bezpośrednio na powierzchnię próbki w celu przyłożenia do niej napięcia. W bezkontaktowym elektroodbiciu (CER z ang. contactless electroreflectance) pole elektryczne wytwarzane w otoczeniu próbki powoduje zmiany w jej wewnętrznym polu elektrycznym. Pomiar taki wymaga użycia uchwytu pełniącego funkcję kondensatora, w którym jedną z dwóch okładek stanowi przeźroczysta elektroda. Podczas pomiaru próbka umieszczana jest pomiędzy okładkami. Po przyłożeniu zmiennego napięcia do obu okładek wytwarzane jest pole elektryczne [11]. Dzięki temu, że elektroda jest przeźroczysta wiązka promieniowania padającego może dotrzeć do powierzchni próbki, a wiązka promieniowania odbitego może dotrzeć do detektora, bez większych strat na absorpcji czy odbiciu przez elektrodę. Następnie badane jest i analizowane odbicie światła od powierzchni próbki. Na podstawie otrzymanego widma spektralnego i obecnych linii rezonansowych wyznaczyć można energię przejść optycznych badanego materiału półprzewodnikowego. Dotychczas stosowane kondensatory z elektrodą przeźroczystą wykonaną z drucianej, miedzianej siatki wymagały użycia wysokich napięć rzędu kilku kilowoltów. Spowodowane było to dużą odległością elektrody od próbki – ok. 1 mm wymuszoną rozmiarem ścieżek, z których wykonana była ta siatka [12].

2.2 Spektroskopia termomodulacyjna

Technika spektroskopii termomodulacyjnej również należy do spektroskopii modulacyjnej tak jak spektroskopia elektromodulacyjna z tą różnicą, że zaburzenia wywoływane są w badanym materiale poprzez periodyczną zmianę temperatury próbki, a nie pola elektrycznego w próbce. W tej technice prąd grzewczy pochodzi ze źródła prądu stałego, a impulsy ciepła z generatora funkcyjnego co przedstawione jest na Rys. 3. Tak jak poprzednio można wyróżnić różne techniki, a jedną z nich jest technika termoodbicia (TR z ang. thermoreflectance).

Wprowadzane zmiany tak jak w poprzednim przypadku wpływają na widmo odbicia badanej próbki. Zaburzenia termiczne mogą być zarówno bezpośrednie jak i pośrednie. W pierwszym przypadku, jeśli badana próbka jest przewodząca, termiczna modulacja może być osiągnięta poprzez przyłożenie prądu zmiennego bezpośrednio do próbki poprzez dwa kontakty omowe. Druga sytuacja zakłada wykorzystanie radiatora rozprowadzającego ciepło w badanej próbce. Takim radiatorem może być podłoże szklane lub szafirowe z warstwą przewodzącą na wierzchu, przez którą w trakcie przepływu prądu wydzielane jest ciepło Joule'a. Do przeprowadzenia takiego pomiaru niezbędna jest grzałka, która będzie zarówno równomiernie dostarczała ciepło do całej powierzchni próbki jak i je odprowadzała. Dzięki temu możliwa będzie szybka zmiana temperatury próbki, a tym samym możliwość wykorzystania jej jako czynnika modulującego. Eksperyment taki może być wykonywany w dwóch trybach – trybie odbiciowym i trybie transmisyjnym. W pierwszym przypadku, próbka umieszczana jest na grzałce, a światło na nią padające odbija się jedynie od jej powierzchni. W przypadku trybu transmisyjnego próbka umieszczana jest za grzałką, co powoduje, że musi być ona przeźroczysta dla światła, by mogło ono dotrzeć do powierzchni próbki i od niej się odbić. Zarówno szkło jak i szafir są odpowiednimi materiałami do rozprowadzania ciepła, a przy tym są one przeźroczyste więc mogą być zastosowane do pomiaru termoodbicia w trybie zarówno transmisyjnym jak i odbiciowym [13–15].

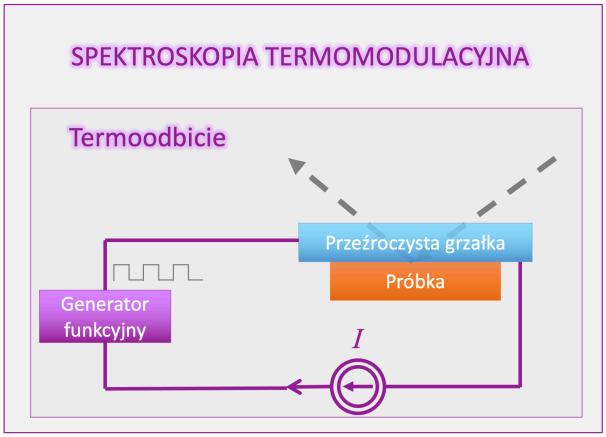

Rysunek 3. Fragment schematu blokowego obejmujący otoczenie próbki w układzie pomiarowym stosowanym w technice termoodbicia.

2.3 Spektroskopia fotonapięcia powierzchniowego

Kolejną z metod spektroskopii optycznej również wykorzystującą przeźroczystą elektrodę jest spektroskopia fotonapięcia powierzchniowego (SPV z ang. surface photovoltage). W tym przypadku elektroda nie jest używana do modulowania widma odbicia próbki, jak odbywa się to w przypadku pomiaru bezkontaktowego elektroodbicia, ale do zbierania wygenerowanego sygnału na skutek efektu fotoelektrycznego występującego w trakcie oświetlenia jej powierzchni. Światło to jest modulowane za pomocą „choppera", a jego częstotliwość jest podawana jako wartość referencyjna bezpośrednio do nanowoltomierza fazoczułego typu lock-in. Kluczowe w tej metodzie jest przepuszczenie modulowanej wiązki do powierzchni próbki, a następnie odprowadzenie wygenerowanych fotoelektronów. Jest to możliwe dzięki umieszczeniu tuż przed próbką przeźroczystej elektrody, która spełnia obie te funkcje [16]. Przykładowy schemat układu przedstawiony jest na Rys. 4.

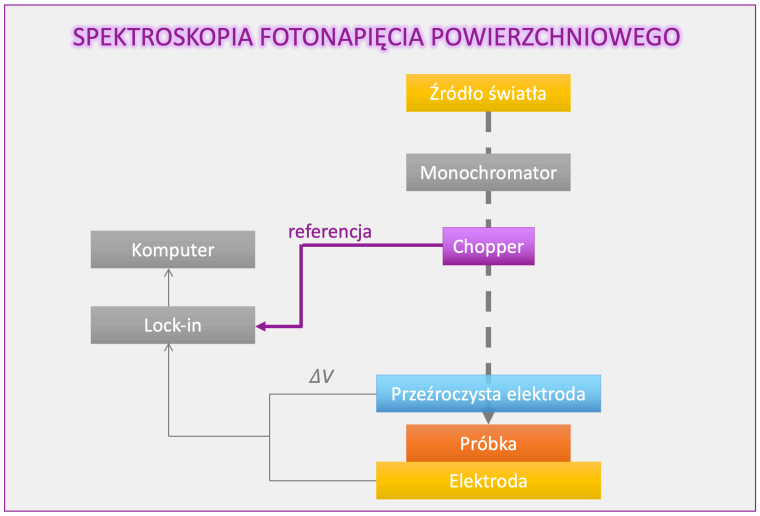

Rysunek 4. Schemat blokowy układu pomiarowego stosowanego w spektroskopii fotonapięcia powierzchniowego.

3. Przeźroczyste elektrody

W przemyśle urządzeń optoelektrycznych przeźroczyste elektrody odgrywają kluczową rolę. W ostatnich latach odpowiadają za szybkość rozwoju technologicznego, gdyż mogą być wykorzystane przy produkcji wyświetlaczy, oświetlenia, inteligentnych okien i wielu innych. Ciągle pojawiają się nowe pomysły wykorzystujące przeźroczyste elektrody na elastycznych podłożach, by móc zastosować je na niepłaskich powierzchniach, np. na ubraniach [17]. Elektroda przeźroczysta może być w łatwy sposób opisana i parametryzowana biorąc pod uwagę jej właściwości optyczne i elektryczne. W pierwszym przypadku oceniana jest wydajność optyczna, np. przez pomiar transmisji (zazwyczaj przy długości fali 550 nm, przy której oko ludzkie ma największą czułość widzenia). W drugim, badane są właściwości elektryczne, np. przez pomiar rezystancji, obliczanie rezystywności czy też rezystancji powierzchniowej. Brana jest również pod uwagę wytrzymałość mechaniczna przeźroczystych elektrod – w kontekście elektrod elastycznych często badana jest ich wytrzymałość na zginanie. Dodatkowym parametrem porównawczym będą oczywiście koszty produkcji, które potrafią znacząco się różnić w zależności od wykorzystywanych materiałów i technik [18–21].

Temat przeźroczystych elektrod pojawia się często w literaturze w kontekście ogniw słonecznych, w których kluczową rolę stanowi tzw. elektroda górna (ujemna), która ma na celu odprowadzić zgromadzony ładunek elektryczny, a równocześnie przepuszczać promieniowanie słoneczne. Ważne jest, by przeźroczysta elektroda nie absorbowała promieniowania, które ma dotrzeć do głębszych warstw w celu przekonwertowania ich na energię elektryczną. Z tego powodu dosyć szczegółowo omawiane są wszelkie warstwy przewodzące zachowujące jak największą przeźroczystość, a dodatkowo charakteryzujące się wysoką wytrzymałością mechaniczną i odpornością na zmienne czynniki zewnętrzne [22–24].

W tej pracy zakres rozważań skupia się na szczególnym typie przeźroczystych elektrod, których schemat jest przedstawiony na Rys. 5. Elektrody te są przygotowywane w skali laboratoryjnej, ok. 2 cm x 2 cm na przeźroczystych, litych dielektrycznych materiałach, a warstwa przewodząca znajduje się na ich powierzchni. Wraz z odpowiednim uchwytem wykorzystywane są one w układach do pomiarów optoelektrycznych.

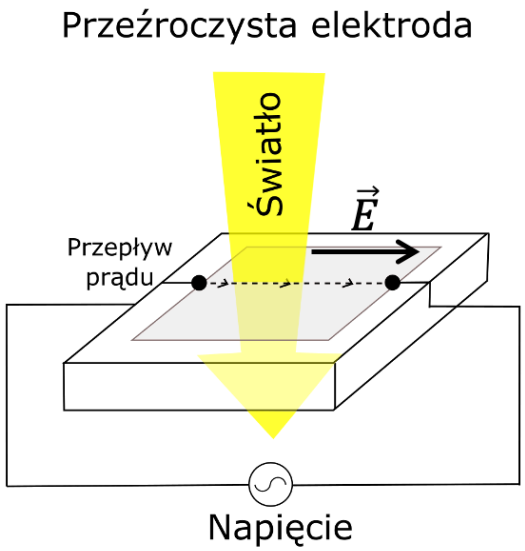

Rysunek 5. Schemat koncepcji przeźroczystej elektrody.

Nie uwzględniano podłoży elastycznych, czy też materiałów przewodzących i przeźroczystych niewymagających podłoża. Poza przeźroczystym podłożem drugim rozważanym w tej pracy elementem składowym elektrody jest przewodząca warstwa znajdująca się na powierzchni. Istnieje wiele różnych sposobów na otrzymanie warstwy przewodzącej na dielektryku. Należą do nich między innymi fotolitografia [25], drukowanie cienkich ścieżek [26] – z ciekawym przypadkiem efektu „coffee ring" [27], transfer grafenu [28,29], strukturyzacja laserowa warstw metalicznych [30], nanoszenie warstw nanodrutów srebra [31,32,21] a także nowe, ciągle pojawiające się pomysły takie jak adaptowanie przykładów występujących w przyrodzie np. pękający szablon („cracking template") czy odwzorowanie użyłkowania liścia [33–36]. Z wyżej wymienionych metod w tej pracy wykorzystano: druk ultraprecyzyjnej depozycji, syntezę grafenu na folii miedzianej z jego transferem na podłoże, ale też opracowano od podstaw dwie nowe techniki: „laser lift-off", czyli wykorzystanie strukturyzacji laserowej warstwy polimerowej oraz „crack-templated lift-off", czyli samorzutne powstawanie nieregularnego wzoru na skutek pękania.

W literaturze przedmiotu można znaleźć rozwiązania wykorzystujące do pomiarów optoelektrycznych przeźroczystą elektrodę umieszczoną w bardzo małej odległości lub na styku z próbką [10,37]. W przytoczonych pracach znaleźć można odniesienie do pomiarów, w których użyta została elektroda na przeźroczystym podłożu z cienką warstwą przewodzącego materiału tlenku indu cyny (ITO z ang. indium tin oxide). W tej pracy nie była brana pod uwagę tak wykonana elektroda, ponieważ jest ona ograniczona spektralnie co zawężyłoby możliwości aplikacyjne. Dodatkowo z powodu deficytowych złóż indu skupiono się na materiałach ogólnodostępnych.

3.1 Materiały wykorzystywane do wytwarzania przeźroczystych elektrod

Do badań nad przeźroczystymi elektrodami wykorzystywano każdorazowo przeźroczyste podłoże i warstwę przewodzącą umieszczoną na powierzchni podłoża. Przetestowano trzy rodzaje materiałów: szkło, kwarc oraz szafir (Tab. 1).

Tabela 1. Porównanie parametrów i kosztów przeźroczystych podłoży. Oznaczenia D1-D4 to odnośniki do poszczególnych prac własnych umieszczonych w bibliografii.

Parametr / *Materiał*	**Transmisja [%, przy 550 nm]**	**Przewodność cieplna [W/(mK)]**	**Względna przenikalność elektryczna [-]**	**Wytrzymałość na ściskanie [MPa]**	**Twardość [mohs]**	**Koszt* [zł]**
Szkło [D1, D4]	90	1,2	4,6	1000	5	0,30
Kwarc [D2, D4]	92	3	3,7-3,9	1100	7	180,00
Szafir [D3, D4]	85	30	9,3	2000	9	350,00

*ceny sklepu sigmaaldrich.com na dzień 24.08.2022 r.

Dla zapewnienia dobrej przewodności elektrycznej jako warstwę przewodzącą na podłożach zastosowano różne rodzaje metali (między innymi srebro i miedź), ale również materiał nie będący metalem o znakomitych właściwościach elektrycznych jakim jest grafen [38]. Jest on jedną z alotropowych odmian węgla i składa się z jednej warstwy atomów ułożonych w dwuwymiarową siatkę o strukturze plastra miodu. Grafen bardzo efektywnie przewodzi ciepło i prąd elektryczny wzdłuż swojej płaszczyzny oraz silnie absorbuje światło widzialne,

pozostając jednocześnie przeźroczystym dzięki swojej jednoatomowej grubości warstwy [39,40]. By możliwe było wykorzystanie tego materiału do zastosowań optoelektrycznych konieczne jest osadzenie go na trwałym i wygodnym w obsługiwaniu podłożu. Z tego też względu podczas omawiania technik syntezy grafenu rozważane są różne techniki transferu tego materiału na docelowe podłoża [38,41,42].

3.2 Typy przeźroczystych elektrod

W niniejszej pracy przedstawiono trzy typy elektrod różniące się warstwami przewodzącymi umieszczonymi w różny sposób na przeźroczystym podłożu (Rys. 6):

a) Przewodzący, nieprzeźroczysty materiał naniesiony na przeźroczyste podłoże w sposób zapewniający przewodzenie na całej powierzchni podłoża jednak tak, by nie ograniczać znacząco transmisji światła mającego przejść przez powierzchnię elektrody. Podstawowym kształtem spełniającym te wymagania jest siatka o odpowiednim rozstawie i szerokości linii.
b) Ciągła, przewodząca i przeźroczysta warstwa naniesiona na przeźroczyste podłoże.
c) Przewodzący, przeźroczysty materiał naniesiony na przeźroczyste podłoże, jednak nie na całej powierzchni, tylko w sposób zapewniający przewodzenie na całej powierzchni podłoża (podobnie jak w typie I kształtem spełniający odpowiednie warunki jest siatka).

Kształt siatki daje możliwość regulacji transmisji poprzez szerokość linii oraz ich rozstaw.

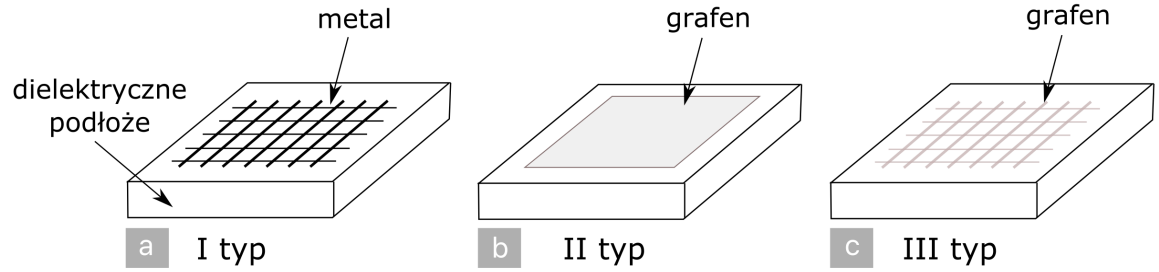

Rysunek 6. Schemat przedstawiający trzy typy przeźroczystej elektrody: a) siatka wykonana z metalu, b) ciągła warstwa grafenowa, c) siatka wykonana z grafenu.

3.3 Techniki wytwarzania przeźroczystych elektrod

3.3.1 Druk – ultraprecyzyjna depozycja

Pierwszą z zastosowanych technik był druk przy użyciu technologii ultraprecyzyjnej depozycji na podłoże przeźroczyste [43]. Został on wybrany ze względu na możliwość otrzymania bardzo wąskich linii przewodzących, które przy zaprojektowaniu odpowiedniego kształtu nie zmniejszały znacznie przeźroczystości podłoża. W tej metodzie kluczowy jest dobór parametrów druku, tak by zapewniona była ciągłość ścieżki, a tym samym prawidłowe przewodzenie całej elektrody. Parametry jakie mogą być kontrolowane w celu otrzymania lepszej jakości wydruku to szybkość druku, ciśnienie przykładane do kapilary wypełnionej tuszem oraz kierunek ruchu głowicy.

3.3.2 Laser lift-off

Kolejny sposób otrzymywania przeźroczystych elektrod był procesem wieloetapowym i wymagał opanowania i optymalizowania każdego z nich. Łączy on użycie systemu laserowego do strukturyzacji warstwy polimerowej razem z techniką usuwania fotorezystu należącego do technik fotolitograficznych. W tej technice fotorezyst może być dowolnym materiałem, który na skutek ablacji laserowej odparuje z powierzchni podłoża. Na pierwszym etapie opracowano odpowiednie stężenie roztworu polimerowego pełniącego rolę fotorezystu, tak by możliwe było wytworzenie ciągłej, cienkiej warstwy na przeźroczystym podłożu techniką powlekania obrotowego (z ang. spin-coating). Następnie planowany był wzór, który bazując na zjawisku ablacji laserowej był odwzorowywany we wcześniej przygotowanej warstwie polimerowej. Tak przygotowana warstwa stanowiła jednorazową maskę potrzebną do kolejnego etapu, którym było nanoszenie warstwy metalicznej metodą fizycznego odparowania z fazy gazowej. Następnie przygotowana próbka z warstwą polimerową i metaliczną umieszczana była w rozpuszczalniku dobranym w ten sposób, by rozpuścił on polimer. Na skutek wymywania maski polimerowej spod warstwy metalu, odrywały się fragmenty metalu w efekcie pozostawiając go tylko w miejscach, w których polimer został usunięty laserowo i metal mógł być osadzony bezpośrednio na przeźroczystym podłożu.

3.3.3 Synteza i transfer grafenu

Ostatnią techniką stosowaną w tej pracy była synteza, a następnie transfer grafenu na przeźroczyste podłoże. Grafen otrzymany został przez chemiczne osadzanie z fazy gazowej na folię miedzianą stanowiącą podłoże katalityczne. Jest to znana metoda, która umożliwia otrzymywanie grafenu dobrej jakości nawet na dużą skalę. W celu otrzymania przeźroczystej elektrody, cienka i delikatna warstwa grafenowa na podłożu miedzianym została przetransferowana na przeźroczyste podłoże szafirowe. Wykorzystano do tego technikę delaminacji elektrochemicznej, która polega na oddzieleniu warstwy grafenu od powierzchni podłoża, na którym został on zsyntezowany. Ten proces odbywa się przez zanurzenie podłoża z grafenem przykrytym warstwą poli(metakrylanu metylu) w cieczy, w której uwalniane są bąbelki wodoru będące wynikiem elektrolizy wody na katodzie miedzianej. W momencie zanurzania podłoża w cieczy warstwa grafenowa wraz z warstwą polimerową unoszą się na powierzchni wody. Ostatnim krokiem jest umieszczenie grafenu w odpowiednim miejscu na docelowym podłożu, rozpuszczenie warstwy polimerowej oraz wysuszenie grafenu. Efektem jest otrzymana w procesie syntezy warstwa grafenowa na przeźroczystym podłożu stanowiąca w całości przeźroczystą elektrodę o ciągłej warstwę przewodzącej.

3.3.4 Crack-templated lift-off

W w ramach doktoratu wytworzono również przeźroczystą elektrodę metodą „crack-templated lift-off”. Metoda ta nie wymaga użycia systemu laserowego, ponieważ proces strukturyzacji zachodzi samorzutnie podczas pękania na skutek wyższej temperatury i zmniejszonego ciśnienia. Etap nanoszenia warstwy metalicznej, a następnie proces rozpuszczania maski polimerowej przebiega tak samo jak w przypadku metody „laser lift-off”. Uzyskana przeźroczysta elektroda o nieregularnych kształtach nie zalicza się do żadnego z wymienionych typów (Rys. 6), ponieważ jej kształt nie układa się w regularne linie, tj. siatkę, ani warstwa przewodząca nie jest ciągła na całej powierzchni. Przewodzący kształt powstały samorzutnie jest drugim wariantem I typu przeźroczystej elektrody – składa się z nieprzeźroczystego materiału srebrnego o niepowtarzalnie ułożonych liniach.

4. Wyniki

Elektrody I typu wytwarzane były metodą druku z wykorzystaniem technologii ultraprecyzyjnej depozycji [D1] oraz techniką „laser lift-off" [D2]. Elektroda I typu w drugim wariancie otrzymana została metodą „crack-templated lift-off" [D4]. Elektroda II typu o ciągłej przewodzącej warstwie otrzymana została poprzez syntezę, a następnie transfer grafenu na przeźroczyste podłoże [D3]. Ostatni, III typ elektrod został otrzymany poprzez strukturyzację warstwy grafenowej w celu otrzymania kształtu siatki z przeźroczystego materiału na przeźroczystym podłożu [D3].

4.1 Modelowanie rozkładu potencjału elektrycznego w kondensatorach z elektrodami przeźroczystymi

W celu zilustrowania wytworzonego przez przeźroczystą elektrodę rozkładu potencjału elektrycznego w kondensatorach do pomiarów spektroskopii struktur półprzewodnikowych wykonano zestaw symulacji korzystając z programu COMSOL Multiphysics. Zamodelowano uproszczony projekt przeźroczystej elektrody o ścieżkach przewodzących wykonanych ze srebra w kształcie siatki (o szerokości ścieżki 100 μm, rozstawie linii 400 μm i grubości warstwy srebra 500 μm) z dwiema srebrnymi elektrodami wyprowadzeniowymi (2 mm x 2 mm) (Rys.7).

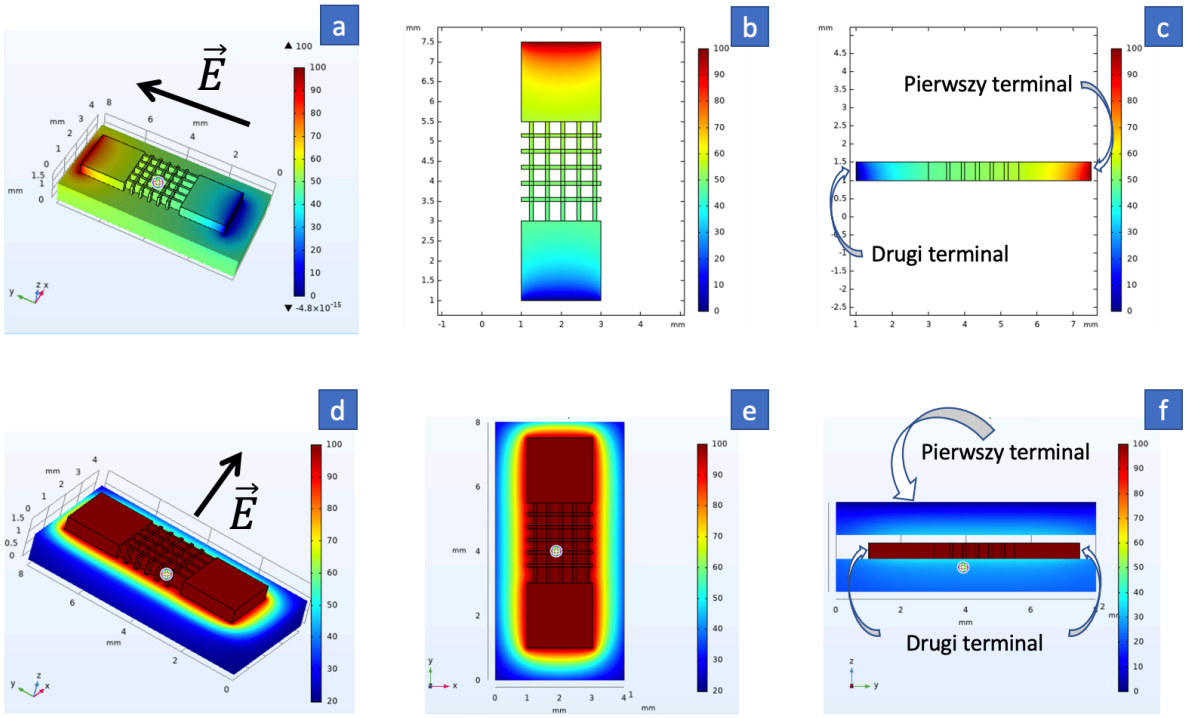

Rysunek 7. Wyniki symulacji rozkładu potencjału elektrycznego na powierzchni elektrody przeźroczystej o uproszczonym kształcie. Przedstawiono dwa tryby pomiarowe: (a-c) w przypadku przyłożenia napięcia pomiędzy prawą (pierwszy terminal) i lewą (drugi terminal) elektrodą wyprowadzeniową oraz (d-f) pomiędzy górną, miedzianą okładką (pierwszy terminal), a elektrodami wyprowadzeniowymi (drugi terminal).

Symulacje przeprowadzono dla dwóch przypadków przykładanego napięcia elektrycznego o wartości 100 V:

a) W pierwszym (Rys. 7a-c), napięcie przykładane było pomiędzy dwiema elektrodami wyprowadzeniowymi oddalonymi o 2,5 mm w tej samej płaszczyźnie XY. Pomiędzy tymi elektrodami umieszczona była siatka. Taki układ występuje podczas standardowego pomiaru właściwości elektrycznych elektrody: dwupunktowy pomiar rezystancji.
b) W drugim (Rys. 7d-f), napięcie przykładano pomiędzy okładką miedzianą oddaloną o 250 μm od siatki w kierunku osi Z. Układ taki stosowany jest podczas wykorzystania przeźroczystej elektrody do pomiarów bezkontaktowego elektroodbicia w celu wytworzenia zewnętrznego pola elektrycznego w otoczeniu próbki.

Wyniki symulacji dla pierwszego przypadku Rys. 7a pokazują, że potencjał elektryczny rozchodzi się równomiernie przez siatkę od lewej do prawej elektrody, a napięcie na siatce jest jednakowe, co jest dobrze widoczne w przekroju elektrody na Rys. 7b i 7c. W przypadku drugiego wariantu symulacji widoczne jest równomierne rozłożenie potencjału w całej objętości siatki. Na poniższych rysunkach przedstawiono bardziej szczegółowo rozkład potencjału na górnej okładce oraz na siatce (Rys. 8).

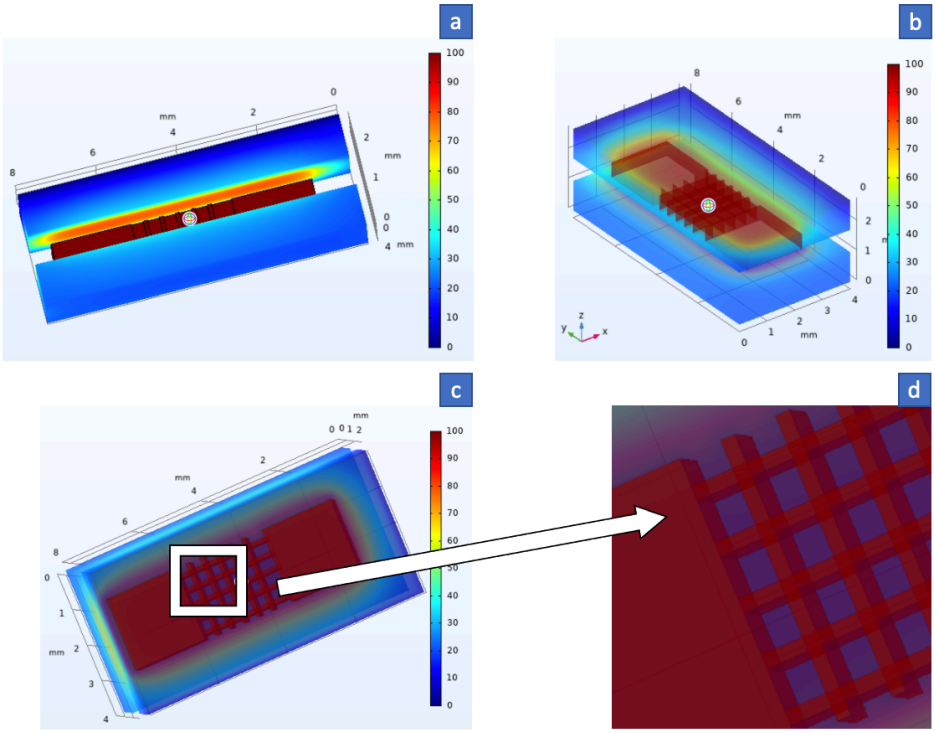

Rysunek 8. Wyniki symulacji przedstawiajace rozkład potencjału elektrycznego a) i b) na górnej miedzianej okładce oraz c) i d) na srebrnej siatce.

Zarówno w przypadku płaskiej powierzchni okładki miedzianej (Rys. 8a-b) jak i w przypadku srebrnej elektrody w kształcie siatki (Rys. 8c-d) łatwo zaobserwować, że rozkład potencjału elektrycznego jest równomierny. Potwierdza to założenie, że pomiędzy siatką a płaską powierzchnią można wytworzyć jednakowe pole elektryczne, a tym samym przeźroczysta elektroda w kształcie siatki może być wykorzystywana do wytwarzania jednorodnego pola elektrycznego, co było celem przeprowadzenia symulacji.

4.2 Wytwarzanie i zastosowanie przeźroczystych elektrod

4.2.1 Publikacja D1

Pierwsza praca opisuje wykorzystanie przeźroczystej elektrody wykonanej techniką druku z wykorzystaniem technologii ultraprecyzyjnej depozycji do zastosowania w pomiarach bezkontaktowego elektroodbicia (CER) próbki fosforku indu (InP). W pracy zostały przetestowane siatki o różnym rozstawie oraz porównano wpływ architektury elektrody na transmisję światła. Przetestowano również dwie konfiguracje elektrody względem uchwytu wykorzystywanego w układzie optycznym. Wyprowadzono również wzór opisujący zależność sygnału otrzymanego widma od odległości przeźroczystej elektrody od próbki. W zoptymalizowanych warunkach przeprowadzono pomiar jeszcze trzech materiałów: diselenku wolframu (WSe_2), diselenku molibdenu ($MoSe_2$) oraz dwusiarczku molibdenu (MoS_2), by pokazać pełne możliwości opracowanej metody.

Measurement 169 (2021) 108361

Contents lists available at ScienceDirect

Measurement

journal homepage: www.elsevier.com/locate/measurement

Contactless electroreflectance spectroscopy with a semitransparent capacitor made of a silver mesh of ultrathin lines

A. Ślusarz [a,b], J. Kopaczek [a], F. Dybała [a], A. Wiatrowska [c], F. Granek [c], R. Kudrawiec [a,b,*]

[a] Departament of Semiconductor Materials Engineering, Wroclaw University of Science and Technology, Wybrzeże Wyspiańskiego 27, 50-370 Wrocław, Poland
[b] LUKASIEWICZ Research Network, PORT Polish Center for Technology Development, Stablowicka 147, 54-066 Wroclaw, Poland
[c] XTPL SA, ul. Stablowicka 147, 54-066 Wroclaw, Poland

ARTICLE INFO

Keywords:
Transparent electrodes
Printed electronics
Electroreflectance
Semiconductors
van der Waals crystals

ABSTRACT

Semitransparent electrodes operating in the broad spectral region are needed for many applications and one of them is contactless electroreflectance (CER) spectroscopy. In this work, the technology of printed electronics has been applied to fabricate mesh-like semitransparent electrodes composed of ultrathin (10 μm) silver lines of different densities. These electrodes have been printed on borosilicate glass and used in CER measurements. It has been shown that the CER signal is linearly proportional to the applied voltage and inversely proportional to the distance. In addition, a shadow effect has been observed for some distances because of non-transparent silver paths. Finally, a phenomenological formula has been proposed to describe the intensity of the CER signal in the capacitor with the semitransparent electrode. Moreover, the mesh-like printed electrodes have been applied to measure CER spectra for van der Waals crystals and perspectives for further development of semitransparent electrodes for CER measurements have been discussed.

1. Introduction

Electromodulation (EM) spectroscopy is a powerful tool to study semiconductor materials and heterostructures [1–5]. The idea of this modulation method is to apply periodic perturbation to the sample, which causes changes in the reflectance spectrum. The quantity, which is changing periodically in EM, is a built-in electric field. The most important advantage of EM spectroscopy is its differential character, which allows an unwanted background to be eliminated and weak signals, related to the optical transitions, to be highlighted.

One type of EM spectroscopy is contactless electroreflectance (CER) [5–13]. This method provides a non-destructive approach to investigate the optical transitions in semiconductor samples. Like other EM techniques (electroreflectance and photoreflectance) CER gives not only information about ground state transitions, but also about excited states transitions since it is an absorption-like method [5,6,9]. Besides, a significant advantage of EM spectroscopy is its high sensitivity to the Franz-Keldysh effect [14–16]. Measurements of Franz-Keldysh oscillations allow studying the built-in electric field in semiconductor heterostructures [16–21]. For proper samples, i.e., so-called van Hoof structures [17], such measurements allow determining the surface potential barrier, i.e., the Fermi level position on the semiconductor surface [17–21]. In this case, CER spectroscopy is strongly recommended since the sample surface is not modified by electrical contacts, which are necessary for a regular electroreflectance [3,22,23]. Comparing to photoreflectance [24–28], which is also a contactless EM method, the unwanted photovoltaic effect is strongly reduced in CER, and thereby the potential barrier determined with this method is significantly higher than obtained with photoreflectance [28]. Because of these advantages, CER spectroscopy is often applied to study the surface potential barrier in semiconductors [18–21] but the efficient band bending modulation in CER, including the development of proper semitransparent electrode, is still a challenge.

The band bending modulation in the CER method is caused by a redistribution of carriers. It occurs because the sample is placed in a capacitor to which an alternating voltage is applied. The generated electric field is directed alternately according to or opposite to the built-in field. It sequentially corresponds to an increase or decrease of the surface potential barrier [6].

To perform the CER experiment a special capacitor is required, which provides modulation of the internal electric field in the sample [6,7]. So far, two constructions of capacitors for the CER method were proposed.

* Corresponding author at: Departament of Semiconductor Materials Engineering, Wroclaw University of Science and Technology, Wybrzeże Wyspiańskiego 27, 50-370 Wrocław, Poland.
E-mail address: robert.kudrawiec@pwr.edu.pl (R. Kudrawiec).

https://doi.org/10.1016/j.measurement.2020.108361
Received 3 May 2020; Received in revised form 15 July 2020; Accepted 10 August 2020
Available online 18 August 2020

The first includes an electrode made of a substrate coated with a thin, continuous and (semi) transparent film of conductive material. The second concerns the metal – mesh electrode. Until now, this mesh was made of 0.5 mm thick copper wires spaced at a distance of 0.5 mm. This type of arrangement with the macroscopic electrode has been successfully used by our group in recent years [6,18–21].

Moreover, the solution with mesh electrode does not limit the range of spectrum available in the experiment in contrast to the uniform conducting layer covering the whole electrode surface, in which the spectrum is determined by the type of electrode/substrate material, which often is non-transparent in UV or other spectral ranges.

The magnitude of the electric field generated between electrodes of the capacitor depends primarily on two described here quantities: (i) First is a distance between the electrode and the sample, where its smaller value corresponds to the greater electric field strength. However, during measurements with high values of voltage and an arrangement of the electrodes with too small distances between them, a problem of the electric breakdown may occur (other effects than electric discharge are not expected at high voltages). Due to this, the distance is carefully estimated to prevent any sample damage. Nevertheless, the high values of the voltage are necessary to obtain a strong enough electric field, generated by the grid-shaped electrode, to observe optical transitions in CER spectra. (ii) The second parameter is a line width on which the shape of the electric field depends. The smaller the dimension of the path, the more homogeneous and stronger the electric field is expected. As a result, decreasing path size in the mesh will allow the electrical breakdown to be avoided, which can be harmful to the sample. Additionally, the intensity of light reflected from the sample is changing with the electrode to sample distance due to the "shadow" effect. In general, it is expected that the thicker the line, the bigger the shadow and the weaker the intensity of light reflected from the sample. However, no theoretical formula is known for the intensity of CER signal. In this context, it is interesting to study experimentally how the intensity of CER signal depends on the voltage and the distance between the sample and the semitransparent electrode in the mesh capacitor.

Considering fabrication of semitransparent mesh-like electrodes, printed electronics can be seen as a beneficial tool to reduce mesh width since it is possible to obtain ultrathin paths of different architecture [29,30]. Using this technology, namely based on printed electronics, meshes composed of 10 μm wide silver lines of different densities can be prepared. So far, such meshes were not tested as semitransparent electrodes operating at high voltages. In this work, it is shown that printed meshes of silver lines are excellent as semitransparent electrodes for CER measurements. We examined five types of such electrodes of different densities of lines and showed that reducing the dimensions of the printed mesh could decrease the "shadow" effect and thus also lower the applied value of voltage. Reducing the voltage will lead to a cost decrease in the experiment and will increase safety for both the operator and the sample. Moreover, we investigated the dependence between the voltage and the electrode to sample distance in the mesh capacitor. The intensity of CER signal for the studied capacitor was described with a phenomenological formula.

2. Experimental methods

2.1. Description of the measurement system

The examined sample was placed in contact with one of the electrodes. Whereas the second plate was semitransparent to allow the light to pass through it and reach the sample. The electrode printed on glass (borosilicate glass transparent substrate – 1 mm thick) was placed in setup for the contactless electroreflectance spectra measurements as a second plate of the capacitor [7]. The distance between a sample and a semitransparent electrode can be adjusted with the use of a micrometer screw - the schematic arrangement is shown in Fig. 1. The conducted experiment aimed to test different semitransparent mesh electrodes. The shape of the mesh on the substrate/electrode started with the distances between the ultrathin silver lines (mesh pitch, *P*) from 100 μm and ended in 1000 μm.

A halogen lamp, the source of the broad white light spectrum, was used to probe the changes of the reflection coefficient caused by the modulation of the built-in electric field. The measurements were performed in a dark configuration with a 1 m focal length GDM monochromator. In the case of such experimental setup, the white light is first directed by concave mirrors to a monochromator and then dispersed light by two diffraction gratings, illuminate the surface of the sample [31]. Eventually, the monochromatic light, reflected from the sample, falls on the detector and its two components, namely AC and DC, are measured by the lock-in amplifier. The scheme of the measurement system is shown in Fig. 2.

To get a modulation of a band bending, and consequently, the modulation of the abovementioned built-in electric field, an alternating voltage (max. 3 kV) is applied to the plates of the capacitor. The dielectric strength of the air determines the maximum value of the applied voltage - an electrical breakdown occurs within a gas of ambient pressure when ~30 kV/cm is exceeded. In order to avoid unwanted electrical breakdowns, which can destroy the sample and/or electrode, CER measurements are performed up to safe voltages.

2.2. Characterization of semitransparent electrodes

The semitransparent electrodes with the ultrathin silver mesh, which allow reducing the "shadow" effect, were fabricated with the use of XTPL Lab Printer and XTPL nano-ink based on silver nanoparticles. XTPL printing head equipped with dedicated nozzle deposits the ink on the substrate using ultra precise dispensing technology (UPD). This innovative technology allows to print the structures with different geometry (parallel lines, meshes, crosses, microdots) and obtains feature size in the range of 1 to 20 μm for medium- to high-viscosity inks [32]. The described printing process is a direct-write method which does not

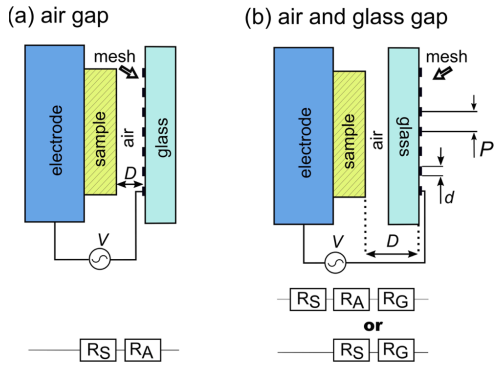

Fig. 1. The arrangements of the printed mesh-shaped electrode in the capacitor-like system. (a) The printed electrode can be moved toward the sample and only air is a spacer. (b) The printed electrode also can be moved toward the sample; however, the spacer is composed of air and glass. In the case of the air gap configuration (a), the distance between the sample and the printed mesh-shaped electrode D is adjustable in the range of 0–2 mm. In the case of the air and glass gap configuration (b), the distance D is in the range of 1–2 mm because of the constant thickness of the glass, which equals 1 mm. The width of the printed line d is around 10 μm. The pitch - distances between the parallel silver paths - is in the range of 100–1000 μm. The voltage V applied between electrodes in the capacitor is in the range of 1500–3000 V. In addition, schematic presentation of resistance in a series circuit of capacitor-like system is presented: (a) the equivalent resistance consists of a sample and air resistance, (b) the equivalent resistance consists of a sample, air and a glass resistance.

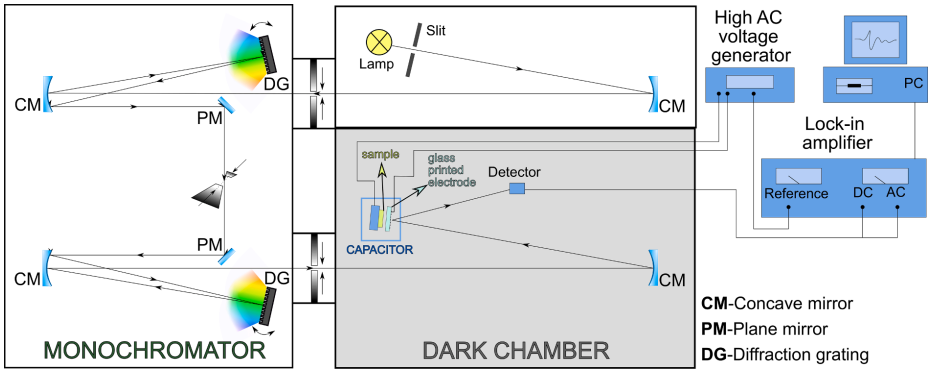

Fig. 2. The scheme of the experimental set-up, in dark configuration, for contactless electroreflectance measurements. DG – diffraction grating, PM – plane mirror, CM – concave mirror.

require any masking or patterning steps. For the purpose of this article, geometry of the conductive meshes were designed to effectively reduce shadow effect and were define as line width: 10 μm; line length: 1 cm; pitch: from 100 μm to 1000 μm. Printed meshes were sintered in the convection oven in air, at 150 °C.

The silver, parallel paths were printed with the following distances, *P*: 100, 200, 400, 600 and 1000 μm - three selected electrodes are shown in Fig. 3(a). The light transmission measurements showed that the transparency of all electrodes is above 75% and the highest value occurs for the electrodes with the pitch above 400 μm, for which the transmission of the light is above 88% in the entire visible and infrared spectral range, see Fig. 3(b). Please note that the optical transparency of the bare glass substrate used in this experiment equals 92%. Thus the printed metal mesh reduced the overall transparency between 17% and 4% respectively.

Next, the chosen glass electrode was placed in front of the sample and connected to a power supply, as shown in Fig. 4. All distances were precisely measured and adjusted so that the sample was in the center of the silver mesh. The capacitor presented in Fig. 4(a) was mounted in the experimental setup for CER measurements, Fig. 2.

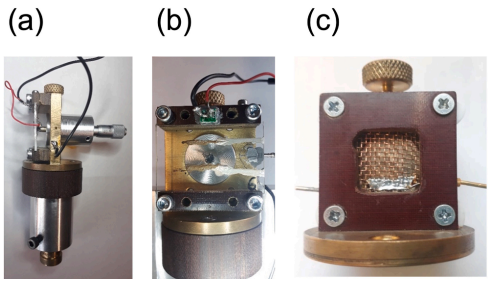

Fig. 4. Pictures of capacitor-like elements with the adjustable sample to electrode distance by the micrometer screw. (a) and (b) The capacitor with the microscopic mesh-shaped electrode, which is made with the technology of printed electronics. (c) The capacitor with the macroscopic mesh-shaped copper electrode commonly used in contactless electroreflectance measurements in recent years.

2.3. Samples

The 0.5 μm thick InP epilayer grown by metalorganic chemical vapor epitaxy on InP substrate was used to test CER measurement with different semitransparent electrodes and different parameters in this experiment (i.e., various voltages and distance between the sample and

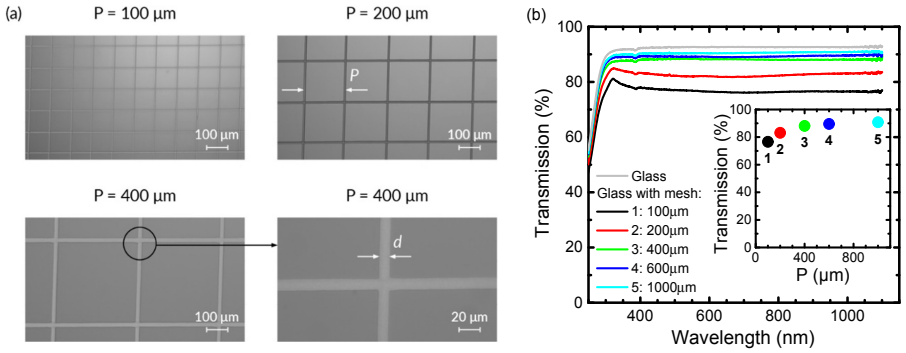

Fig. 3. (a) Optical microscope images of the printed silver meshes on borosilicate glass with the pitches P equal, respectively, to 100, 200 and 400 μm. The width of the printed line d is around 10 μm. (b) The transmission of light for five different electrodes. The inset shows the relationship between transmission at 600 nm and P.

the electrode). Furthermore, to demonstrate the usefulness of the tested semitransparent electrodes in CER measurements, we selected WSe_2, $MoSe_2$, and MoS_2 crystals from 2DSemiconductors company.

3. Results and discussion

Fig. 5 shows room temperature CER spectra of InP epilayer measured in capacitors built of semitransparent electrodes of different mesh densities. All these measurements were performed in the arrangement with an air gap of 1 mm as shown in Fig. 1(a). The observed CER signal corresponds to a band-to-band transition in InP. The amplitude (A) of this signal slightly changes due to different transparency of the studied electrodes, weaker efficiency of electromodulation in areas of different distances from silver wires, and the "shadow" effect. Obtained results indicate that the electrode with the pitch *P* equals to 400 μm (number 3) gives the highest CER signal. This electrode is more transparent than electrodes 1 and 2, see Fig. 3(b) and therefore higher transparency can explain higher signal in this case. On the other hand electrodes 4 and 5 are of very similar transparency as the electrode 3 but the intensity of CER signal is weaker for these electrodes. This observation is associated with weaker modulation of electric field in in the areas furthest away from the silver wires. This shows that there is a trade-off between electrode transparency and electric field intensity/homogeneity in the sample. It is worth noting that all tested electrodes are very useful in CER spectroscopy, because the difference in CER signal intensity is very small, see Fig. 5.

The third electrode was chosen for further studies. For this electrode, CER measurements were done for different distances *D*, adjusted with the micrometer screw, in the configuration with the air gap shown Fig. 1 (a). The range of distances was from 2.0 to 0.075 mm. The plate printed with silver, was gently shifted towards to the surface of the investigated sample. Measurements were performed for various voltages and distances. Some of them were selected and presented in Fig. 6. In conditions of too high voltage and with too small distance between the electrodes, the electrons can go directly through the air – electric breakdown of the air. Since this phenomenon can destroy the sample (and the printed electrode), it is crucial to know the minimal value of the distance. Therefore, CER measurements at high voltage and small distances were avoided. Compared to previous spectra, the poorer signal-to-noise ratio for these spectra is associated with a shorter time constant on the Lock-in amplifier during measurements (1 s vs. 3 s). In general the signal-to-noise ratio in CER measurements is also affected by the stability of probing beam, the stability of modulation frequency, and the dark current of the detector. In our case the signal-to-noise ratio resulting from these factors is the same for all measurements.

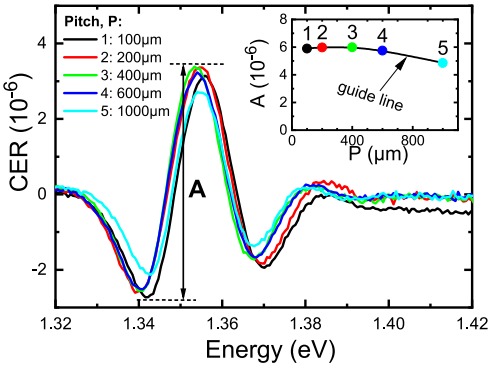

Fig. 5. Room temperature contactless electroreflectance spectra of the InP sample measured with the capacitor with the printed semitransparent electrode of different pitch P. The inset shows the dependence of a signal amplitude A versus a mesh pitch P.

First, the obtained results, namely amplitude of the signal, were collected as a function of the voltage for each distance separately in Fig. 6(e). As seen in this figure, the voltage *V* dependence of the amplitude *A* is linear at the constant distance *D*. The coefficient, which was used to fit the data, is signed as α' and placed in the table in the upper part of Fig. 6(e). From this analysis, we concluded that the α' coefficient also depends on distance *D* and therefore, the relationship between the amplitude *A* and the distance *D* should be determined.

In the second step, obtained results were collected as a function of the distance for each voltage separately. As seen in Fig. 6(f) the amplitude *A* is inversely proportional to the distance *D,* but in some range of distances, the amplitude is insensitive to the size of the air gap. This range is assigned as a "shadow" effect area in this figure. Finally, the dependence of the amplitude on the distance was divided into two regions, which were analyzed separately using the formula:

$$A = \frac{\alpha V}{D + \beta}, \tag{1}$$

where β is a parameter, which depends on the semitransparent electrode and is also related to the shadow effect. Parameters extracted from fitting are shown in tables in Fig. 6(f). The table placed in the upper part of this figure is related to distances from 0.7 to 1.45 mm (right part of the graph). The table placed in the lower part refers to the range of a distance from 75 μm to 0.325 mm (left part).

Summarizing parameters derived from fitting, we can conclude that the amplitude dependence on the voltage and distance is very well described with the phenomenological formula given by Eq. (1). The studied semitransparent capacitor for CER measurements is described by following parameters: $\alpha = 4.6 \pm 0.3 \times 10^{-9}$ mm/V and $\beta = 0.6 \pm 0.2$ mm in the range of large distances $D > 0.7$ mm; $\alpha = 2.8 \pm 0.2 \times 10^{-9}$ mm/V and $\beta = 0.36 \pm 0.02$ mm in the range of small distances $D < 0.4$ mm. It is expected that the proposed formula will work for capacitors with other mesh densities, but parameters describing these capacitors (α and β) will be different.

The next measurements were done using the setup with the configuration of air/glass gap, as shown in Fig. 1 (b), where the thickness of the glass was constant and equal to 1 mm and the gap of air was increased from 0 to 1 mm in steps of 0.25 mm. In this case, the printed mesh electrode is moved towards the sample surface and there is no risk of an electrical breakdown because of the glass barrier.

As in the previous case, CER measurements were done for various voltages and distances. Some of them were selected and presented in Fig. 7(a)-(d). In Fig. 7(e), similar as in the previous arrangement, i.e., Fig. 1(a), the voltage *V* dependence of the amplitude *A* is linear, and the highest amplitudes occur when the semitransparent electrode is as close as possible to the sample surface. The dependencies plotted in Fig. 7(f) differs from the obtained for the previous case because of another arrangement in the capacitor-like system. In this case, the glass substrate determines the minimal distance at which the electrode can approach the sample - this distance in Fig. 7(f) is marked with the blue area. Since the thickness of the glass substrate is larger than the previously estimated distance range, for which the "shadow" effect is observed, the amplitude *A* to separation *D* dependencies can be approximated by single formula Eq. (1) it means the shadow effect is not observed in this range of distances between the electrode and the sample. The fitting procedure was applied to each set of experimental data and the obtained parameters were collected in tables included in Fig. 7(e) and (f).

As for the previous configuration, we can conclude that the amplitude dependence on the voltage and the distance is well described with the phenomenological formula given by Eq. (1). In this configuration the amplitude of CER signal is described by the following parameters: $\alpha = 5.4 \pm 0.3 \times 10^{-9}$ V^{-1} and $\beta = -0.51 \pm 0.04$ mm. The negative value of the β parameter is associated with the fact that the dielectric permittivity

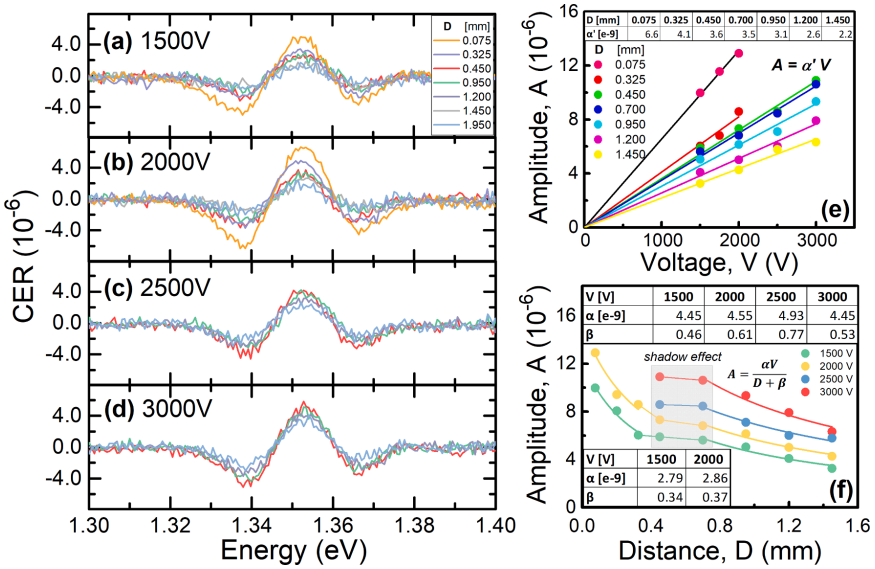

Fig. 6. (a)–(d) Room temperature contactless electroreflectance spectra of the InP sample measured with the capacitor with the printed semitransparent electrode for a few selected voltages. The arrangement of the electrode in the device is with the air gap, like in Fig. 1(a). (e) The dependence of the obtained signal amplitude versus the voltage V applied to the capacitor. (f) The dependence of the obtained signal amplitude versus the distance D between the electrode and the sample surface.

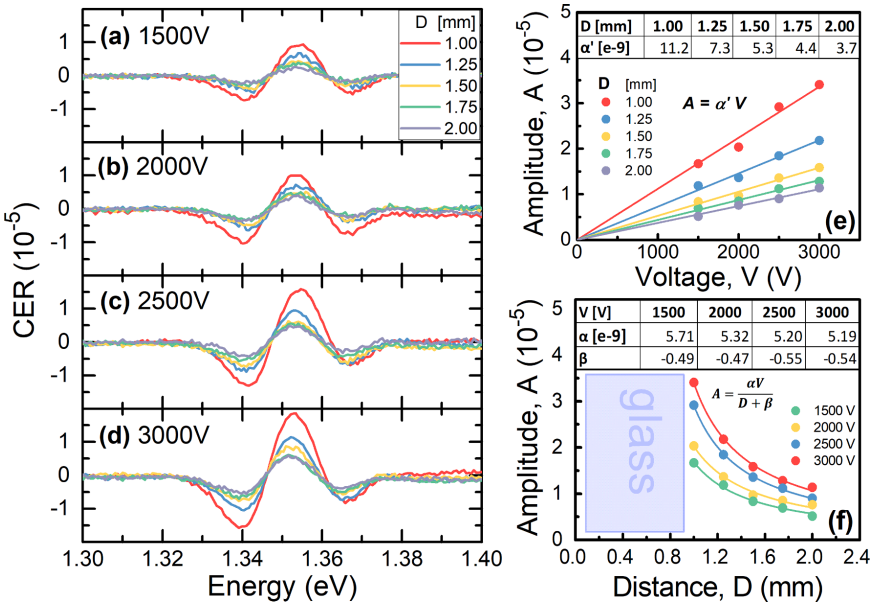

Fig. 7. (a–d) Room temperature contactless electroreflectance spectra of the InP sample measured with the capacitor with the printed semitransparent electrode for a few selected voltages. The arrangement of the electrode in the device is with air and a glass gap, like in Fig. 1(b). (e) The dependence of the obtained signal amplitude versus the voltage V applied to the capacitor. (f) The dependence of the obtained signal amplitude versus the distance D between the electrode and the sample surface.

is not included in the applied formula. In general, the proposed phenomenological formula can be improved by adding proper dielectric permittivities, but the present fit is good enough and therefore it is not necessary to introduce an extra parameter.

The results of these two configurations of semitransparent electrodes are directly compared in Fig. 8. The highest CER signal occurs for the second configuration, Fig. 1(b), where there is only glass between the printed electrode and the sample, compare solid circles with open diamonds. Therefore, it is very clear from this comparison that the increase in the dielectric permittivities of the medium between the mesh electrode and the sample surface enhances CER signal because of larger band bending modulation inside the investigated sample. Taking into account plotted series resistance for the capacitors, see Fig. 1, the stronger CER signal can be explained by the fact that the voltage drop in the medium between the sample surface and the mesh electrode is smaller for glass because of its lower resistivity. In addition, it is worth noting that the configuration with glass between the mesh electrode and the sample surface is also the most accurate and easiest to repeat because the distance is determined by the constant thickness of the glass plate. Therefore, this configuration can be considered as the most promising for further development of CER spectroscopy.

Another important issue for further development of CER spectroscopy is a reduction of external voltage needed for modulation of the electric field inside the capacitor, which leads to modulation of the built-in electric field of the investigated samples. This reduction should be from commonly used kilovolts to a few volts since it will ensure better safety for operators. Besides, it will reduce measurement costs because it allows eliminating the generator of high AC voltage. In place of this generator, a voltage signal from the Lock-in amplifier with the amplitude of a few volts can be used. In order to investigate in detail the stated above issue and check the lowest voltage for which CER spectrum can be obtained with the acceptable signal-to-noise ratio, CER measurements have been performed for the capacitor configuration, Fig. 1(b), with the air and glass gap. Fig. 9 shows room temperature CER spectra of InP sample obtained for different voltages on the capacitor. As for previous studies, it is visible that the intensity of CER varies linearly with the voltage and its lowest value, for which the optical transition is detectable in CER spectrum, equals ~100 V. This voltage is much safer for the operator than that of the order of kV. Nevertheless, the required voltage seems to be on the level of a few volts, i.e., the voltage which can be taken from the Lock-in amplifier.

In the context of studies presented in this work, it can be concluded

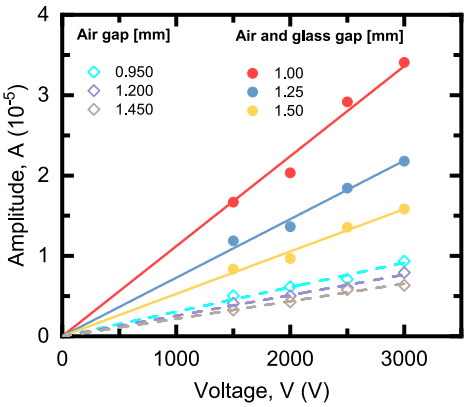

Fig. 8. Comparison of the amplitude of CER signal of InP sample measured with capacitors with the air gap (open diamonds) and with air and the glass gap (solid circles).

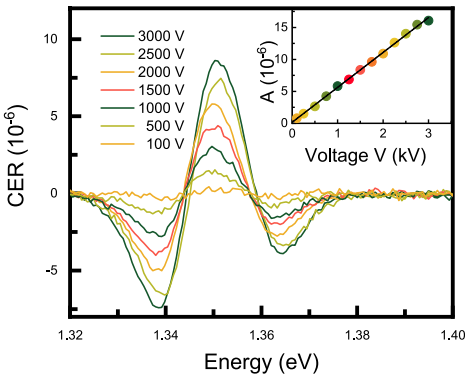

Fig. 9. Room temperature contactless electroreflectance spectra of InP sample measured with the capacitor with the air and glass gap in the function of the applied voltage in the step of 250 V. The inset shows the signal amplitude versus the applied voltage to the capacitor.

that the further reduction of voltage is possible but the thickness of dielectric spacer between the mesh electrode and the sample surface should be below ~0.4 mm, i.e., below the distance for which the "shadow" effect seems to be significant for a given architecture of silver mesh (in this case this architecture corresponds to 10 μm thick lines with the pitch equal 400 μm). However, it is not excluded that other effects (diffraction effects, etc.) can be present in this regime of distances between the mesh electrode and the sample surface; therefore, further experimental studies are necessary.

Summarizing, a reduction of glass thickness below the shadow effect regime is very perspective for the further development of capacitors for CER measurements. However, the construction of capacitors proposed in this work is a milestone in the development of CER measurements. In order to show the utility of our capacitors to measure semiconductor samples, CER experiment has been performed for van der Waals crystals since this material system is intensively studied for recent years. The application of CER spectroscopy to study van der Waals crystals is interesting because of the high sensitivity of this method to direct optical transitions and the effective elimination of unwanted background. In case of single layers of van der Waals crystals with strong photoluminescence the application of CER spectroscopy is recommended because no photoluminescence signal in contrast to photoreflectance where the unwanted photoluminescence signal can be a real problem in measurements.

Fig. 10 shows room temperature CER spectra of WSe_2, $MoSe_2$, and MoS_2 crystals obtained with the capacitor with the glass spacer between the silver mesh and the sample surface at the voltage of 3000 V. The obtained signal-to-noise ratio is very satisfactory for the detection of the optical transitions in these materials. For the three crystals, the observed CER signal is composed of two resonances. Therefore, CER spectra have been fitted by the Aspnes formula [33] containing two resonances. According to previous studies, these transitions have been attributed to the direct optical transition at the K (transition A_K) and H (transition A_H) point of the Brillouin zone [34]. The A_K transition is observed in regular reflectance/absorption measurements [35] while the A_H transition is not visible in such measurements. This transition is detected in the CER spectrum due to the differential nature of CER spectroscopy and signal elimination that may be associated with indirect optical transitions as well as the background signal. Because many van der Waals crystals, both bulk and single layers, have still not been studied by CER spectroscopy, this example shows that CER spectroscopy is very promising for further study of van der Waals crystals.

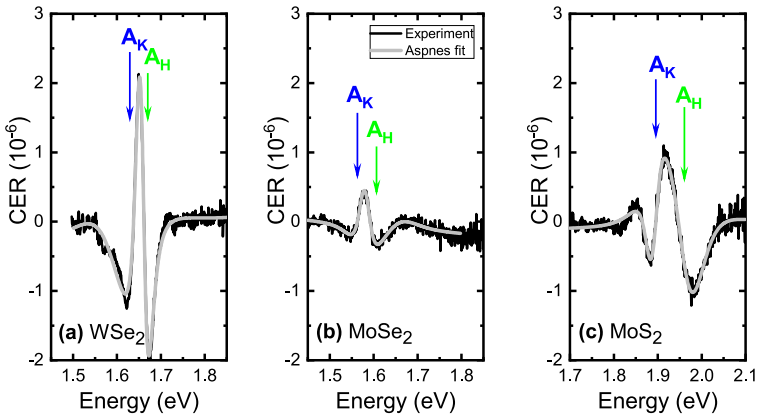

Fig. 10. Exemplary room temperature contactless electroreflectance spectra of van der Waals crystals: (a) WSe_2, (b) $MoSe_2$, and (c) MoS_2.

Regarding this family of semiconductors and the progress in their exfoliation, a very perspective seems to be CER measurements of the following material systems: graphene/h-BN/MX_2/h-BN/graphene, where the graphene layer is a semitransparent electrode, h-BN is a dielectric spacer, and MX_2 is the studied dichalcogenide (M = Mo, W, and Re; X = S, Se, and Te). In this case, the graphene/h-BN electrode or other graphene-based electrode is expected to be the solution that allows avoiding shadow effect and reducing the operating voltage to a few volts. Therefore, this approach is also a perspective for further development of capacitors for CER studies. We expect that for van der Waals layers with strong photoluminescence this approach can be very interesting because of no problems with photoluminescence signal typical for photoreflectance measurements as well as the possibility to introduce the DC voltage to such heterostructures.

4. Summary and outlook

The concept of semitransparent electrodes composed of silver paths of different architectures printed on borosilicate glass has been tested in CER measurements with two constructions of capacitors. One with the air gap between the mesh electrode and the sample surface and second with the air/glass gap. The second construction is more promising for CER spectroscopy since a stronger CER signal can be achieved with this construction due to the higher dielectric permittivity of glass. This kind of construction is also safer for samples, i.e., the electric breakdown in the capacitor can be eliminated in this construction. It has been clearly observed that CER signal is linearly proportional to the voltage applied to the capacitor and inversely proportional to the distance between the silver mesh and the sample surface. These relations can be described by a phenomenological formula, which has been derived within this study. Additionally, it has been observed that for some distances between the metal mesh and the sample surface, the intensity of the CER signal does not change according to the derived formula due to the "shadow" effect. The further development of semitransparent electrodes containing non-transparent metal mesh needs careful optimization of the architecture of metal mesh (width of lines and their densities) and the distance between the mesh electrode and the sample surface. As previously stated, this distance should be filled with a medium of high dielectric permittivity since it enhances CER signal. All these observations show directions for further development of capacitor construction for CER measurements operating at low voltages. For the present construction of capacitors, an acceptable CER spectrum, due to signal-to-noise ratio, of InP has been observed for the voltage of 100 V. It is still far from the voltage of a few volts, which is available directly from the Lock-in amplifier, but we believe that the further development of semitransparent electrodes will allow a significant reduction of this voltage. It is also worth emphasizing that the proposed construction of semitransparent electrodes is already useful for studies of semiconductor samples, including the van der Waals crystals, as shown for WSe_2, $MoSe_2$, and MoS_2.

CRediT authorship contribution statement

A.S. performed measurements, analyzed the results, and wrote the first draft of the manuscript, J. K. and F. D. prepared the experiment and contributed in measurements, A.W. and F.G. prepared the semi-transparent electrodes for CER measurements, R.K. proposed the idea and experiments, coordinated experimental work and analysis of the results. All the authors reviewed the manuscript.

Declaration of Competing Interest

The authors declare that they have no known competing financial interests or personal relationships that could have appeared to influence the work reported in this paper.

Acknowledgments

This work was supported by the National Science Centre (NCN) Poland OPUS 11 no. 2016/21/B/ST3/00482.

References

[1] O.J. Glembocki, B.V. Shanabrook, Photoreflectance spectroscopy of microstructures, in: D.G. Seiler, C.L. Littler (Eds.), Semiconductors and Semimetals, vol. 36, Academic Press, New York, 1992, pp. 221.
[2] H. Pollak, H. Shen, Modulation spectroscopy of semiconductors: Bulk/thin films, microstructures, surfaces/interfaces and devices, Mater. Sci. Eng. R 10 (1993) 275–374.
[3] F.H. Pollak, Modulation spectroscopy of semiconductors and semiconductor microstructures in: M. Balkanski (Ed.), Hand−book on Semiconductors, vol. 2, Elsevier Science B.V., Amsterdam, 1994, pp. 527.
[4] J. Misiewicz, P. Sitarek, G. Sek, R. Kudrawiec, Semiconductor heterostructures and device structures investigated by photoreflectance spectroscopy, Mater. Sci. 21 (2003) 263.
[5] J. Misiewicz, R. Kudrawiec, Contactless electroreflectance spectroscopy of optical transitions in low dimensional semiconductor structures, Opto-Electron. Rev. 20 (2012) 101.
[6] R. Kudrawiec, W. Walukiewicz, Electromodulation spectroscopy of highly mismatched alloys, J. Appl. Phys. 126 (2019) 141102.
[7] X. Yin, F.H. Pollak, Novel contactless mode of electro-reflectance, Appl. Phys. Lett. 59 (1991) 2305.

[8] L. Aigouy, T. Holden, F.H. Pollak, N.N. Ledentsov, W.M. Ustinov, P.S. Kop'ev, D. Bimberg, Contactless electroreflectance study of a vertically coupled quantum dot-based InAs/GaAs laser structure, Appl. Phys. Lett. 70 (1997) 3329.
[9] R.C. Tu, Y.K. Su, D.Y. Lin, C.F. Li, Y.S. Huang, W.H. Lan, S.L. Tu, S.J. Chang, S. C. Chou, W.C. Chou, Contactless electroreflectance study of $Zn_{0.79}Cd_{0.21}Se$/ZnSe strained double quantum wells, J. Appl. Phys. 83 (1998) 1043.
[10] S. Datta, S. Ghosh, B.M. Arora, Electroreflectance and surface photovoltage spectroscopies of semiconductor structures using an indium–tin–oxide-coated glass electrode in soft contact mode, Rev. Sci. Instr. 72 (2001) 177.
[11] C.H. Chang, D.P. Wang, C.C. Wu, C.L. Hsiao, L.W. Tu, Contactless electroreflectance and photoreflectance studies of *n*- and *p*-type doped GaN with Ga and N face, Appl. Phys. Lett. 87 (2005) 202103.
[12] L. Bhusal, A.J. Ptak, R. France, A. Mascarenhas, Contactless electroreflectance studies of ultra-dilute $GaAs_{1-x}Bi_x$ alloys, Semicond. Sci. Technol. 24 (2009) 035018.
[13] J. De Jesus, T.A. Garcia, S. Dhomkar, A. Ravikumar, C. Gmachl, G. Chen, A. Shen, D. Ferizovic, M. Muñoz, M.C. Tamargo, Characterization of the three-well active region of a quantum cascade laser using contactless electroreflectance, J. Vac. Sci. Technol. B 31 (2013) 03C134.
[14] D.E. Aspnes, Band nonparabolicities, broadening, and internal field distributions: The spectroscopy of Franz–Keldysh oscillations, Phys. Rev. B 10 (1974) 4228.
[15] H. Shen, F.H. Pollak, Generalized Franz–Keldysh theory of electromodulation, Phys. Rev. B 42 (1990) 7097.
[16] H. Shen, M. Dutta, Franz-Keldysh oscillations in modulation spectroscopy, J. Appl. Phys. 78 (1995) 2151.
[17] C. Van Hoof, K. Deneffe, J. De Boeck, D.J. Arent, G. Borghs, Franz-Keldysh oscillations originating from a well-controlled electric field in the GaAs depletion region, Appl. Phys. Lett. 54 (1989) 608.
[18] R. Kudrawiec, H.P. Nair, M. Latkowska, J. Misiewicz, S.R. Bank, W. Walukiewicz, Contactless electroreflectance study of the Fermi level pinning on GaSb surface in *n*-type and *p*-type GaSb Van Hoof structures, J. Appl. Phys. 112 (2012) 123513.
[19] A. Tolloczko, J. Kopaczek, R. Szukiewicz, A. Gocalińska, E. Pelucchi, D. Hommel, R. Kudrawiec, Contactless electroreflectance study of the surface potential barrier in n-type and p-type InAlAs van Hoof structures lattice matched to InP, J. Phys. D: Appl. Phys. 51 (2018) 215104.
[20] R. Kudrawiec, L. Janicki, M. Gladysiewicz, J. Misiewicz, G. Cywinski, M. Boćkowski, G. Muzioł, C. Chèze, M. Sawicka, C. Skierbiszewski, Contactless electroreflectance studies of surface potential barrier for N- and Ga-face epilayers grown by molecular beam epitaxy, Appl. Phys. Lett. 103 (2013).
[21] Ł. Janicki, M. Gładysiewicz, J. Misiewicz, K. Klosek, M. Sobanska, P. Kempisty, Z. R. Zytkiewicz, R. Kudrawiec, Contactless electroreflectance studies of the Fermi level position at the air/GaN interface: Bistable nature of the Ga-polar surface, Appl. Surf. Sci. 396 (2017) 1657.
[22] S.R. Kurtz, A.A. Allerman, D.D. Koleske, G.M. Peake, Electroreflectance of the AlGaN/GaN heterostructure and two-dimensional electron gas, Appl. Phys. Lett. 80 (2002) 4549.
[23] A.T. Winzer, R. Goldhahn, G. Gobsch, A. Dadgar, A. Krost, O. Weidemann, M. Stutzmann, M. Eickhoff, Electroreflectance spectroscopy of Pt/AlGaN/GaN heterostructures exposed to gaseous hydrogen, Appl. Phys. Lett. 88 (2006) 024101.
[24] D.P. Wang, C.C. Chen, T.L. Shen, T.M. Hsu, W.C. Lee, Pumping-beam-induced photovoltaic effect on the photoreflectance of a δ-doped GaAs film, J. Appl. Phys. 80 (1996) 6980.
[25] D.F. de Sousa, M.J.V. Bell, L.A.O. Nunes, Photoreflectance and time-resolved photoreflectance in delta-doped superlattices, J. Appl. Phys. 83 (1998) 2806.
[26] D.P. Wang, K.R. Wang, K.F. Huang, T.C. Huang, A.K. Chu, Determination of built-in field by applying fast Fourier transform to the photoreflectance of surface-intrinsic –type doped GaAs, Appl. Phys. Lett. 74 (1999) 475.
[27] H. Takeuchi, Y. Kamo, Y. Yamamoto, T. Oku, M. Totsuka, M. Nakayama, Photovoltaic effects on Franz-Keldysh oscillations in photoreflectance spectra: Application to determination of surface Fermi level and surface recombination velocity in undoped -type GaAs epitaxial layer structures, J. Appl. Phys. 97 (2005) 063708.
[28] R. Kudrawiec, M. Syperek, M. Motyka, J. Misiewicz, R. Paszkiewicz, B. Paszkiewicz, M. Tlaczała, Contactless electromodulation spectroscopy of AlGaN/GaN heterostructures with a two-dimensional electron gas: A comparison of photoreflectance and contactless electroreflectance, J. Appl. Phys. 100 (2006) 013501.
[29] Z.Y. Fan, J.C. Ho, T. Takahashi, R. Yerushalmi, K. Takei, A.C. Ford, Y.L. Chueh, A. Javey, Toward the development of printable nanowire electronics and sensors, Adv. Mat. 21 (2009) 3730.
[30] D.J. Finn, M. Lotya, J.N. Coleman, Inkjet printing of silver nanowire networks, ACS Appl. Mat. & Interf. 17 (2015) 9254.
[31] Z. Gumienny, J. Misiewicz, Measuring setup with a GDM-1000 monochromator to measure the anisotropy of optical properties of Zn_3P_2, Opt. Appl. 12 (1982) 37.
[32] A. Wiatrowska, P. Kowalczewski, M. Dusza, M. Zięba, K. Fiączyk, P. Cichoń, K. Fijak, F. Granek, XTPL approach to print conductive structures in microscale for next-generation displays, in: SID Symposium Digest of Technical Papers, vol. 50, 2019, pp. 773–774. doi:10.1002/sdtp.13035.
[33] D.E. Aspnes, Third-derivative modulation spectroscopy with low-field electroreflectance, Surf. Sci. 37 (1973) 418.
[34] J. Kopaczek, M.P. Polak, P. Scharoch, K. Wu, B. Chen, S. Tongay, R. Kudrawiec, Direct optical transitions at K- and H-point of Brillouin zone in bulk MoS_2, $MoSe_2$, WS_2, and WSe_2, J. Appl. Phys. 119 (2016) 235705.
[35] Y. Li, A. Chernikov, X. Zhang, A. Rigosi, H.M. Hill, A.M. van der Zande, D. A. Chenet, E.-M. Shih, J. Hone, T.F. Heinz, Measurement of the optical dielectric function of monolayer transition-metal dichalcogenides: MoS_2, $MoSe_2$, WS_2, and WSe_2, Phys. Rev. B 90 (2014) 205422.

4.2.2 Publikacja D2

Druga praca opisuje wieloetapową metodę wytwarzania przeźroczystych elektrod techniką wykorzystującą ablację laserową na warstwie polimerowej. Szczególny nacisk położono na eliminację niebezpiecznych substancji chemicznych z poszczególnych etapów procesu ostatecznie pozwalając na przeprowadzenie procesu w warunkach wodnych. Praca zawiera również opis badań przeprowadzonych w ramach optymalizacji mocy wiązki laserowej poprzez dobór odpowiednich uczulaczy dodawanych do warstwy strukturyzowanej. Wyznaczone są najkorzystniejsze parametry metody do otrzymywania przeźroczystych elektrod, a ich funkcjonalność jest zaprezentowana w pomiarze kryształu van der Waalsa, dwusiarczku molibdenu (MoS_2) dwiema technikami pomiarowymi: bezkontaktowego electroodbicia (CER) i termoodbicia (TR). W tej ostatniej przeźroczysta elektroda pełni funkcję przeźroczystej grzałki co jest dodatkowym wynikiem przeprowadzonych badań. Na końcu pracy przedstawiono również możliwości techniki „laser lift-off" wybiegające poza wytwarzanie przeźroczystych elektrod. Jako przykład przedstawiono srebrne logo Politechniki Wrocławskiej ukazując możliwości skalowania dowolnych kształtów.

ACS Sustainable Chemistry & Engineering

pubs.acs.org/journal/ascecg

Research Article

Transparent Metal Mesh Electrodes Microfabricated by Structuring Water-Soluble Polymer Resist via Laser Ablation

Anna M. Ślusarz,* Katarzyna Komorowska, Tomasz Baraniecki, Szymon J. Zelewski, and Robert Kudrawiec*

Cite This: *ACS Sustainable Chem. Eng.* 2022, 10, 8196–8205

Read Online

ACCESS | Metrics & More | Article Recommendations

ABSTRACT: We present a method of manufacturing semitransparent mesh-shaped electrodes using laser structuring of a polymer followed by resistive thermal evaporation of a metallic layer. Toluene, used for preparing a polymer solution and its layer deposition, has been replaced with ethanol, thus eliminating a hazardous solvent from the process. The influence of adding photosensitizers to the polymer base on the structuring laser ablation threshold has been investigated, with most prominent reduction from 1.3 to ∼0.3 W for a UV laser line irradiation. Finally, and most importantly, the key step of this method, the development step that includes the removal of a resist, was carried out in water, thus ruling out completely other environmentally hazardous solvents from the process. Additionally, it does not require cleanroom conditions. The final electrode prototype was tested in electro- and thermomodulation measurements, proving its usefulness in spatial control of electric field and heat generation. Consequently, our work paves the way for other applications requiring patterned semitransparent electrodes made in a sustainable process.

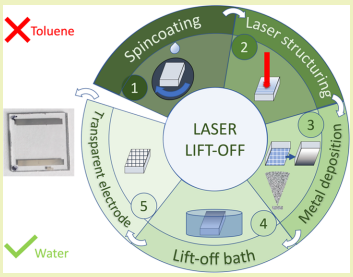

KEYWORDS: *mask-less lithography, water lift-off, microstructuring, picosecond laser, ethyl cellulose, poly(vinylpyrrolidone), contactless electroreflectance, thermoreflectance*

INTRODUCTION

Nowadays, transparent electrodes (TEs) are crucial mainly in optoelectronic applications, but additionally they provide the basis for material and biological fundamental research. In daily applications, TEs can be found in displays, solar panels, smart windows, or windscreen heaters.[1−5] Apart from conducting electricity, those electrodes transmit light and can induce elevated temperature conditions through Joule heating, so as a result TEs vary in terms of their transparency in the visible range, electrical resistivity, and specific heat as benchmark parameters. As those parameters are interrelated, they must be balanced depending on the target application.[6]

Two types of TEs can be distinguished: continuous conductive coatings and spaced narrow-shaped paths (e.g., mesh-shaped).[7] In the first case, the most common materials used as the thin conducting layers are transparent metal oxides, with indium tin oxide (ITO)[8] being an industrial standard despite the high cost of indium. Graphene,[9,10] owing to established methods for large-scale manufacturing of atomically thin sheets, also receives great attention, additionally not exhibiting diminished transparency in the infrared range, typical for high-carrier-concentration oxides.[11,12] Second type of TEs, the patterned mesh structure, is made of highly conductive metals such as gold, silver, or copper. Among many manufacturing methods of such semitransparent electrodes, there are two main groups: top−down and bottom−up techniques (e.g., inkjet printing).[13,14] The first approach covers a wide range of lithographic methods like optical lithography, laser lithography, direct laser sintering, 3D laser writing, electron or ion beam lithography (EBL/IBL), nanoimprinting lithography, and others.[15−21] The demand for new methods and new materials for nano- and microstructuring has increased due to a wide variety of new applications and, what is even more noticeable in recent years, focuses on designing processes that minimize the use and generation of hazardous substances. More interest in environmentally friendly alternatives to conventional resins for all kinds of lithography can result in more ecological methods. Novel solutions must meet certain conditions, which are highly dependent on the application, while simultaneously finding a compromise between price and quality. This research area is evolving toward materials that facilitate custom-tailored fast and cheap techniques not requiring cleanroom conditions,

Received: March 29, 2022
Revised: May 24, 2022
Published: June 16, 2022

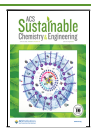

https://doi.org/10.1021/acssuschemeng.2c01835
ACS Sustainable Chem. Eng. 2022, 10, 8196–8205

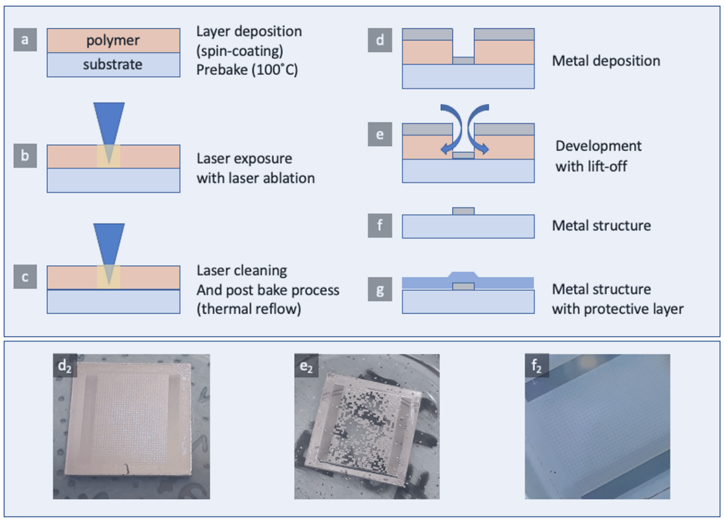

Figure 1. Schematic presentation and pictures of chosen steps of polymer resist laser ablation and the lift-off process for manufacturing metal structures with a protective coating. (a) Spin-coated polymer layer onto the substrate and pre-baking process. (b) Hardened layer exposure to the laser beam (laser ablation). (c) Cleaning paths from the polymer debris by passing the beam along the same pattern several (2−5) times. The post-baking process with thermal reflow as an optional method for smoothing path edges. (d) Deposition of the metal layer onto the structured polymer mask. (e) Dissolution of the polymer mask with the lift-off of the metal layer. (f) Final result of the transparent electrode made of the metal mesh structure. (g) Securing the structure with a protective layer.

contrary to standard resists and solvents consisting of hazardous and harmful ingredients and, for instance, which may cause skin irritation, damage to the respiratory tract, and be harmful to aquatic organisms when improperly disposed of.

In this work, we present a method for manufacturing a metal grid semitransparent electrode by applying a mask-less technique based on an identical resist as a reference in photolithography. We adapt the existing method of structurization[22,23] and materials to an efficient, fast, microsize-resolution, and water-based process. A TE is obtained with the technique of selective polymer layer structuring by laser ablation, which goes hand-in-hand with the increasing availability of industrial-grade lasers. Laser ablation is the process of removal of materials from a solid surface by laser beam irradiation.[24] The polymer layer, which in this method is used as a sacrificial layer, absorbs the laser energy and as a result heats up and evaporates. This process is best carried out with a pulsed laser and ultrashort laser pulses due to the minimal interaction of light with the material.

In a similar way, Yeo et al. used a laser structuring technique for sintering nanoparticle ink without the use of a mask.[21] However, toxic chemicals are used in the preparation of the nanoparticle ink in this method. In our work, we concentrated on substitution of the environmentally hazardous sacrificial layer material with an ecological polymer layer. Also, organic solvents originally used in the developing process (dissolution of photoresist) were replaced by water, which is easily accessible and handled, inexpensive, nontoxic, and can be simply disposed of. A similar attempt of reducing risk was previously made in the case of nanoimprinting lithography[25] and electron beam lithography,[26] which shows that environmentally friendly techniques of fabricating TEs are still in demand. We focused on optimization of transparent mesh electrode fabrication with laser ablation microstructuring. The emphasis of our research was put on the selection of a water-soluble base material, the appropriate sensitizer depending on the used ablation, and on the writing scheme using two laser lines of different wavelengths in one fabrication system. The requirement for the development step was to perform it in water or ethanol instead of a harmful developer.

The application of manufactured electrodes is demonstrated in two representative modulation spectroscopy experiments, commonly utilized in state-of-the-art electronic band structure materials characterization.[27−29] Their requirements of local periodic perturbation of electric field in contactless electroreflectance (CER)[30,31] or temperature elevation in thermoreflectance (TR)[32−37] while maximizing the light transmission for optical access make a perfect test field for TEs. Analyses of modulated reflectance spectra of a reference semiconductor crystal demonstrate the usefulness of TE in vastly different conditions requiring simultaneous electronic conductivity and optical transparency.

RESULTS AND DISCUSSION

Procedure for Laser Lift-Off Microstructure Manufacturing. Manufacturing of a transparent electrode using the laser lift-off method consists of several stages shown in Figure 1a−g.

Substrate Material Selection. Since the obtained electrode is expected to be transparent, the base substrate itself must exhibit high light transmission across the desired spectrum, which in this case includes visible and near-infrared ranges. Three optical-grade materials were tested: soda-lime glass, quartz, and sapphire. At first, the endurance of each material to

https://doi.org/10.1021/acssuschemeng.2c01835
ACS Sustainable Chem. Eng. 2022, 10, 8196−8205

intense laser illumination has been tested to determine the upper limit for average laser beam power available for polymer structuring. The laser ablation threshold of substrate damage at 1064 nm was similar for all substrates around 15.2 W. Upon illumination with the 355 nm line, quartz and sapphire remained intact even at the highest available power of 2.3 W, while the glass substrate was modified at 1.38 W. Such effect can be attributed to different ablation rates, which vary with the material parameters, predominantly optical absorption (including impurities), thermal transport, and lattice structure.[38−40] The quartz substrate was chosen because it showed good durability while maintaining an affordable price. It was prepared for the process by cleaning in solvents: acetone, isopropanol, and deionized water with an ultrasonic washer for 10 min in each solvent. Next, it was rinsed with water and dried with nitrogen. Also, air plasma was used for a thorough cleaning, which is optional.

Polymer Layer Deposition. Two ecological standard polymers were tested: ethyl cellulose (EC), which is a nontoxic, biocompatible, tasteless, and colorless substance,[41] and poly(vinylpyrrolidone) (PVP), which is a water-soluble, light, and hygroscopic powder polymer used in the cosmetic industry with a good film formation property.[42] The polymer layer, with reduced environmental impact compared to a typical photoresist, was spin-coated onto the prepared surface. The specimen was baked on a hot plate: for EC at 110 or 80 °C and for PVP at 100 or 80 °C due to the evaporation temperature of solvents; the sample was then left to cool down to room temperature.

Irradiation. Then, the heat-cured polymer layer was subjected to laser irradiation. After the selection of a proper laser power (adequately for substrate type and the polymer material), the sacrificial layer was irradiated by scanning the laser beam to form the designed pattern.

Path Laser Cleaning. Due to dust formation after the first laser irradiation, cleaning the paths was necessary, which was performed in a simple way by directing the beam along the same pattern several (2−5) times. Also, the sample surface was blown with nitrogen from any remaining polymer debris created during the ablation.

Edge Smoothing−Thermal Reflow. An optional step was performed for some of the polymer samples. The structured polymer layer was heated once again at a strictly defined temperature close to the softening point to smooth the edges by melting the polymer.

Metal Deposition. A metallic material with an adhesive layer was deposited on the prepared disposable polymer mask (Figure 1d_2). The materials used were alternatively gold, silver, aluminum, and copper. Titanium was optionally deposited as the initial, 10 nm adhesive layer. The thickness of the metal layer was controlled by deposition time and adjusted to meet a target. The target thickness ranged from 170 to 840 nm. It was selected so that the material was as continuous as possible over the entire surface but bearing in mind that the layer must lift off and detach after dissolving the polymer underneath it.

Lift-off. The sample with the polymer and metal layers prepared as described was put in a Petri dish with proper solvent matched to the polymer: ethanol (for EC and PVP) and water (for PVP). The dissolution of the sacrificial layer induced lifting-off and then complete detachment of the deposited metal part in polymer regions, which were not irradiated by the laser (Figure 1e_2). The sample was washed with a solvent (EtOH or H_2O) a few times until every redundant metal element was debonded from the substrate. The obtained structure was flushed once more with a suitable solvent, then with water, and, in the end, it was dried with nitrogen (Figure 1f_2).

Electrode Protection/Encapsulation. A protective layer was deposited on the final TE to prevent its uncontrolled degradation and mechanical damage. Two encapsulation methods were used: PMMA spin coating with post-baking and SiO_2 sputtering, which is better than PMMA in terms of protection against oxidation during heating of the electrodes.

Procedure for Obtaining Solution and Thin Layer of the Resist Polymer. The sacrificial layer, used as a disposable mask, was prepared from the EC or PVP polymer in a powder form. First, dissolution methods of polymers were tested, and then, various concentrations were examined. In the case of EC, a few hours of magnetic stirring at room temperature were required. The mixture of ethanol and toluene was used as a solvent. This solution was stable, clear, and slightly yellow. To obtain the target sacrificial layer thickness of 2−3 μm, several concentrations were prepared to find the optimum. Such thickness is optimal, as a thinner layer would make it difficult to detach the metal as the polymer dissolves during lift-off. The step between the substrate and the resist top surface must be high enough to allow the solvent to penetrate under the metal layer but not too high that it generates too much dust during laser structuring. In addition, excess layer thickness might worsen the method resolution (the smallest possible pattern size) by hampering access to the substrate when depositing the metallic layer. To eliminate toluene (which is typically used to dissolve EC[43]), a hazardous element of the solvent mixture, identical solutions of EC were prepared using only ethanol.

The EC in ethanol solution with a mass concentration equal to 0.071 g/mL was chosen for further examination (marked with a circle in Figure 2). However, all concentrations below

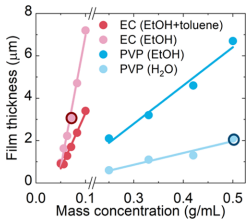

Figure 2. Obtained spin-coated polymer film thickness dependence on mass concentrations of polymer solutions: ethyl cellulose (EC) and poly(vinylpyrrolidone) (PVP) in organic solvents and water.

this value gave continuous layers of the polymer and can also be used in the described procedure. Then, the step of thin-film preparation was repeated.

The second polymer, PVP, was dissolved in ethanol and independently in water. This solution was mixed using a vortex. Again, a few different concentrations were tested. Thin films of the polymer were obtained using the same method as before, with identical spin coater parameters. Only hot plate temperatures were changed because of the different evaporation temperatures of solvents. All samples gave uniform, continuous polymer layers. The PVP solution in water with a mass concentration of 0.5 g/mL was used in the subsequent examination.

https://doi.org/10.1021/acssuschemeng.2c01835
ACS Sustainable Chem. Eng. 2022, 10, 8196−8205

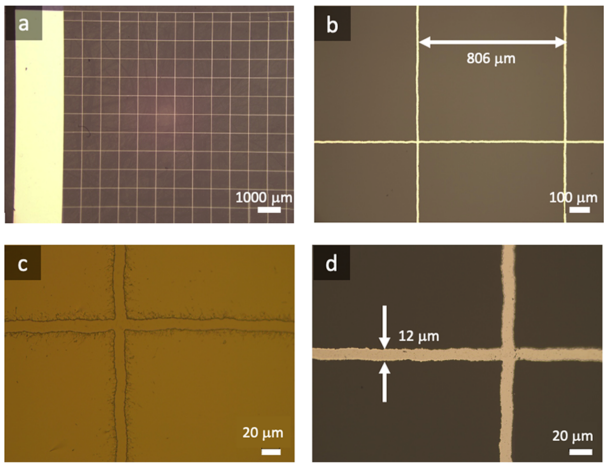

Figure 3. Optical microscope images of the transparent metal mesh electrode on a quartz substrate with a pitch of 800 μm, path width of 12 μm, and thickness of 200 nm, taken at magnifications (a) 40×, (b) 500×, and (d) 2000×. (c) Laser-structured EC layer. (d) Silver pattern is consistent with the one structured by the laser.

Optimization of the Laser Irradiation Process. After preparing the polymer layer, the sample was irradiated to form the designed structure. The mesh pattern used as a transparent electrode template is shown in Figure 3.

Edge Smoothing. Before the metal layer deposition, the path edge was smoothed by thermal reflow of the polymer in a heating stage microscope. A sample with a structured polymer layer was heated gradually (10 °C/min) to the softening point of the polymer and held at this temperature for 10 min (Figure 4). As a result, the polymer edges were more uniform, represented by a narrower path width distribution (Figure 4c).

A number of studies have been carried out to optimize the step of laser exposure (Figure 1b). The optimization comprises reducing the laser power required to structure the polymer layer to make the whole process more economically viable and sustainable. We tested the influence of adding absorbing substances (sensitizers) on ablation efficiency. The two most important benchmark parameters to be met were the compatibility of the absorption band with the structuring laser beam wavelength and the preserved ability to form a homogeneous layer after mixing with the polymer (Figure 5).

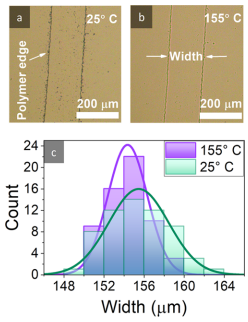

Figure 4. Thermal reflow of the EC polymer on a ∼155 μm width representatively structured area. Optical microscope images of the structured layer at temperatures of (a) 25 °C and (b) 155 °C. (c) Histogram representing width distribution of the structured area based on 60 measurements.

Ethyl Cellulose. In the case of EC, the purpurin dye (1,2,4-trihydroxy-9,10-anthracenedione) was used due to its good solubility in ethanol and absorption spectrum (Figure 5a) compatible with the laser beam wavelength in the UV range (355 nm). The additive was mixed with the EC polymer solution using a vortex for 10 min, yielding a concentration of 0.5% w/v. The polymer layer with an absorber was prepared using spin coating and then cured on a hot plate. The sample was irradiated with increasing laser power, and, after crossing a threshold, some parts of the polymer were removed. Results of the performed studies are shown in Figure 6 with a graph illustrating path width as a function of the used laser power. For power values below the threshold, there was no interaction between the laser beam and the polymer; however, after crossing the ablation threshold, the polymer was completely removed and the path widened upon increasing the laser power.

Figure 6c shows that the addition of a dye allowed a reduction of the ablation threshold for UV laser structuring from 1.14 down to 0.78 W (32% decrease). Sensitizing the layer to absorption of the laser beam wavelength also contributed to the narrowing of the obtained path. The path width power dependence can be approximated by an asymptotic curve, which converges to different values: 18.9 and 19.3 μm for the layers with and without the additive, respectively.

Poly(vinylpyrrolidone). During irradiation of the PVP layer with a laser, an issue of edge quality occurred; due to laser ablation, some microexplosions on line edges appeared (Figure 7a). An appropriate additive was searched to improve the structuring process, i.e., to control condition of the edge and reduce the laser power, so the polymer layer removal would

https://doi.org/10.1021/acssuschemeng.2c01835
ACS Sustainable Chem. Eng. 2022, 10, 8196−8205

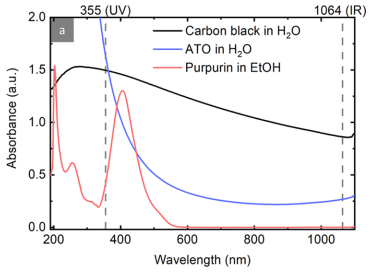

b

Polymer	EC	PVP	
Additive	Purpurin	Carbon black	ATO
Solvent	EtOH	Dispersion in H_2O	H_2O
Laser beam	UV	UV	UV and IR

c Ablation threshold for UV laser beam

Polymer	EC	PVP	
	1.14 W	1.3 W	
With additive	Purpurin	Carbon black	ATO
	0.78 W	0.3 W	0.27 W

Figure 5. (a) Absorption spectrum of carbon black, antimony tin oxide (ATO), and 1,2,4-Trihydroxy-9,10-anthracenedione (purpurin). (b) Matching sensitizers for ethyl cellulose (EC) and poly-(vinylpyrrolidone) (PVP) polymers consider their solubility (of both the polymer and the additive) and the absorption peak. (c) Laser ablation thresholds for tested polymers and additives.

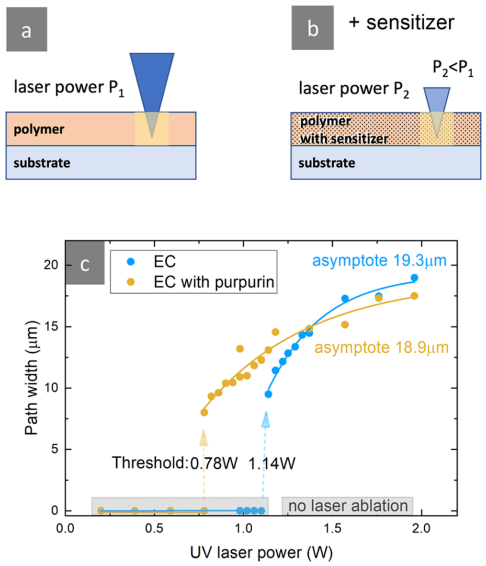

Figure 6. Scheme of laser structuring for the layer (a) without the sensitizer and (b) with the sensitizer; reduction of the laser power (P) after adding a sensitizing substance to the polymer layer. The graph (c) shows the dependence of the path width as a function of the UV laser power for both samples.

not occur so rapidly. The addition of carbon black as an absorber to the polymer solution was used. PVP requires solubility in ethanol or water, so the sensitizing substance was carefully mixed in a polymer solution using an ultrasonic homogenizer.

The obtained polymer layer with a photosensitizer after laser irradiation dissipates heat evenly over the entire surface and results in a homogeneous edge of the structured path (Figure 7b). To clean the inner part of the path from the dust, the sample was irradiated several (2−5) times according to the same pattern (Figure 7c).

The addition of the absorber also led to a significant reduction of the material structuring threshold power from 1.3 W for a sample with a pure polymer to 0.3 W for a layer with the carbon black for the laser beam at 355 nm (about 77% decrease) (Figure 7d).

For comparison, structuring of pure PVP with the near-infrared laser line (1064 nm) turned out to be impossible, with the polymer layer remaining unaffected when the laser power reached the quartz substrate damage threshold. For that reason, another sensitizer was needed, with significant absorption in the IR range. Antimony tin oxide (ATO) was selected for these studies because it is a commonly known and commercially available IR absorber, alongside indium tin oxide.[44] ATO was chosen to be mixed with PVP also because of its solubility in water. An appropriate mass of the substance was mixed using a vortex with PVP solution. Polymer layers were spin-coated and baked, following the previously described procedure. Results of PVP with ATO after laser structuring are presented in Figure 8a and compared with that of the commercially available photoresist AR-P3250.

The measurements were performed for PVP with a concentration of ATO 0.5, 1, and 2.5%. The results for PVP with a concentration of ATO 1 and 2.5% w/v are comparable and give similar path widths. However, the narrowest path was obtained on the PVP polymer layer with a 0.5% additive. This experiment was repeated for confirmation of the results (Figure 8b). The obtained two red curves, with a full circle sign for primary structuring and an open circle sign for repeated structuring, both corresponding to 0.5% w/v concentration, are overlapping, which proves the repeatability of the process.

In Figure 8d, it is presented that structurization of pure PVP with the IR laser beam is impossible. However, for PVP with the ATO additive, selective removal of the layer is possible and the process is replicable. This kind of the layer polymer sensitized for the IR range was also subjected to the experiment under UV irradiation (Figure 8c). Pure PVP was presented for reference, as the UV laser beam does not damage the quartz substrate. The resolution (inversely proportional to the line width) of the polymer resist with the additive is higher; this additive enables structuring at both laser beams: UV (355 nm) with minimal path widths of 9 μm and 12 μm for IR (1064 nm). Moreover, in comparison to the commercial resist,

https://doi.org/10.1021/acssuschemeng.2c01835
ACS Sustainable Chem. Eng. 2022, 10, 8196−8205

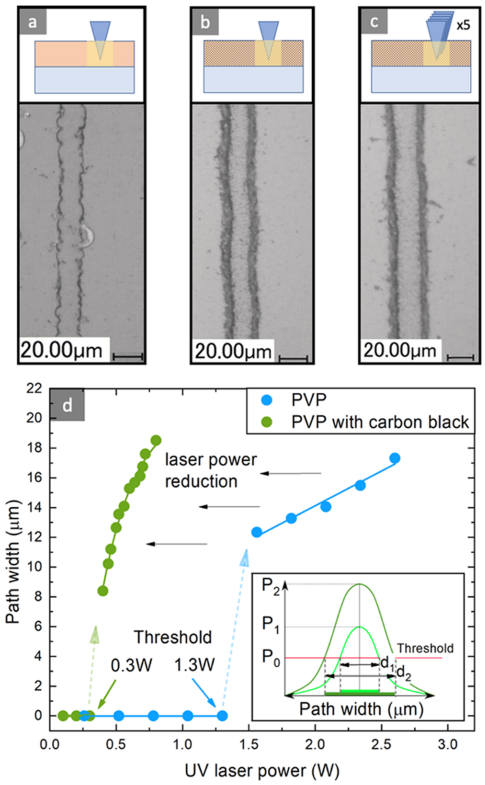

Figure 7. Laser-irradiated PVP layers prepared: (a) without any additive microexplosions are visible along the edge and (b) with additive carbon black. (c) Removal of post-process residues by repeated laser irradiation along the path (cleaning procedure). (d) Path width dependence on the UV laser power for the PVP polymer of concentration 0.5 g/mL before and after addition of carbon black (0.14% w/v) in a layer. The inset presents laser beam distribution and consistently the width (d) of the obtained path for chosen power (P).

PVP with the absorber shows better resolution and laser ablation threshold reduction.

The table in Figure 5c summarizes the results for the structuring of both EC and PVP polymers with additives, directly comparing ablation threshold values for the UV beam, i.e., the minimum laser power required to structure environmentally friendly resists. As a result, both polymers were successfully structured, resulting in a path that was thinner than that of the commercial photoresist, and proper conditions for efficient structuring of both environmentally friendly polymers were found. For the three tested photosensitizers, the laser ablation threshold was shifted to lower power values.

APPLICATIONS

The manufactured electrodes were tested in modulation spectroscopy measurements, broadly used in experimental band structure investigations of solids. The energy of optical transitions in a structure is determined by analyzing resonance-like features in reflectance or transmission spectra upon applied periodic perturbation. Two representative techniques, CER[30,31] and TR,[33] rely on vastly different modulation mechanisms: the former relies on built-in electric field perturbation in a capacitor-like arrangement and the latter on thermal expansion of the studied material caused by periodic heating. For both of them, the electrode was placed in custom-designed holders and dedicated setups.

For CER, electric field modulation is provided by applying a voltage of 2 kV alternating at a frequency of 280 Hz between the sample and the electrode (Figure 9a). Because of the very fine mesh on the electrode surface, the generated field is homogeneous, which allowed to generate a uniform electric field to modulate periodically the sample built-in electric field. Simultaneously, the electrode remains transparent to monochromatic probing light (transmittance of 85%, as shown in Figure 10a). The experimental setup used for CER uses a lock-in synchronous demodulation with the triggering of the high voltage generator, with spectral dependence of relative reflectivity changes ($\Delta R/R$) providing information on optical transitions in the studied material. The spectra are composed of one or more characteristic resonances resembling the third derivative of the dielectric function and occurring at singularities in joint density of states. As a consequence, CER (along with other modulation spectroscopy methods) provides accurate characterization of optical transitions, including their energy and broadening, which is often used for studying fundamental properties or evaluating the quality of semiconductors. CER spectra of bulk MoS_2, a semiconducting van der Waals crystal used as a reference material, reveal resonances $E_A = 1.843 \pm 0.001$ eV and $E_B = 1.911 \pm 0.002$ eV, at the expected band-edge excitonic transitions[45−47] (Figure 10c). The results are reproducible for two electrodes made of different metals, silver and copper, with an identical resonance shape and magnitude. The electrodes were prepared using the same pattern with a pitch of 400 μm, which was previously determined as the best compromise between electrode transparency and electrical conductivity.[7]

The second measurement technique (i.e., TR) allows to test TE from a different angle to check its application possibilities as heaters. In this technique, the sample is placed directly on an electrode, which is connected to a power source. By passing periodically modulated electric current pulses through the TE acting as a resistive metallic layer, the energy is lost as heat (Joule heating) and causes indirect thermomodulation of the reference MoS_2 crystal (Figures 9b and 10b). TR measurements are performed in two configurations, namely, the reflection and the transmission modes, with the latter feasible only with electrodes that are transparent and allow for broadband optical measurements across the spectral range of interest. In the first configuration, the sample is placed in front of the electrode and the light beam directly illuminates the sample surface, thus the TE only functions as a heater. In the second configuration, the electrode with the sample is reversed, so that the probing light beam is transmitted through the transparent electrode onto the sample and reflected back to the detection system. In this case, the electrode has a new, combined functionality: a transparent heater.

The results of the measurement in both TR configurations of the reference MoS_2 crystal are presented in Figure 10d,e. From fitting the spectra according to the Aspnes formula,[47] we conclude that both methods give correct information about the semiconductor band structure of MoS_2. When compared to the

https://doi.org/10.1021/acssuschemeng.2c01835
ACS Sustainable Chem. Eng. 2022, 10, 8196−8205

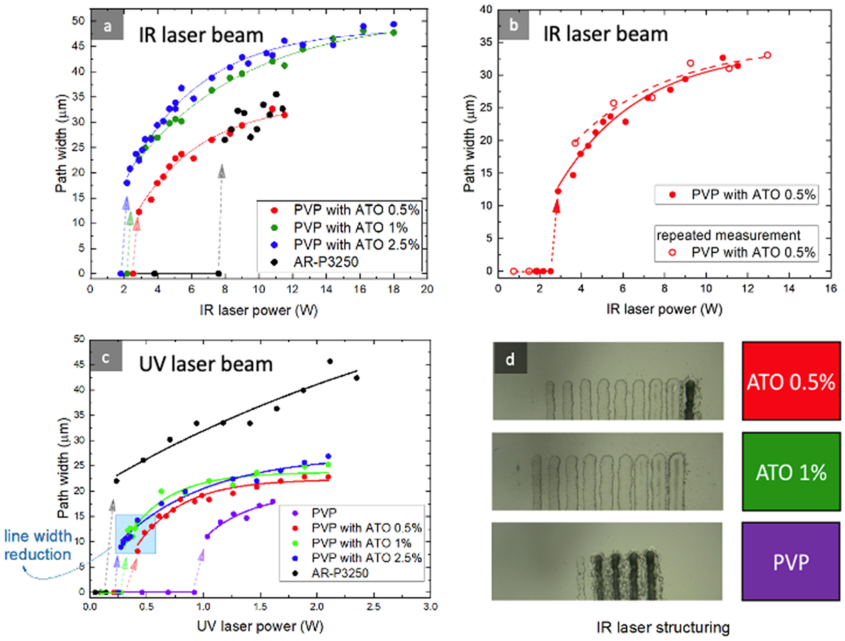

Figure 8. Obtained path width dependence on (a) IR laser power for PVP water solution of concentration 0.5 g/mL with a concentration of infrared absorber ATO 0.5−2.5% w/v; for comparison, results obtained with a commercial photoresist AR-P3250 are presented, revealing 4 times higher IR laser power required for material structuring, (b) IR laser power for PVP with a concentration of infrared absorber ATO 0.5% w/v (repeated measurement), (c) UV laser power for pure PVP and with a concentration of infrared absorber ATO 0.5−2.5% w/v; for comparison, results obtained with a commercial photoresist AR-P3250 are presented. (d) IR laser-structured polymer layers for ATO 0.5%, 1%, and pure polymer.

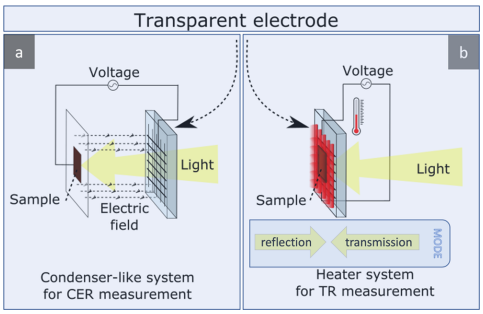

Figure 9. Experimental arrangement of TE holders for two modulation spectroscopy techniques: (a) contactless electroreflectance (CER) and (b) thermoreflectance (TR).

resonance obtained from CER, slight transition energy shifts were noticed for the reflection mode TR, and more significant in the transmission mode, which results from additional static temperature elevation of the sample in TR measurements.

This topic offers prospects for further explorations in this research area. TE made using the elucidated procedure can be implemented in such materials characterization methods where the key role is played by overall high or controlled (by mesh pitch) light transmission of the electrode and uniformity of the electric field or heat distribution. Also, the developed TE can be used repeatedly since no deterioration was observed after multiple experiments in either transparency or total electrode resistance.

CONCLUSIONS

We developed a green technology for manufacturing transparent electrodes (TEs), based on laser structuring of representative environmentally friendly polymer layers. For the ethyl cellulose (EC) polymer, purpurin was matched as a sensitizing substance absorbing in the UV range, allowing structurization with a 355 nm laser beam. It contributed to path width reduction, directly corresponding to the better spatial resolution of the method. Also, a harmful ingredient, toluene, which is typically used for thin-layer formation, was eliminated. In the case of the poly(vinylpyrrolidone) (PVP) polymer, as a result of introducing the carbon black additive to the layer, heat generated by laser light absorption in the polymer upon structuring was transferred from the edge, microexplosions were eliminated, and edges were smoothed. A second additive, ATO, sensitized the polymer layer in IR, which enabled structurization with the fundamental Nd:YAG laser wavelength of 1064 nm. The whole lift-off process was possible to be performed only with water. As a result, substitutes for a commercial photoresist were obtained, which

https://doi.org/10.1021/acssuschemeng.2c01835
ACS Sustainable Chem. Eng. 2022, 10, 8196−8205

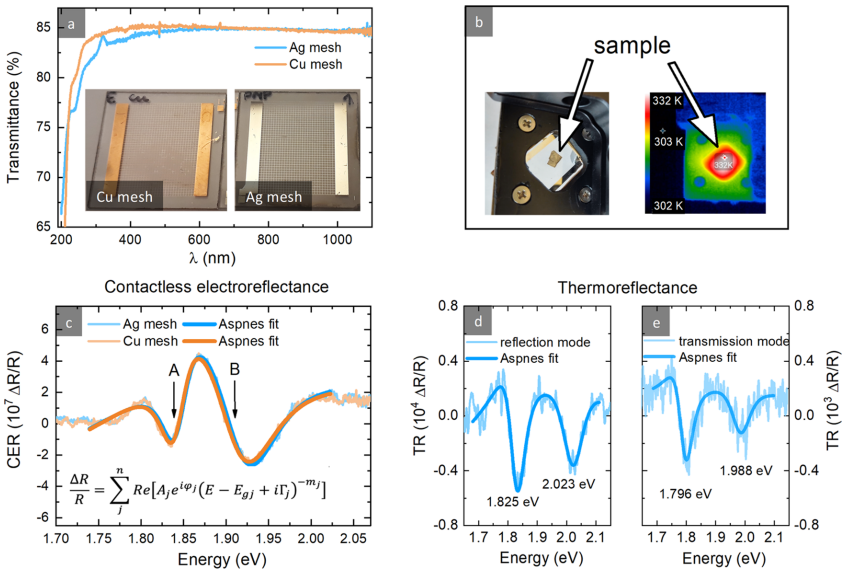

Figure 10. (a) Light transmittance spectrum of semitransparent electrodes manufactured using the laser ablation technique on the ethyl cellulose layer and the lift-off process of two different metals: silver (thickness of 170 nm, resistance of 7.3 Ω) and copper with an adhesive layer (thickness of 840 nm and resistance 5.3 Ω). (b) Picture of the transparent heater holder used for thermoreflectance measurements and equivalent in thermal imaging during thermoreflectance measurements. (c) Contactless electroreflectance spectra of a bulk MoS_2 crystal fitted with the Aspnes formula.[47] (d, e) Thermoreflectance spectrum in reflection and transmission modes, respectively, taken on the same sample using the silver electrode as a plane transparent heater.

were customized based on requirements. The health risks associated with harmful solvents were reduced. We have shown two scientific applications (CER and TR measurements) of manufactured TEs. While in the case of CER, two different metal mesh electrodes gave the same result, the TR measurement predicts divergent results due to a different thermal modulation depending on the sample-heater configuration. The next steps will focus on fabricating electrodes from other materials and testing them in TR measurements, aiming for customized heat distribution potentially leading to intrinsic optimization of TR. However, electrodes produced using the developed method also have utility applications. It allows to obtain structures with the smallest size of a dozen micrometers and to create any pattern that reaches beyond just producing transparent electrodes. The prospects for this method are promising and provide great application possibilities, as demonstrated in Figure 11.

Different shapes with sharp and rounded edges can be manufactured to create various patterns, allowing the shape to be adjusted depending on the application. Furthermore, resizing this shape (scaling) is easier and quicker in comparison to traditional lithography, where each image change requires the creation of a new mask. Also, since the ingredient that could damage the surface has been eliminated, this method can be adapted to flexible polymeric substrates and, moreover, used in industrial manufacturing once the individual steps of deposition,[48] laser structuring[49] and polymer film preparation[50] are introduced into large-scale production.

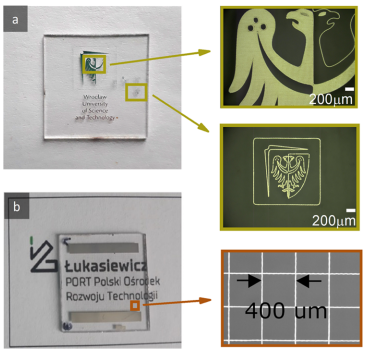

Figure 11. (a) WUST logo was manufactured with the laser lift-off technique, presenting method versatility. Enlargements of selected fragments are shown in squares as a comparison of method resolution possibilities. (b) Silver mesh with a pitch of 400 μm, demonstrating excellent transparency of the designed electrode with a paper Ł-PORT logo under the electrode. Logos are used with permission.

MATERIALS AND METHODS

Ethyl cellulose and poly(vinylpyrrolidone) polymers were bought from Sigma-Aldrich. The purpurin dye (1,2,4-Trihydroxy-9,10-anthracenedione) was from Fluorochem and the antimony tin oxide dye from Alfa Aesar. Photoresist AR-P3250 was from Allresist company.

https://doi.org/10.1021/acssuschemeng.2c01835
ACS Sustainable Chem. Eng. 2022, 10, 8196−8205

The tested transparent substrates were commercially available: soda-lime glass from Thermo Scientific Menzel-Gläser, quartz from Continental Trade, and sapphire from EKSMA Optics.

An air plasma generator from DIENE was used for thorough cleaning of substrates with a power of 80 W and a time of 30 s.

Layers were obtained by spin coating (POLOS spin coater) with parameters of 4000 rpm and 40 s.

Laser micromachining system parameters (OPTEC SP450-TO) for polymer layer structurization were laser repetition rate 500 kHz, pulse duration 15 ps, and maximum average power 36 W. The system enables switching the output between the fundamental Nd:YAG laser line (1064 nm) and higher harmonics (532, 355 nm). The UV laser beam has a spot size of 20 μm and the IR laser beam has a spot size of 30 μm.

Metal layers were deposited using Evaporator MBraun EVAP with the following parameters: resistive thermal evaporation system (for Ag, Au, Al, and Cu) and electron beam (for Ti, SiO_2); parameters for Ag and Cu include the following: rate 5 Å/s and pressure 2×10^{-6} mbar.

The spectrophotometer used for absorption spectrum measurement of the used additive was Thermo Fisher Scientific Evolution 300 UV−VIS. For the measurement of TE, a light transmission Reflectometer FILMETRICS F10-RT was used.

Measurements of CER in the so-called dark configuration were performed with an optical system consisting of a 1 m grating monochromator GDM-1000 (Carl Zeiss Jena) equipped with an amplified balanced silicon photodiode detector. A 150 W quartz tungsten halogen lamp was used as a broadband probing light source. The AC (electroreflectance) and DC (proportional to reflectance) components of the signal were analyzed with an SR510 lock-in amplifier.

For TR measurements, a bright configuration (the sample illuminated with full broadband light) optical system with an SR830 lock-in amplifier was used. The metal mesh was connected to a custom transistor switching unit, allowing for a high current supply that was synchronized with a sinusoidal reference signal (oscillating between 0 and 5 V) from an external generator set to a frequency of 2 Hz. The thermal image was acquired with a microbolometer infrared camera (Seek Thermal Compact).

The MoS_2 bulk crystal was bought from the 2D Semiconductors company. A flake around 100 μm thick was cleaved from a big crystal and used for modulation spectroscopy experiments without further treatment, except for exfoliating the top surface with Scotch tape to ensure a clean interface.

AUTHOR INFORMATION

Corresponding Authors

Anna M. Ślusarz − *ŁUKASIEWICZ Research Network − PORT Polish Center for Technology Development, 54-066 Wrocław, Poland; Department of Semiconductor Materials Engineering, Faculty of Fundamental Problems of Technology, Wrocław University of Science and Technology, 50-370 Wrocław, Poland;* orcid.org/0000-0002-1537-2961; Email: anna.slusarz@pwr.edu.pl

Robert Kudrawiec − *ŁUKASIEWICZ Research Network − PORT Polish Center for Technology Development, 54-066 Wrocław, Poland; Department of Semiconductor Materials Engineering, Faculty of Fundamental Problems of Technology, Wrocław University of Science and Technology, 50-370 Wrocław, Poland;* orcid.org/0000-0003-2593-9172; Email: robert.kudrawiec@pwr.edu.pl

Authors

Katarzyna Komorowska − *Department of Optics and Photonics, Faculty of Fundamental Problems of Technology, Wrocław University of Science and Technology, 50-370 Wrocław, Poland*

Tomasz Baraniecki − *ŁUKASIEWICZ Research Network − PORT Polish Center for Technology Development, 54-066 Wrocław, Poland*

Szymon J. Zelewski − *Department of Semiconductor Materials Engineering, Faculty of Fundamental Problems of Technology, Wrocław University of Science and Technology, 50-370 Wrocław, Poland;* orcid.org/0000-0002-6037-3701

Complete contact information is available at: https://pubs.acs.org/10.1021/acssuschemeng.2c01835

Author Contributions

The manuscript was written through contributions of all authors. All authors have given approval to the final version of the manuscript.

Notes

The authors declare no competing financial interest.

REFERENCES

(1) Layani, M.; Kamyshny, A.; Magdassi, S. Transparent Conductors Composed of Nanomaterials. *Nanoscale* **2014**, *6*, 5581−5591.

(2) He, W. W.; Yan, X. H.; Liang, Y. M.; Long, Y. F.; Pan, C.; Zhao, J. L.; Chen, L.; Xiong, W.; Liu, Q. X. Scalable and Cost-Effective Ag Nanowires Flexible Transparent Electrodes. *RSC Adv.* **2018**, *8*, 12146−12151.

(3) Papanastasiou, D. T.; Schultheiss, A.; Muñoz-Rojas, D.; Celle, C.; Carella, A.; Simonato, J.-P.; Bellet, D. Transparent Heaters: A Review. *Adv. Funct. Mater.* **2020**, *30*, No. 1910225.

(4) Liu, Q.; Tian, B.; Liang, J.; Wu, W. Recent Advances in Printed Flexible Heaters for Portable and Wearable Thermal Management. *Mater. Horiz.* **2021**, *8*, 1634−1656.

(5) Kim, H.-J.; Kim, J.; Kim, Y. A Fluoropolymer-Coated Nanometer-Thick Cu Mesh Film for a Robust and Hydrophobic Transparent Heater. *ACS Appl. Nano Mater.* **2020**, *3*, 8672−8678.

(6) Anand, A.; Islam, M. M.; Meitzner, R.; Schubert, U. S.; Hoppe, H. Introduction of a Novel Figure of Merit for the Assessment of Transparent Conductive Electrodes in Photovoltaics: Exact and Approximate Form. *Adv. Energy Mater.* **2021**, *11*, No. 2100875.

(7) Ślusarz, A.; Kopaczek, J.; Dybała, F.; Wiatrowska, A.; Granek, F.; Kudrawiec, R. Contactless Electroreflectance Spectroscopy with a Semitransparent Capacitor Made of a Silver Mesh of Ultrathin Lines. *Measurement* **2021**, *169*, No. 108361.

(8) Naik, G.; Kim, J.; Kinsey, N.; Boltasseva, A. Alternative Plasmonic Materials. In *Handbook of Surface Science* Richardson, N. V.; Holloway, S., Eds.; Modern Plasmonics: North-Holland, 2014; Vol. *4*, Chapter 6, pp 189−221.

(9) Wang, X.; Zhi, L.; Müllen, K. Transparent, Conductive Graphene Electrodes for Dye-Sensitized Solar Cells. *Nano Lett.* **2008**, *8*, 323−327.

(10) Nair, R. R.; Blake, P.; Grigorenko, A. N.; Novoselov, K. S.; Booth, T. J.; Stauber, T.; Peres, N. M. R.; Geim, A. K. Fine Structure Constant Defines Visual Transparency of Graphene. *Science* **2008**, *320*, 1308.

(11) Stadler, A. Transparent Conducting Oxides—An Up-To-Date Overview. *Materials* **2012**, *5*, 661−683.

(12) Edwards, P. P.; Porch, A.; O Jones, M.; V Morgan, D.; M Perks, R. Basic Materials Physics of Transparent Conducting Oxides. *Dalton Trans.* **2004**, *0*, 2995−3002.

(13) Meng, X.; Xu, Y.; Wang, Q.; Yang, X.; Guo, J.; Hu, X.; Tan, L.; Chen, Y. Silver Mesh Electrodes via Electroless Deposition-Coupled Inkjet-Printing Mask Technology for Flexible Polymer Solar Cells. *Langmuir* **2019**, *35*, 9713−9720.

(14) Zhang, Z.; Zhu, W. Controllable Fabrication of a Flexible Transparent Metallic Grid Conductor Based on the Coffee Ring Effect. *J. Mater. Chem. C* **2014**, *2*, 9587−9591.

(15) Lawson, R. A.; Robinson, A. P. G. Overview of Materials and Processes for Lithography. In *Frontiers of Nanoscience*, Robinson, A.;

Lawson, R., Eds.; Materials and Processes for Next Generation Lithography; Elsevier, 2016; Vol. *11*, Chapter 1, pp 1−90.
(16) Levinson, H. J. *Principles of Lithography*, SPIE Press, 2005.
(17) Ikumapayi, O. M.; Akinlabi, E. T.; Adeoye, A. O. M.; Fatoba, S. O. Microfabrication and Nanotechnology in Manufacturing System − An Overview. *Mater. Today: Proc.* **2021**, *44*, 1154−1162.
(18) Gabran, S. R. I.; Mansour, R. R.; Salama, M. M. A. Maskless Pattern Transfer Using 355nm Laser. *Opt. Lasers Eng.* **2012**, *50*, 710−716.
(19) Jia, W.; Yu, J.; Chai, L.; Wang, C.-Y. Micromachining Soda-Lime Glass by Femtosecond Laser Pulses. *Front. Phys.* **2015**, *10*, 1−4.
(20) Qin, R.; Hu, M.; Zhang, N.; Guo, Z.; Yan, Z.; Li, J.; Liu, J.; Shan, G.; Yang, J. Flexible Fabrication of Flexible Electronics: A General Laser Ablation Strategy for Robust Large-Area Copper-Based Electronics. *Adv. Electron. Mater.* **2019**, *5*, No. 1900365.
(21) Yeo, J.; Hong, S.; Lee, D.; Hotz, N.; Lee, M.-T.; Grigoropoulos, C. P.; Ko, S. H. Next Generation Non-Vacuum, Maskless, Low Temperature Nanoparticle Ink Laser Digital Direct Metal Patterning for a Large Area Flexible Electronics. *PLoS One* **2012**, *7*, No. e42315.
(22) *Laser Ablation for Thin Film Structuring*, Fraunhofer ILT, 2022, https://www.ilt.fraunhofer.de/en/media-center/brochures/b-laser-ablation-thin-film-structuring.html (accessed June 13, 2022).
(23) *Structuring by ablation of the resist materials*, Allresist, 2022, https://www.allresist.com/resist-wiki-structuring-by-ablation-of-the-resist-materials/ (accessed June 13, 2022).
(24) Miller, J. C. *Laser Ablation: Principles and Applications*, Springer Science & Business Media, 2013.
(25) Dore, C.; Osmond, J.; Mihi, A. A Water-Processable Cellulose-Based Resist for Advanced Nanofabrication. *Nanoscale* **2018**, *10*, 17884−17892.
(26) Takei, S.; Maki, H.; Sugahara, K.; Ito, K.; Hanabata, M. Inedible Cellulose-Based Biomass Resist Material Amenable to Water-Based Processing for Use in Electron Beam Lithography. *AIP Adv.* **2015**, *5*, No. 077141.
(27) Bottka, N.; Gaskill, D. K.; Sillmon, R. S.; Henry, R.; Glosser, R. Modulation Spectroscopy as a Tool for Electronic Material Characterization. *J. Electron. Mater.* **1988**, *17*, 161−170.
(28) Kudrawiec, R.; Walukiewicz, W. Electromodulation Spectroscopy of Highly Mismatched Alloys. *J. Appl. Phys.* **2019**, *126*, No. 141102.
(29) Kudrawiec, R.; Misiewicz, J.Optical Modulation Spectroscopy. In *Semiconductor Research: Experimental Techniques*, Springer, 2012; p 95.
(30) Yin, X.; Pollak, F. H. Novel Contactless Mode of Electroreflectance. *Appl. Phys. Lett.* **1991**, *59*, 2305−2307.
(31) Kudrawiec, R. Application of Contactless Electroreflectance to III-Nitrides. *Phys. Status Solidi B* **2010**, *247*, 1616−1621.
(32) Berglund, C. N. Temperature-Modulated Optical Absorption in Semiconductors. *J. Appl. Phys.* **1966**, *37*, 3019−3023.
(33) Matatagui, E.; Thompson, A. G.; Cardona, M. Thermoreflectance in Semiconductors. *Phys. Rev.* **1968**, *176*, 950−960.
(34) Ho, C.-H.; Lee, H.-W.; Cheng, Z.-H. Practical Thermoreflectance Design for Optical Characterization of Layer Semiconductors. *Rev. Sci. Instrum.* **2004**, *75*, 1098−1102.
(35) Muhimmah, L. C.; Ho, C.-H. Dual Phase Two-Color Emission Observed in van Der Waals GaTe Planes. *Appl. Surf. Sci.* **2021**, *542*, No. 148593.
(36) Ryu, Y. K.; Carrascoso, F.; López-Nebreda, R.; Agraït, N.; Frisenda, R.; Castellanos-Gomez, A. Microheater Actuators as a Versatile Platform for Strain Engineering in 2D Materials. *Nano Lett.* **2020**, *20*, 5339−5345.
(37) Ho, C.-H.; Hu, S.-F.; Chang, H.-W. Thermoreflectance Characterization of the Band-Edge Excitons Observed in Multilayered $CuInP_2S_6$. *FlatChem* **2021**, *29*, No. 100290.
(38) Wædegaard, K.; Frislev, M.; Balling, P. Femtosecond Laser Excitation of Dielectric Materials: Experiments and Modeling of Optical Properties and Ablation Depths. *Appl. Phys. A* **2013**, *110*, 601−605.
(39) Christensen, M. N.; Byskov-Nielsen, J.; Christensen, B. H.; Balling, P. Single-Shot Ablation of Sapphire by Ultrashort Laser Pulses. *Appl. Phys. A* **2010**, *101*, 279−282.
(40) Pietroy, D.; Maio, Y. D.; Moine, B.; Baubeau, E.; Audouard, E. Femtosecond Laser Volume Ablation Rate and Threshold Measurements by Differential Weighing. *Opt. Express* **2012**, *20*, 29900−29908.
(41) *Safety Data Sheet of Ethylcellulose*, Sigma Aldrich, 2019. https://www.sigmaaldrich.com/PL/en/sds/sial/phr1374.
(42) *Safety Data Sheet of Polyvinylpyrrolidone*, Sigma Aldrich, 2020. https://www.sigmaaldrich.com/PL/en/sds/sial/81420.
(43) *Ethocel Standard Premium Application Data*, Colorcon Ltd.: Dartford England, 2022. https://www.industrialcellulosics.com/insights/ethocel-printing-inks.
(44) *Transparent IR Absorbers and Antistatic Additives*, Nyacol Nano Technologies, Inc.: Ashland, USA, 2022, https://www.nyacol.com/application/ir-absorbers-antistatic-additives/ (accessed June 13, 2022).
(45) Mak, K. F.; Lee, C.; Hone, J.; Shan, J.; Heinz, T. F. Atomically Thin MoS_2: A New Direct-Gap Semiconductor. *Phys. Rev. Lett.* **2010**, *105*, No. 136805.
(46) Vella, D.; Ovchinnikov, D.; Martino, N.; Vega-Mayoral, V.; Dumcenco, D.; Kung, Y.-C.; Antognazza, M.-R.; Kis, A.; Lanzani, G.; Mihailovic, D.; Gadermaier, C. Unconventional Electroabsorption in Monolayer MoS 2. *2D Mater.* **2017**, *4*, No. 021005.
(47) Aspnes, D. E. Third-Derivative Modulation Spectroscopy with Low-Field Electroreflectance. *Surf. Sci.* **1973**, *37*, 418−442.
(48) Cordill, M. J.; Kreiml, P.; Mitterer, C. Materials Engineering for Flexible Metallic Thin Film Applications. *Materials* **2022**, *15*, 926.
(49) Industrial Laser Ablation by Laserax, 2020. https://www.laserax.com/blog/what-is-laser-ablation#industrial-applications (accessed April 28, 2022).
(50) Large-Scale Deposition by Ossila. https://www.ossila.com/pages/opv-large-scale-deposition (accessed April 28, 2022).

4.2.3 Publikacja D3

W trzeciej pracy opisana została metoda otrzymywania elektrody o ciągłej warstwie przewodzącej wykonanej z grafenu. Opisany został proces syntezy i transferu grafenu na podłoża szafirowe o trzech grubościach. Wykorzystując nowo zaprojektowany uchwyt zapewniający kontakt z cienką i delikatną warstwą grafenową zmierzono dobrze znane dwie standardowe próbki półprzewodnikowe: fosforek indu (InP) i arsenek galu (GaAs) oraz dwa kryształy van der Waalsa: dwusiarczek molibdenu (MoS_2) i diselenek wolframu (WSe_2). Podczas pomiarów badane były różne konfiguracje grafenowej elektrody względem próbki w każdej z opisanych technik pomiarowych. Pierwszą z metod było bezkontaktowe elektroodbicie (CER), drugą elektroodbicie w „miękkim kontakcie" (SCER z ang. soft contact electroreflectance), a trzecią spektroskopia fotonapięcia powierzchniowego (SPV). Dla każdej opracowano optymalne warunki pomiarowe. Na końcu pracy została przedstawiona elektroda typu III (Rys. 6), tj. elektroda grafenowa w kształcie siatki, a jej możliwości zostały zestawione z elektrodą typu II (ciągłą warstwą grafenową) w pomiarach bezkontaktowego elektroodbicia.

Praca została złożona do publikacji w czasopiśmie Applied Surface Science 17 maja 2022 i obecnie jest w recenzji. Za zgodą czasopisma praca została opublikowana bez recenzji 13 czerwca 2022 w serwisie SSRN (Social Science Research Network).

Electro-Modulation and Surface Photovoltage Spectroscopy with Semi-Transparent Graphene Electrodes

38 Pages • Posted: 13 Jun 2022

Anna M. Melnychenko
affiliation not provided to SSRN

Szymon J. Zelewski
affiliation not provided to SSRN

Daria Hlushchenko
affiliation not provided to SSRN

Krzysztof Lis
affiliation not provided to SSRN

Alicja Bachmatiuk
affiliation not provided to SSRN

Robert Kudrawiec
affiliation not provided to SSRN

Abstract

Investigating fundamental properties of new semiconductor materials and structures requires the use of a wide range of optical spectroscopy techniques. Among them, there are those that exploit the use of electrodes that are semi-transparent to light, a requirement arising from the need to either apply external perturbation to the studied material or sense the effects generated by light excitation. In this work, semi-transparent graphene electrodes were obtained by chemical vapour deposition of graphene on a copper substrate and transferring these layers to a sapphire substrate. The fabricated electrodes were tested in contactless electroreflectance, soft-contact electroreflectance, and surface photovoltage spectroscopy on III-V epilayers (InP and GaAs) and van der Waals crystals (MoS 2 and WSe 2), reference industry-standard and emerging semiconductors. The obtained results clearly show that graphene electrodes are suitable for these measurements and have many advantages over the commonly used approaches for ensuring transparent conducting layers in optoelectronic devices. On the other hand, compared to indium-tin oxide, their transparency covers a wide spectral range, including UV, revealing another important advantage. We also demonstrate that further structuring of the graphene layer enables maximizing the transparency up to the limit imposed by the hosting substrate.

Keywords: transparent electrode, contactless electroreflectance, soft-contact electroreflectance, surface photovoltage spectroscopy, van der Waals crystals

Suggested Citation:

Melnychenko, Anna M. and Zelewski, Szymon J. and Hlushchenko, Daria and Lis, Krzysztof and Bachmatiuk, Alicja and Kudrawiec, Robert, Electro-Modulation and Surface Photovoltage Spectroscopy with Semi-Transparent Graphene Electrodes. Available at SSRN: https://ssrn.com/abstract=4134845 or http://dx.doi.org/10.2139/ssrn.4134845

Electro-modulation and surface photovoltage spectroscopy with semi-transparent graphene electrodes

Anna M. Melnychenko[†,‡*], *Szymon J. Zelewski*[‡], *Daria Hlushchenko*[†,‡], *Krzysztof Lis*[†],

Alicja Bachmatiuk[†], *and Robert Kudrawiec*[†,‡**]

† ŁUKASIEWICZ Research Network – PORT Polish Center for Technology Development,

Stabłowicka 147, 54-066 Wrocław, Poland

‡ Department of Semiconductor Materials Engineering,

Faculty of Fundamental Problems of Technology,

Wrocław University of Science and Technology,

Wybrzeże Wyspiańskiego 27, 50-370 Wrocław, Poland

Corresponding authors:
*e-mail address: anna.slusarz@pwr.edu.pl
**e-mail address: robert.kudrawiec@pwr.edu.pl

Abstract

Investigating fundamental properties of new semiconductor materials and structures requires the use of a wide range of optical spectroscopy techniques. Among them, there are those that exploit the use of electrodes that are semi-transparent to light, a requirement arising from the need to either apply external perturbation to the studied material or sense the effects generated by light excitation. In this work, semi-transparent graphene electrodes were obtained by chemical vapour deposition of graphene on a copper substrate and transferring these layers to a sapphire substrate. The fabricated electrodes were tested in contactless electroreflectance, soft-contact electroreflectance, and surface photovoltage spectroscopy on III-V epilayers (InP and GaAs) and van der Waals crystals (MoS_2 and WSe_2), reference industry-standard and emerging semiconductors. The obtained results clearly show that graphene electrodes are suitable for these measurements and have many advantages over the commonly used approaches for ensuring transparent conducting layers in optoelectronic devices. On the other hand, compared to indium-tin oxide, their transparency covers a wide spectral range, including UV, revealing another important advantage. We also demonstrate that further structuring of the graphene layer enables maximizing the transparency up to the limit imposed by the hosting substrate.

Keywords

transparent electrode, contactless electroreflectance, soft-contact electroreflectance, surface photovoltage spectroscopy, van der Waals crystals

1. Introduction

Advancement in the field of electronic and optoelectronic materials requires a broad range of characterization methods, with their properties often revealed by a variety of optical spectroscopy experiments [1]. Certain spectroscopic methods are commonly recognized as state-of-the-art for studying semiconductor band structure, with the family of modulation spectroscopy techniques leading in precise determination of optical transitions arising from the band-to-band absorption or excitonic effects. Among optical spectroscopies there are those that require the use of electrodes that are semi-transparent to light, for either inducing or sensing effects involving the pumping/probing beams. Electro-modulation methods [1–3] and surface photovoltage (SPV) spectroscopy [4,5] are some of them. The former, representatives of modulation spectroscopy, rely on applied periodic perturbation of a parameter revealing resonance-like features at energies corresponding to direct optical transitions, assuming they are sensitive to the modulating factor.

One of the commonly used electro-modulation methods is electroreflectance (ER), where the change of the built-in electric field is induced by applying an external voltage directly to the Schottky barrier created at the structure interface. However, this method modifies the surface of the studied sample and cannot be used to investigate the surface potential barrier by measuring Franz-Keldysh oscillations [6–8]. Therefore, a frequently used variation of the ER method is the contactless electroreflectance (CER) [9–12]. For this method the semi-transparent electrode is the key component, since to modulate the built-in electric inside the sample two plates are required where one of them must be semi-transparent to pass incident and reflected light. Then, after applying voltage between them, electric field is generated. To create such conditions, external voltage generator and a proper sample holder forming a capacitor between the transparent electrode and the sample are needed. Typical voltages in CER are around a few kilovolts due to the air gap present in the capacitor and a voltage drop across it [2]. A very important advantage of CER spectroscopy is its contactless character, where the sample surface remains intact, and the possibility to study the surface potential barrier or its modification upon additional factors, i.e. in different gas atmospheres or due to the deposition of various nanomaterials [9,13–18].

Another type of ER, which is very similar to the CER variant, is the soft-contact electroreflectance (SCER) [19,20]. Those methods can be considered parallelly because the measurement setup can utilize the same holder design as CER, which will be described here in detail. The only changes are in the sample placement and values of the applied voltage. In SCER, the examined semiconductor softly touches the surface of a semitransparent electrode. The important advantage of this method is reduction of the voltage inducing electromodulation in comparison to CER. In addition, deposition of electric contacts permanently affecting the material surface is not required. It is possible because along with a position of the sample, which depends on a position of the plate, also the effective capacitance seen between the electrodes is changing, consequently minimizing the voltage drop across the air-gap separation. Interestingly, in such conditions, the voltage drop across the sample is of the same order as the applied voltage, corresponding to a comparable modulation amplitude to CER upon using high (>1000 V) voltages, as discussed by Datta et al. [19]. As a result, the experiment may be performed without any electrical hazard, eliminating the risk of interrupting the experiment by uncontrolled sparks caused by dielectric breakdown in air. However, this approach was not intensively explored since the character of semi-transparent soft contact (Schottky vs ohmic) may vary with the applied materials (electrode material vs investigated sample). In this case, the material of the semi-transparent electrode can play a key role since no modulation of the built-in electric field is expected for ohmic contact.

SPV is another technique which requires a semi-transparent electrode and is used for studying optical transitions in semiconductor materials and heterostructures [4,5,21–23]. The

mechanism of this method lays in measuring illumination-induced changes in a surface potential [4,5] produced due to optically excited electron-hole pair generation and following carrier redistribution, which is related to a surface photovoltaic effect. In order to efficiently detect those changes, the illumination has to be periodically chopped and the SPV signal is detected using the *lock-in* technique. The sample is placed as close as possible but without any contact to the transparent electrode, and can be performed using the same sample holder with the transparent electrode as in CER measurements. Until now, various electrodes have been used to measure SPV, CER, and SCER, but graphene electrodes have not yet been tested in these applications.

In general, the aforementioned electrodes must meet appropriate electrical, optical, and mechanical conditions. These, however, will vary depending on a type of the electrode [24]. One of the distinguished electrode families are semitransparent electrodes made of a non-transparent, conductive material (e.g. metal), but of such a fine pattern that reflection of the light beam does not cause large transmission losses of an entire electrode. Many different manufacturing methods were already demonstrated, such as inkjet printing [25,26], lithography [27,28], manufacturing using nanowires and nanotubes [29–32], and other methods which enable to create micro- and nano-size structures of grids, rings, and different intersecting structures to ensure continuous conductivity across a large area [33,34]. However, this kind of electrodes can cause a shadow effect that was observed during CER measurements with a micro-size mesh electrode, caused by grid lines covering a substantial portion of the probing light beam in close proximity to the sample surface [35].

Another types of transparent electrodes are electrodes with a continuous layer made of transparent conducting material covering all surface of an adequately transparent substrate. This category often includes conducting oxides with a subcategory of doped metal oxides such as indium-tin oxide (ITO), fluorine-doped tin oxide (FTO), tin dioxide (SnO_2), aluminum doped zinc oxide ZnO:Al, and others [36,37]. They are commercially available, but some of them are affected by issues such as brittleness, and limited transparency in the near infrared region. The major problem occurs with the industry-standard ITO which concerns deficiency of indium and related to that high costs [38]. Continuous transparent electrodes made of thin metal layer can be distinguished as another category, but the major drawback lays in their transparency that can be maximum up to 60% [39,40]. Beyond that, transparent conductive polymer layers were also used as TE in the context of photovoltaic and light-emitting applications e.g. fluorene-containing polymers [41], or poly(3,4-ethylene dioxythiophene): polystyrene sulfonic acid (PEDOT:PSS). PEDOT:PSS shows higher transparency up to 90%, unfortunately it degrades under unfavorable conditions of high humidity, temperature, and UV exposure [24].

It is well known that graphene exhibits extraordinary transparency across wide range of the electromagnetic radiation spectrum from UV down to deep-IR[42], is compatible with flexible substrates thanks to impressive mechanical properties including high stretchability, exhibits excellent properties of thermal and chemical stability, and has high in-plane conductance [24,43]. Due to these features, the use of graphene in semi-transparent electrodes for various applications was considered [3,19,44], though its exploration in hands-on modulation-based measurements seems to be lacking, with the considered CER, SCER, and SPV experiments using graphene electrodes not reported so far.

In this work, we present a constructed holder for semi-transparent graphene electrodes, with continuous surface and structured into a mesh shape one, suitable for various complementary optical spectroscopy methods. Also, a proof of the concept of using these electrodes for CER, SCER, and SPV spectra measurements on selected semiconductor materials is shown. We analyzed the optimal conditions for acquiring the spectra using the graphene electrode, where in CER and SCER it is used to modulate the electric field in the sample, while in SPV measurements it is used to detect photovoltage. We show that for both

cases the same experimental configuration can be used, preserving the sample preparation in-situ for multiple measurements. We also discuss the differences in the utilized experimental methods since each sample was tested with every technique, emphasizing that all these measurements were performed with the use of one holder for the graphene electrode.

2. Materials and methods

Sapphire substrates were bought from LAMBDA SYSTEM with three thicknesses of 1.0, 0.5, and 0.1 mm, all double side polished. The copper foil used for graphene growth was purchased from Alfa Aesar. Polymer poly(methylmethacrylate) (PMMA), molecular weight 950 kDa, AR-P 679.04. solution of potassium chloride (1 M) was purchased from Sigma Aldrich.

All optical images were taken with a Leica optical microscope using a 50× objective lens. The morphologies of the sample surfaces were investigated using a FEI Helios 660 Scanning Electron Microscope (SEM) in a high vacuum. The SEM micrographs are taken at 2 kV accelerating voltage with a current of 25 pA. For Raman spectra measurements and mapping, a confocal micro-Raman spectrometer (WiTEC) with grating 600 g/mm and laser of 532 nm wavelength used. Laser power of 2 mW was chosen to avoid sample heating. The Raman signal was collected in a backscattering configuration through a 100× objective with numerical aperture (NA) 0.95. Measurements were carried out in ambient air at room temperature. The transferred material has dimensions of 0.5 cm x 1.5 cm and was placed onto three different thicknesses of a sapphire substrate.

The InP and GaAs samples are standard epilayers grown by metalorganic vapor phase epitaxy on InP and GaAs substrates, respectively. The MoS_2 and WSe_2 bulk crystals were bought from 2D Semiconductors company (USA). A thin flake was cleaved from a bulk crystal, then it was used for modulation spectroscopy experiments with no further processing. The sample surface was cleaved by exfoliation with Scotch tape ensuring clean interface.

Parameters of laser micromachining system (OPTEC SP450-TO) for structurization of graphene layer were as follows: maximum average power 36 W (20% of this value was used for laser structurization), laser repetition rate 500 kHz, and pulse duration 15 ps. The system output wavelength was 355 nm, which is a higher harmonic of the Nd:YAG laser line (1064 nm). The UV laser beam spot size is equal 20 μm.

Measurements of electroreflectance and surface photovoltage spectroscopy were performed using the system shown in Figure 1.

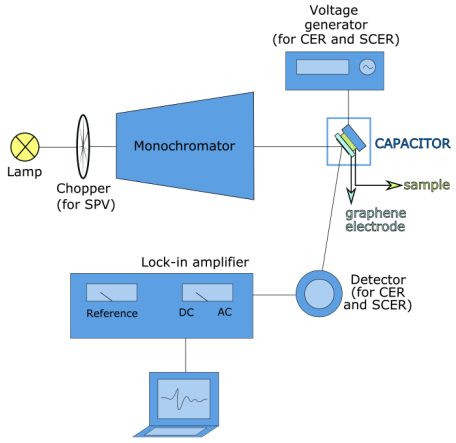

Figure 1. The scheme of the measuring system for contactless electroreflectance (CER), soft-contact electroreflectance (SCER), and surface photovoltage (SPV) experiments.

In all cases (for CER, SCER, and SPV) a halogen lamp was used as a broad-spectrum light source, and thanks to a monochromator placed before the capacitor (this configuration is called "dark"), the sample was illuminated with a specific wavelength, scanned within a desired range to obtain a full spectral dependence. The reflected beam was directed towards the detector during CER and SCER measurements. At the same time, a varying voltage was applied to the sample for both electroreflectance techniques. This method can be performed using the same procedure as in case of CER but the advantage is that we do not use high-voltage generator. In the case of the SPV, the capacitor with the sample inside was directly connected to the lock-in amplifier (Stanford Research Systems, SRS SR830) along with a mechanical chopper (SRS SR540) responsible for periodic illumination.

3. Results and Discussion

By using chemical vapour deposition (CVD) method, it is possible to receive continuous graphene films with over 95% surface coverage [45,46]. It is one of the most efficient methods for graphene transfer on a large scale [40–43]. We synthesized graphene layers on a copper foil (Cu), which was used as a catalytic substrate. Electrochemical delamination was applied to transfer graphene from Cu directly onto a sapphire substrate. At first, during electrochemical delamination, a poly(methylmethacrylate) (PMMA) layer was spin-coated on graphene/Cu samples as a protection layer. During electrochemical etching, voltage from a DC supply was applied to the PMMA/graphene/Cu cathode and a glassy carbon anode, which was immersed in electrolyte (potassium chloride solution). The graphene/Cu electrode was cathodically polarized at -3 V, and hydrogen bubbles occurred at the graphene/Cu interface due to reduction of water. Sapphire substrates of three different thicknesses (0.1, 0.5, and 1 mm) have been cleaned using the following procedure: first, the target substrate was sonicated for 5 min in acetone, followed by immersion in isopropyl alcohol (IPA) for 5 min. After this procedure, the substrates were dried with a N_2 gun. Afterwards, the graphene/PMMA films were transferred onto sapphire substrates and graphene/PMMA films dried using N_2 gun for a few seconds for better contact to the substrate. The structures were then annealed at 80 °C for 5 min and next cooled down. The PMMA layer was removed using immersion in acetone for 30 min followed by annealing in N_2 atmosphere.

Each sample was characterized by scanning electron microscopy (SEM) and Raman spectroscopy. By using SEM, the continuity of the graphene layer was confirmed on each sample, see Fig. 2. From the SEM observations, we see that the few layers of graphene on sapphire gave a brighter image and can be easily identified contrasting on the sapphire surface.

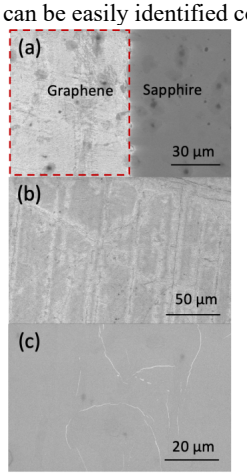

Figure 2. SEM images of transferred graphene on sapphire substrate: a) the edge of the graphene; b) – c) graphene surface with appropriate magnification.

By using Raman spectroscopy, graphene thickness was determined, ranging from 2 to 4 layers depending on sapphire substrates and examined sites on the surface (Fig. 3). It was possible to transfer the entire graphene flake onto some substrates, covering a surface sufficient for further measurement purposes. In other cases, two overlapping flakes were transferred to the substrate to ensure conductivity over the entire working surface of the electrode (inset in Fig. 4; area surrounded by a white dashed line). This resulted in the occurrence of different thicknesses of graphene layers, however, it did not affect the results of optical spectroscopy measurements. Raman spectrum of graphene on sapphire contains the main Raman modes, D, G, and 2D (Fig. 3a) appearing at 1362 cm^{-1}, 1594 cm^{-1}, and 2690 cm^{-1} (for bilayer), respectively. The peak position of the 2D line was analysed indicating a shift in frequency with increasing graphene thickness (Fig. 3b). This frequency shift is in agreement with previously reported results [47–53].

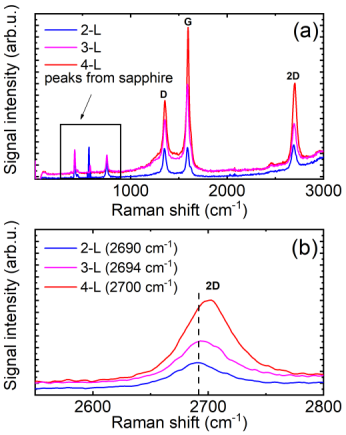

Figure 3. Raman scattering spectra of: (a) bilayer (2-L), three layers (3-L), and four layers (4-L) graphene on sapphire substrate with representative thicknesses of 0.1 mm and 1 mm, excited by 532 nm laser; (b) 2D Raman peak position analysis used for elucidating the layer thickness.

3.1 Holder preparation – possible sets

The fabricated graphene electrode was placed in a specially designed holder for soft contact, where the studied sample is approached in a gentle way toward the electrode, preventing the sample surface from unintentional damage and thus extend electrode viability, see Fig. 4. It is possible because the graphene electrode is laid onto a flat copper frame with outlet in form of three metal pins, and then carefully closed in an isolating textolite frame. The electrode can be placed in the holder in two ways: with the graphene layer facing inwards or outwards, as these interchangeable configurations are ensured by the frame design. The holder is also equipped with an element adjustable by a micrometric screw, allowing precise and repetitive regulation of sample-graphene electrode distance with an accuracy of 10 μm. The scheme of the experimental set-up for CER, SCER, and SPV measurements is included in the *Materials and methods* section.

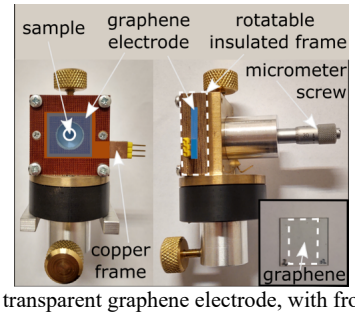

Figure 4. Holder dedicated for transparent graphene electrode, with front (left panel) and side (right panel) of the holder shown. The inset presents graphene placement on the sapphire substrate.

3.2 Influence of the substrate thickness on the graphene electrode performance in CER

At first, the optimal thickness of the sapphire window was studied, since the distance between the graphene electrode and the sample ($D_{E\text{-}S}$) in this measurement is crucial for a proper choice of the modulating voltage applied to the system. For this purpose, CER measurements

were performed using sapphire windows of three different thicknesses: 1.0, 0.5, and 0.1 mm. The slot size between the two parts of the holder body was chosen so the 1 mm electrode would be firmly secured inside, so for the thinner substrates insulated distancing pads were put between the holder body and the electrode to preserve 1 mm thickness inside the frame and prevent any displacement of the fixed graphene electrode. Then, the InP sample (chosen arbitrarily as a reference material) was glued at the end of the micrometer screw using silver paste. After that, series of CER measurements were performed with the three electrodes at different distances between the sample and the graphene layer, see Fig. 5. The resonance observed in Fig. 5 (c) is associated with the band-to-band absorption and is typical for InP epilayers [54]. Its spectral position corresponds to the band-gap of InP (1.35 eV), broadening to the layer quality, and the amplitude is proportional to the magnitude of modulation of the built-in electric field in the sample. The amplitude is marked on the two exemplary spectra in Fig. 5 (c) by two-side arrows. It is also worth noting that the shape of the CER resonance does not vary with the change of the electrode and the applied voltage. Therefore, the CER resonance amplitude is analyzed as an indicator of the efficiency of band bending modulation in CER measurements with different electrodes.

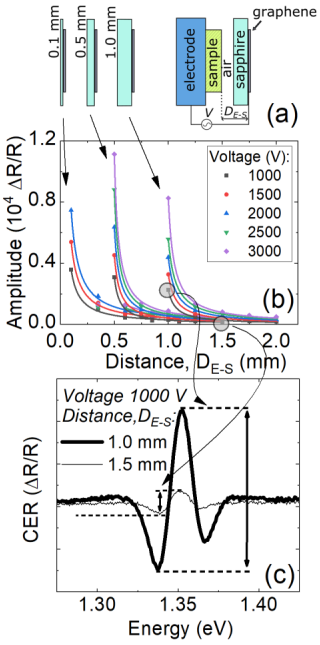

Figure 5. (a) Graphene electrode design and a scheme of the sample holder. (b) Graph of amplitude in function of distance from a reference InP sample approaching the graphene electrode. (c) Contactless electroreflectance spectra for configuration of the electrode where: 1) the distance is equal 1 mm – sample is in contact with sapphire, 2) the distance is equal 1.5 mm – the sample and the sapphire separated by a 0.5 mm air gap.

The highest resonance amplitudes occur for the configuration in which the sample touches the sapphire surface and the distance from the graphene electrode is the smallest – the distance limitation results from the sapphire thickness, see Fig. 5 (b). For the thinner electrode of about 0.1 mm, it was possible to conduct experiments with a maximum voltage up to 2 kV –

larger values can damage the electrode due to mechanical strength of such thin substrate. The most optimal conditions for CER measurements were obtained using the 0.5 mm substrate with applied voltage of 3 kV. Using these parameters we obtained fourfold signal increase comparing to set with 0.5 mm air gap, which was so far widely used for semi-transparent electrodes made of copper mesh [3]. Additionally, as graphene ensures continuous electrode coverage, we do not observe the shadow effect which have appeared with silver micro-mesh electrode occurring in close proximity to the sample due to the presence of non-transparent grid lines [35].

3.3 Optimizing the electrode configuration

Next, we examined graphene electrode configuration with the graphene layer facing outwards the sample and called the dielectric gap set and facing inwards – the air gap set, see Fig. 6 (a). CER spectra were measured for both sets keeping constant distance between the sample and the graphene layer – $D_{E\text{-}S}$ value equal 1 mm. Two group III-V semiconductor samples (GaAs and InP) and two van der Waals crystals (MoS_2 and WSe_2) were tested at the same conditions and CER spectra obtained for these samples are shown in Fig. 6 (b)-(e).

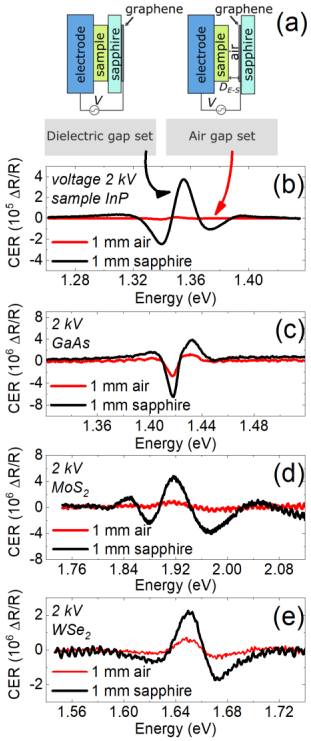

Figure 6. (a) Schemes of two possible sets of a graphene electrode in the holder: with a dielectric gap between the sample and the electrode, and with an air gap between the sample and the electrode. Contactless electroreflectance spectra performed using both configurations for four different samples: (b) InP, (c) GaAs, (d) MoS_2, and (e) WSe_2.

The recorded CER spectra are typical for the studied materials, and the observed resonances are related to direct optical transitions. For InP and GaAs they are observed at 1.35

and 1.42 eV, respectively, and are associated with the band-to-band absorption. In the case of MoS_2 and WSe_2, CER resonances are observed at 1.88-1.96 and 1.65 eV, respectively, and are attributed to exciton transitions at the K/H point of the Brillion zone [55]. In this study we are interested in the intensity of CER resonances. In Fig. 6 it is clearly observed that the air gap set (red curves) correlates with weaker CER signal than for the dielectric gap set for all investigated samples. Hence, we conclude that the dielectric sapphire gap between the examined sample enhances the modulation strength and improves the signal-to-noise ratio. This is related to a difference in the relative permittivity of sapphire (at 20 °C ε = 8.9–11.1 (anisotropic))[56] and air (ε =1) which directly affects the capacitor capacitance, formed between the transparent electrode and the sample, that is responsible for resonance amplitude of a CER spectrum. As a result, the optimal measurement configuration for CER is the one with the sapphire between the sample and the graphene (dielectric gap set).

3.4 The graphene electrode performance in SCER

To extend further the experimental capabilities of the manufactured graphene electrodes, we tested their usefulness in SCER measurements, with the experimental arrangement shown in Fig. 7 (a). In this case we translate the sample closer to the electrode until their surfaces come into contact, confirmed by the appearance of Newton rings [19].

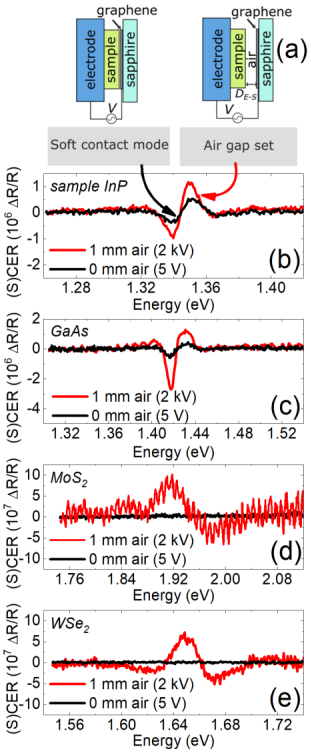

Figure 7. (a) Schemes of the setups in the soft contact electroreflectance (SCER) mode of the graphene electrode in a holder and repeated for the alternative air gap set. SCER spectra compared with contactless electroreflectance spectra in air gap set performed for four different samples: (b) InP, (c) GaAs, (d) MoS_2, and (e) WSe_2.

The spectra presented in Fig. 7 show that the SCER measurement works very well for InP and GaAs samples – resonances related to the band-to-band absorption are clearly visible, see black curves. What is more, measurements of SCER spectra for these samples were possible with 400 times reduction of the applied voltage when compared to the CER method. This method can be performed using the same procedure as in case of CER but the advantage is that we do not use high-voltage generator. However, for the other two samples (MoS_2 and WSe_2) no distinct features are observed in SCER spectra. For better comparison, previously obtained CER spectra were plotted (red curves) to show that all van der Waals samples were possible to characterize in CER with the air gap set. This is because the nature of the junction that forms with the graphene electrode is essential in SCER measurements, i.e., a Schottky barrier is necessary to modulate the built-in electric field. For the studied samples, the I-V characteristics were measured and plotted in Fig. 8. It is clearly visible that a significantly larger current flows through graphene/MoS_2 and graphene/WSe_2 junctions, about two orders of magnitude higher than through graphene/InP and graphene/GaAs ones. Therefore, in the case of van der Waals crystals we deal with ohmic contact at the graphene/MoS_2 and graphene/WSe_2 interface and as a consequence it is difficult to obtain the conditions for modulating the built-in electric field in these crystals. For InP and GaAs samples, the situation is different because of the Fermi-level pining at the surface due to dangling bonds [7]. Because of this it is easier to achieve a Schottky barrier at the graphene/InP and graphene/GaAs interface and modulate the built-in electric field in InP and GaAs. It is worth mentioning that the characteristics of such contacts are neither perfectly ohmic nor perfectly Schottky. However, for SCER measurements this is not critical, as only any potential barrier for modulating the built-in electric field is required.

It is interesting to note that no SCER signal was also observed for other van der Waals crystals ($MoSe_2$, $MoTe_2$, WS_2). This suggests that graphene electrodes have a tendency to form ohmic contacts with van der Waals crystals [57–59]. This can be attributed to no Fermi level pinning on the surface of van der Waals crystals (graphene, MoS_2, WS_2, etc.).

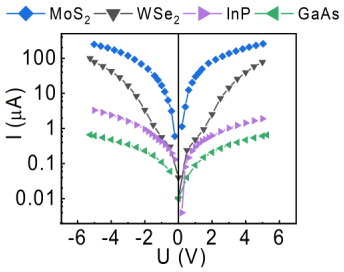

Figure 8. I-V characteristics for soft contact between graphene and InP, GaAs, MoS_2, and WSe_2.

3.5 The graphene electrode performance in SPV

In contrast to the previously demonstrated experimental techniques, SPV spectroscopy requires mechanical modulation of the probing light beam, see experimental set-up in *Materials and methods* section. Using very similar setting of the graphene electrode, the SPV technique was applied for characterizing InP, GaAs, MoS_2, and WSe_2. After creating a small distance between the sample and the graphene layer, SPV spectrum was measured, see Fig. 9. Overall, the intensity of the SPV signal for all four samples decreases upon increasing the distance between the sample surface and the graphene electrode. This is expected as the surface potential decreases with the distance from the surface and means that the optimal conditions for SPV measurements are those where the electrode is close to the sample surface.

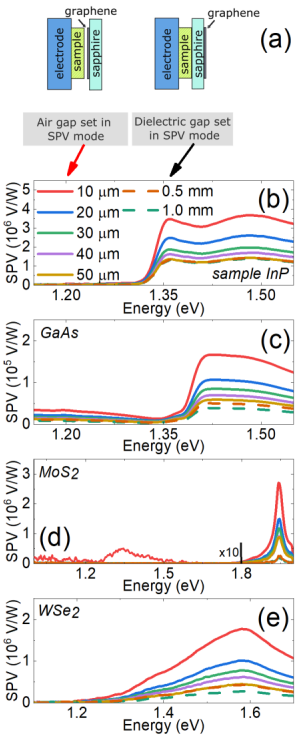

Figure 9. (a) Schemes of the two possible sets of a graphene electrode in the holder: with a dielectric gap between the sample and the electrode, and with an air gap between the sample and the electrode. Surface photovoltage spectra performed for four different samples: (b) InP, (c) GaAs, (d) MoS_2, and (e) WSe_2.

For InP, the SPV signal starts rising at 1.32 eV and peaks at 1.35 eV, which corresponds to a direct band gap in InP. Similarly for GaAs, the SPV signal starts ramping up at 1.35 eV and peaks at the direct band gap in GaAs of 1.42 eV. In this case a weak SPV signal is also observed below 1.35 eV, which can be associated with the generation of the photovoltaic effect after sub-gap excitation of carriers transferred from defect states to the conduction (valence) band. MoS_2 and WSe_2 are indirect gap semiconductors and the SPV signal rises at the indirect gap, which is at 1.2 eV for these crystals [60]. The SPV spectra have peaks at the direct optical transitions since the absorption has a local maximum at such transition. For MoS_2 and WSe_2 the SPV peaks are observed at 1.96 and 1.65 eV, respectively, which corresponds to excitonic transitions observed in CER, see Fig. 6 (d) and (e).

The SPV results obtained for the four samples clearly show that the sample holder with the semi-transparent graphene electrode used for CER and SCER measurements can also be used to measure SPV spectra, significantly extending the experimental possibilities of the proposed system. As a result, the optimal measurement configuration for SPV is the air gap set.

3.6 Influence of the continuous graphene versus mesh-shaped graphene on the electrode performance in CER

To increase the transparency of the electrode the graphene layer was structured in a shape of mesh. It was achieved by removing square parts to obtain 400 μm spacing of a grid pattern. It was done using laser structuring system after parameter selection so as the removal dose would not damage the substrate, see Fig. 10. The Raman mapping of structured sample confirms presence of graphene mesh (Fig. 10b), where the dark areas on the map correspond to total intensity from graphene mesh.

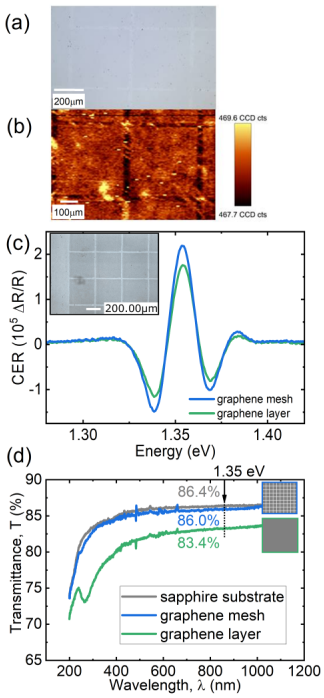

Figure 10. (a) Optical microscope image of graphene grid on sapphire substrate. (b) Raman map of the graphene grid on sapphire. The scale represents total signal intensity (number of counts). (c) Contactless electroreflectance spectra measured with the use of graphene electrode with continuous layer (green line) and with mesh structured layer (blue line). (d) Graph of transmittance as a function of wavelength for those two kinds of graphene electrodes and a result for clear sapphire substrate (grey line).

After structuring graphene layer, the transmittance of the electrode increased from 83.4% to 86.0% at 1.35 eV, which improved CER measurement by enhancing the resonance, as demonstrated in Fig. 10 (c) for InP sample. We attribute this improvement to the higher light transmission through the electrode rather than better modulation of the band bending in the studied sample.

It is also worth emphasizing here that both types of electrodes (structured and unstructured) are transparent in a very wide spectral range. The drop in transparency below 300 nm is related more to the sapphire substrate than to the graphene itself. In this spectral range, the ITO electrodes are no longer transparent.

The described electrodes were used many times in CER measurements and we did not observe their degradation after a year, except for mechanical damage caused by touching the sample to the graphene layer for the SCER configuration. These damages can be eliminated by performing measurements in the graphene/sapphire/sample configuration (dielectric gap set), which is also described here and compared with other alternative electrode arrangements. Currently, the dielectric gap set is most often used in our laboratory in CER measurements.

4. Summary and perspectives

We implement a graphene electrode on sapphire in two varying measurement configurations of electromodulation spectroscopy, with the electrode utilized for generating electric field, and SPV, in which the electrode detects the surface potential. By designing a dedicated sample holder, we were able to perform three different measurements (CER, SCER, and SPV) using the same optical system and to show that graphene electrodes are suitable for these measurements and have some advantages over commonly used semi-transparent electrodes. The most important advantage compared to electrodes made of metal mesh is the lack of a shadow effect revealed during CER measurements with a micro-mesh electrode in close proximity to the sample. Compared to ITO electrodes, the most important advantage is the transparency of graphene electrodes in a wide spectral range, including UV. We are convinced that the proposed graphene electrodes, i.e., a conductive graphene layer and structured graphene layer in mesh-shape on a substrate with high dielectric permittivity (demonstrated using sapphire), can find many other applications in optical spectroscopy, where both optical access to the sample and placing the sample in an external electric field are needed. Such electrodes have also promising application possibilities in biology where a combination of both optical characterization (i.e. fluorescence microscopy with markers) and electrophoresis would be beneficial.

CRediT author statement

Anna M. Melnychenko: Performed optical measurements, analyzed the results, wrote original draft. **Szymon J. Zelewski**: Prepared the experiments and contributed in measurements; reviewing and editing. **Daria Hlushchenko**: Performed graphene transfer and measurements; writing and editing. **Krzysztof Lis**: Performed graphene synthesis. **Alicja Bachmatiuk:** Supervision of graphene synthesis and transfer. **Robert Kudrawiec**: Supervision of all measurement, coordinated experimental work and analysis of the results; writing, reviewing, editing. All the authors reviewed the manuscript.

Declaration of Competing Interest

The authors declare that they have no conflict of interest.

Acknowledgments

This work was supported by the National Science Centre (NCN) in Poland through OPUS Grant No. 2018/29/B/ST7/02135. At PORT this work was supported by the National Centre for Research and Development (NCBiR) in Poland through project POIR.04.01.02-00-0103/17.

References

[1] R. Kudrawiec, J. Misiewicz, Optical Modulation Spectroscopy, in: A. Patane, N. Balkan (Eds.), Semicond. Res., Springer Berlin Heidelberg, Berlin, Heidelberg, 2012: pp. 95–124. https://doi.org/10.1007/978-3-642-23351-7_4.

[2] X. Yin, F.H. Pollak, Novel contactless mode of electroreflectance, Appl. Phys. Lett. 59 (1991) 2305–2307. https://doi.org/10.1063/1.106051.

[3] J. Misiewicz, R. Kudrawiec, Contactless electroreflectance spectroscopy of optical transitions in low dimensional semiconductor structures, Opto-Electron. Rev. 20 (2012) 101–119. https://doi.org/10.2478/s11772-012-0022-1.

[4] L. Kronik, Y. Shapira, Surface photovoltage phenomena: theory, experiment, and applications, Surf. Sci. Rep. 37 (1999) 1–206. https://doi.org/10.1016/S0167-5729(99)00002-3.

[5] L. Kronik, Y. Shapira, Surface photovoltage spectroscopy of semiconductor structures: at the crossroads of physics, chemistry and electrical engineering, Surf. Interface Anal. 31 (2001) 954–965. https://doi.org/10.1002/sia.1132.

[6] C. Van Hoof, K. Deneffe, J. De Boeck, D.J. Arent, G. Borghs, Franz–Keldysh oscillations originating from a well-controlled electric field in the GaAs depletion region, Appl. Phys. Lett. 54 (1989) 608–610. https://doi.org/10.1063/1.100893.

[7] H. Shen, M. Dutta, Franz–Keldysh oscillations in modulation spectroscopy, J. Appl. Phys. 78 (1995) 2151–2176. https://doi.org/10.1063/1.360131.

[8] Ł. Janicki, M. Gładysiewicz, J. Misiewicz, K. Klosek, M. Sobanska, P. Kempisty, Z.R. Zytkiewicz, R. Kudrawiec, Contactless electroreflectance studies of the Fermi level position at the air/GaN interface: Bistable nature of the Ga-polar surface, Appl. Surf. Sci. 396 (2017) 1657–1666. https://doi.org/10.1016/j.apsusc.2016.12.013.

[9] L. Hernandez-Mainet, G. Chen, A. Zangiabadi, A. Shen, M.C. Tamargo, Growth and characterization of II-VI semiconductor multilayer quantum-well structures for two-color quantum well infrared photodetector applications, J. Vac. Sci. Technol. A. 39 (2021) 033205. https://doi.org/10.1116/6.0000947.

[10] A. Tolloczko, J. Kopaczek, R. Szukiewicz, A. Gocalińska, E. Pelucchi, D. Hommel, R. Kudrawiec, Contactless electroreflectance study of the surface potential barrier in n -type and p -type InAlAs van Hoof structures lattice matched to InP, J. Phys. Appl. Phys. 51 (2018) 215104. https://doi.org/10.1088/1361-6463/aabf6b.

[11] Y.F. Chiang, A.H. Tseng, D.P. Wang, Contactless Electroreflectance Spectroscopy of ZnO with Different Polarization-Direction Probe Beams, Appl. Mech. Mater. 535 (2014) 679–682. https://doi.org/10.4028/www.scientific.net/AMM.535.679.

[12] W.-J. Chen, M.-H. Chang, C.-C. Chang, M.-C. Tsai, H.-L. Cheng, W.-Y. Chou, Optical properties of PTCDI thin films studied by contactless electroreflectance, in: S. Yin, R. Guo (Eds.), Photonic Fiber Cryst. Devices Adv. Mater. Innov. Device Appl. V, Spie-Int Soc Optical Engineering, Bellingham, 2011: p. 81201E. https://doi.org/10.1117/12.893479.

[13] Ł. Janicki, J. Misiewicz, M. Siekacz, H. Turski, J. Moneta, S. Gorantla, C. Skierbiszewski, R. Kudrawiec, Sensitivity of N-polar GaN surface barrier to ambient gases, Sens. Actuators B Chem. 281 (2019) 561–567. https://doi.org/10.1016/j.snb.2018.10.157.

[14] A.P. Herman, L. Janicki, H.S. Stokowski, M. Rudzinski, E. Rozbiegala, M. Sobanska, Z.R. Zytkiewicz, R. Kudrawiec, Determination of Fermi Level Position at the Graphene/GaN Interface Using Electromodulation Spectroscopy, Adv. Mater. Interfaces. 7 (2020) 2001220. https://doi.org/10.1002/admi.202001220.

[15] E. Zdanowicz, A.P. Herman, K. Opołczyńska, S. Gorantla, W. Olszewski, J. Serafińczuk, D. Hommel, R. Kudrawiec, Toward h-BN/GaN Schottky Diodes: Spectroscopic Study on the Electronic Phenomena at the Interface, ACS Appl. Mater. Interfaces. 14 (2022) 6131–6137. https://doi.org/10.1021/acsami.1c20352.

[16] J. Kopaczek, S. Zelewski, K. Yumigeta, R. Sailus, S. Tongay, R. Kudrawiec, Temperature Dependence of the Indirect Gap and the Direct Optical Transitions at the High-Symmetry Point of the Brillouin Zone and Band Nesting in MoS_2, $MoSe_2$, $MoTe_2$, WS_2, and WSe_2 Crystals, J. Phys. Chem. C. 126 (2022) 5665–5674. https://doi.org/10.1021/acs.jpcc.2c01044.
[17] J. De Jesus, T.A. Garcia, S. Dhomkar, A. Ravikumar, C. Gmachl, G. Chen, A. Shen, D. Ferizovic, M. Muñoz, M.C. Tamargo, Characterization of the three-well active region of a quantum cascade laser using contactless electroreflectance, J. Vac. Sci. Technol. B. 31 (2013) 03C134. https://doi.org/10.1116/1.4803838.
[18] H. Lu, A. Shen, W. Charles, I. Yokomizo, M.C. Tamargo, K.J. Franz, C. Gmachl, M. Muñoz, Optical characterization of intersubband transitions in $Zn_xCd_{1-x}Se/Zn_{x'}Cd_{y'}Mg_{1-x'-y'}Se$ multiple quantum well structures by contactless electroreflectance, Appl. Phys. Lett. 89 (2006) 241921. https://doi.org/10.1063/1.2405385.
[19] S. Datta, S. Ghosh, B.M. Arora, Electroreflectance and surface photovoltage spectroscopies of semiconductor structures using an indium–tin–oxide-coated glass electrode in soft contact mode, Rev. Sci. Instrum. 72 (2001) 177–183. https://doi.org/10.1063/1.1332114.
[20] R. Kudrawiec, J. Misiewicz, Contactless and soft contact electroreflectance of AlGaN/GaN and GaN/AlGaN/GaN field effect transistor heterostructures, Phys. Status Solidi C. 7 (2010) 96–99. https://doi.org/10.1002/pssc.200982626.
[21] R. Kudrawiec, P. Sitarek, M. Gladysiewicz, J. Misiewicz, Y. He, Y. Jin, G. Vardar, A.M. Mintarov, J.L. Merz, R.S. Goldman, K.-M. Yu, W. Walukiewicz, Surface photovoltage and modulation spectroscopy of E− and E+ transitions in GaNAs layers, Thin Solid Films. 567 (2014) 101–104. https://doi.org/10.1016/j.tsf.2014.07.052.
[22] D. Cavalcoli, A. Cavallini, Surface photovoltage spectroscopy - method and applications, Phys. Status Solidi C. 7 (2010) 1293–1300. https://doi.org/10.1002/pssc.200983124.
[23] D. Cavalcoli, M.A. Fazio, Electronic transitions in low dimensional semiconductor structures measured by surface photovoltage spectroscopy, Mater. Sci. Semicond. Process. 92 (2019) 28–38. https://doi.org/10.1016/j.mssp.2018.05.027.
[24] W. Cao, J. Li, H. Chen, J. Xue, Transparent electrodes for organic optoelectronic devices: a review, J. Photonics Energy. 4 (2014) 040990. https://doi.org/10.1117/1.JPE.4.040990.
[25] M. Layani, M. Gruchko, O. Milo, I. Balberg, D. Azulay, S. Magdassi, Transparent Conductive Coatings by Printing Coffee Ring Arrays Obtained at Room Temperature, ACS Nano. 3 (2009) 3537–3542. https://doi.org/10.1021/nn901239z.
[26] Z. Zhang, W. Zhu, Controllable fabrication of a flexible transparent metallic grid conductor based on the coffee ring effect, J. Mater. Chem. C. 2 (2014) 9587–9591. https://doi.org/10.1039/C4TC01908C.
[27] C.F. Guo, T. Sun, Q. Liu, Z. Suo, Z. Ren, Highly stretchable and transparent nanomesh electrodes made by grain boundary lithography, Nat. Commun. 5 (2014) 3121. https://doi.org/10.1038/ncomms4121.
[28] T. Gao, B. Wang, B. Ding, J. Lee, P.W. Leu, Uniform and Ordered Copper Nanomeshes by Microsphere Lithography for Transparent Electrodes, Nano Lett. 14 (2014) 2105–2110. https://doi.org/10.1021/nl5003075.
[29] W.W. He, X.H. Yan, Y.M. Liang, Y.F. Long, C. Pan, J.L. Zhao, L. Chen, W. Xiong, Q.X. Liu, Scalable and cost-effective Ag nanowires flexible transparent electrodes, RSC Adv. 8 (2018) 12146–12151. https://doi.org/10.1039/C7RA13196H.
[30] H. Hosseinzadeh Khaligh, K. Liew, Y. Han, N.M. Abukhdeir, I.A. Goldthorpe, Silver nanowire transparent electrodes for liquid crystal-based smart windows, Sol. Energy Mater. Sol. Cells. 132 (2015) 337–341. https://doi.org/10.1016/j.solmat.2014.09.006.

[31] J. Sun, R. Wang, Carbon Nanotube Transparent Electrode, IntechOpen, 2013. https://doi.org/10.5772/51783.
[32] C.-L. Kim, C.-W. Jung, Y.-J. Oh, D.-E. Kim, A highly flexible transparent conductive electrode based on nanomaterials, NPG Asia Mater. 9 (2017) e438–e438. https://doi.org/10.1038/am.2017.177.
[33] M. Layani, A. Kamyshny, S. Magdassi, Transparent conductors composed of nanomaterials, Nanoscale. 6 (2014) 5581–5591. https://doi.org/10.1039/C4NR00102H.
[34] H.B. Lee, W.-Y. Jin, M.M. Ovhal, N. Kumar, J.-W. Kang, Flexible transparent conducting electrodes based on metal meshes for organic optoelectronic device applications: a review, J. Mater. Chem. C. 7 (2019) 1087–1110. https://doi.org/10.1039/C8TC04423F.
[35] A. Ślusarz, J. Kopaczek, F. Dybała, A. Wiatrowska, F. Granek, R. Kudrawiec, Contactless electroreflectance spectroscopy with a semitransparent capacitor made of a silver mesh of ultrathin lines, Measurement. 169 (2021) 108361. https://doi.org/10.1016/j.measurement.2020.108361.
[36] A. Stadler, Transparent Conducting Oxides—An Up-To-Date Overview, Materials. 5 (2012) 661–683. https://doi.org/10.3390/ma5040661.
[37] J.-H. Lee, Y.-J. You, M.A. Saeed, S.H. Kim, S.-H. Choi, S. Kim, S.Y. Lee, J.-S. Park, J.W. Shim, Undoped tin dioxide transparent electrodes for efficient and cost-effective indoor organic photovoltaics (SnO2 electrode for indoor organic photovoltaics), NPG Asia Mater. 13 (2021) 1–10. https://doi.org/10.1038/s41427-021-00310-2.
[38] E.J. López-Naranjo, L.J. González-Ortiz, L.M. Apátiga, E.M. Rivera-Muñoz, A. Manzano-Ramírez, Transparent Electrodes: A Review of the Use of Carbon-Based Nanomaterials, J. Nanomater. (2016) e4928365. https://doi.org/10.1155/2016/4928365.
[39] B. O'Connor, C. Haughn, K.-H. An, K.P. Pipe, M. Shtein, Transparent and conductive electrodes based on unpatterned, thin metal films, Appl. Phys. Lett. 93 (2008) 223304. https://doi.org/10.1063/1.3028046.
[40] S.D. Yambem, A. Haldar, K.-S. Liao, E.P. Dillon, A.R. Barron, S.A. Curran, Optimization of organic solar cells with thin film Au as anode, Sol. Energy Mater. Sol. Cells. 95 (2011) 2424–2430. https://doi.org/10.1016/j.solmat.2011.04.019.
[41] C. Brabec, U. Scherf, V. Dyakonov, Organic Photovoltaics: Materials, Device Physics, and Manufacturing Technologies, John Wiley & Sons, 2011.
[42] R.R. Nair, P. Blake, A.N. Grigorenko, K.S. Novoselov, T.J. Booth, T. Stauber, N.M.R. Peres, A.K. Geim, Fine Structure Constant Defines Visual Transparency of Graphene, Science. 320 (2008) 1308–1308. https://doi.org/10.1126/science.1156965.
[43] X. Wang, L. Zhi, K. Müllen, Transparent, Conductive Graphene Electrodes for Dye-Sensitized Solar Cells, Nano Lett. 8 (2008) 323–327. https://doi.org/10.1021/nl072838r.
[44] F.H. Pollak, Contactless electromodulation and surface photovoltage spectroscopy for the nondestructive, room temperature characterization of wafer-scale III–V semiconductor device structures, Mater. Sci. Eng. B. 80 (2001) 178–183. https://doi.org/10.1016/S0921-5107(00)00618-8.
[45] F. Qing, Y. Zhang, Y. Niu, R. Stehle, Y. Chen, X. Li, Towards large-scale graphene transfer, Nanoscale. 12 (2020) 10890–10911. https://doi.org/10.1039/D0NR01198C.
[46] H.C. Lee, W.-W. Liu, S.-P. Chai, A.R. Mohamed, A. Aziz, C.-S. Khe, N.M.S. Hidayah, U. Hashim, Review of the synthesis, transfer, characterization and growth mechanisms of single and multilayer graphene, RSC Adv. 7 (2017) 15644–15693. https://doi.org/10.1039/C7RA00392G.
[47] I. Calizo, W. Bao, F. Miao, C.N. Lau, A.A. Balandin, The effect of substrates on the Raman spectrum of graphene: Graphene- on-sapphire and graphene-on-glass, Appl. Phys. Lett. 91 (2007) 201904. https://doi.org/10.1063/1.2805024.

[48] Z. Ni, Y. Wang, T. Yu, Z. Shen, Raman spectroscopy and imaging of graphene, Nano Res. 1 (2008) 273–291. https://doi.org/10.1007/s12274-008-8036-1.
[49] L.M. Malard, M.A. Pimenta, G. Dresselhaus, M.S. Dresselhaus, Raman spectroscopy in graphene, Phys. Rep. 473 (2009) 51–87. https://doi.org/10.1016/j.physrep.2009.02.003.
[50] Y. Hao, Y. Wang, L. Wang, Z. Ni, Z. Wang, R. Wang, C.K. Koo, Z. Shen, J.T.L. Thong, Probing layer number and stacking order of few-layer graphene by Raman spectroscopy, Small Weinh. Bergstr. Ger. 6 (2010) 195–200. https://doi.org/10.1002/smll.200901173.
[51] S. Siregar, Double resonance Raman spectra of G ′ and G ∗ bands of graphene, (2015). https://www.semanticscholar.org/paper/Double-resonance-Raman-spectra-of-G-%E2%80%B2-and-G-%E2%88%97-bands-Siregar/5c0fdbf3a2ec424724682e3c0ca270ea02368aac (accessed January 11, 2022).
[52] J.-B. Wu, M.-L. Lin, X. Cong, H.-N. Liu, P.-H. Tan, Raman spectroscopy of graphene-based materials and its applications in related devices, Chem. Soc. Rev. 47 (2018) 1822–1873. https://doi.org/10.1039/C6CS00915H.
[53] A.C. Ferrari, D.M. Basko, Raman spectroscopy as a versatile tool for studying the properties of graphene, Nat. Nanotechnol. 8 (2013) 235–246. https://doi.org/10.1038/nnano.2013.46.
[54] X. Yin, X. Guo, F. Pollak, G. Pettit, J. Woodall, T. Chin, C. Tu, Nature of Band Bending at Semiconductor Surfaces by Contactless Electroreflectance, Appl. Phys. Lett. 60 (1992) 1336–1338. https://doi.org/10.1063/1.107335.
[55] J. Kopaczek, M.P. Polak, P. Scharoch, K. Wu, B. Chen, S. Tongay, R. Kudrawiec, Direct optical transitions at K- and H-point of Brillouin zone in bulk MoS2, MoSe2, WS2, and WSe2, J. Appl. Phys. 119 (2016) 235705. https://doi.org/10.1063/1.4954157.
[56] A.K. Harman, S. Ninomiya, S. Adachi, Optical constants of sapphire (α-Al2O3) single crystals, J. Appl. Phys. 76 (1994) 8032–8036. https://doi.org/10.1063/1.357922.
[57] D. Pierucci, H. Henck, J. Avila, A. Balan, C.H. Naylor, G. Patriarche, Y.J. Dappe, M.G. Silly, F. Sirotti, A.T.C. Johnson, M.C. Asensio, A. Ouerghi, Band Alignment and Minigaps in Monolayer MoS2-Graphene van der Waals Heterostructures, Nano Lett. 16 (2016) 4054–4061. https://doi.org/10.1021/acs.nanolett.6b00609.
[58] M.H.D. Guimarães, H. Gao, Y. Han, K. Kang, S. Xie, C.-J. Kim, D.A. Muller, D.C. Ralph, J. Park, Atomically Thin Ohmic Edge Contacts Between Two-Dimensional Materials, ACS Nano. 10 (2016) 6392–6399. https://doi.org/10.1021/acsnano.6b02879.
[59] Y. Liu, H. Wu, H.-C. Cheng, S. Yang, E. Zhu, Q. He, M. Ding, D. Li, J. Guo, N.O. Weiss, Y. Huang, X. Duan, Toward Barrier Free Contact to Molybdenum Disulfide Using Graphene Electrodes, Nano Lett. 15 (2015) 3030–3034. https://doi.org/10.1021/nl504957p.
[60] K.K. Kam, B.A. Parkinson, Detailed photocurrent spectroscopy of the semiconducting group VIB transition metal dichalcogenides, J. Phys. Chem. 86 (1982) 463–467. https://doi.org/10.1021/j100393a010.

4.2.4 Publikacja D4

Czwarta praca opisuje technikę wytwarzania przeźroczystych elektrod o nieregularnych kształtach wykorzystującą pękającą warstwę polimerową jako maskę stosowaną w procesie nanoszenia cienkich warstw metalicznych. Elektrody otrzymane tą metodą są zestawione z wynikami otrzymanymi metodą „laser lift-off". Przeprowadzono również badania opisujące sam etap pękania, poprzez przetestowanie różnych stężeń roztworu polimerowego jak i rodzajów przeźroczystego podłoża, na którym warstwa jest osadzana. W końcowej części pracy zaproponowano nowe zastosowanie tego typu elektrod. Przedstawiony został pomysł kodowania za pomocą elektrody przeźroczystej o nieregularnym kształcie sugerując poszerzenie obszaru zastosowań przeźroczystych elektrod.

Praca została opublikowana w wersji elektronicznej 17 października 2022r.

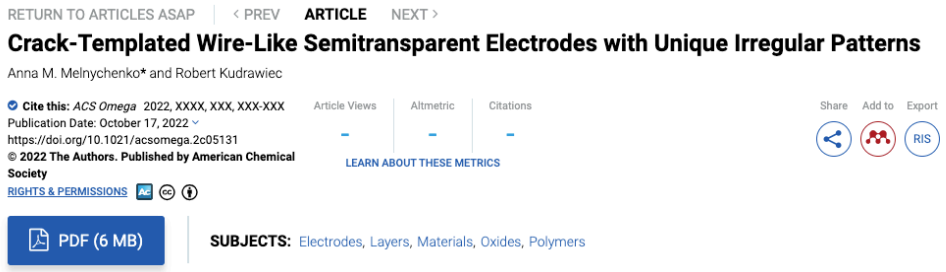
RETURN TO ARTICLES ASAP | < PREV ARTICLE NEXT >

Crack-Templated Wire-Like Semitransparent Electrodes with Unique Irregular Patterns

Anna M. Melnychenko* and Robert Kudrawiec

Cite this: *ACS Omega* 2022, XXXX, XXX, XXX-XXX

Publication Date: October 17, 2022

https://doi.org/10.1021/acsomega.2c05131

© 2022 The Authors. Published by American Chemical Society

RIGHTS & PERMISSIONS

Article Views - | Altmetric - | Citations -

LEARN ABOUT THESE METRICS

Share Add to Export RIS

PDF (6 MB)

SUBJECTS: Electrodes, Layers, Materials, Oxides, Polymers

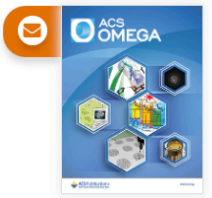

ACS Omega

ACS OMEGA

http://pubs.acs.org/journal/acsodf

Article

Crack-Templated Wire-Like Semitransparent Electrodes with Unique Irregular Patterns

Anna M. Melnychenko* and Robert Kudrawiec

Cite This: https://doi.org/10.1021/acsomega.2c05131

Read Online

ACCESS | Metrics & More | Article Recommendations

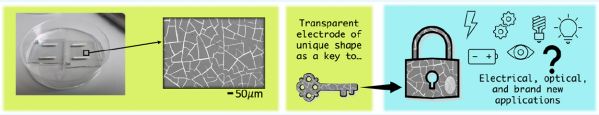

ABSTRACT: The development of novel methods of producing transparent electrodes is important because of their ever-evolving applications and thus the additional parameters they must meet. In this work, we present a method of manufacturing semitransparent silver electrodes. This technique involves cracking the polyvinylpyrrolidone layer in the presence of a colloidal nanodispersion of zinc oxide. The resulting cracked polymer layer serves as the disposable mask for metal deposition. The whole procedure is valuable due to the fast and easy step of cracks formation caused by the elevated temperature and reduced pressure. The obtained electrodes have high transparency (82.4%) in a wide spectral range, which is only limited by the transparency of the applied substrate, and low resistivity (27.3×10^{-7} Ωm). The presence of unique patterns suggests new ideas for the applications of such electrodes, such as coding, security, and antiplagiarism protection.

INTRODUCTION

Transparent electrodes (TEs) are used in many different applications, such as photovoltaics, optoelectronics, and display production, as well as in the automotive industry for windows with heaters and even in highly future-oriented applications of smart home construction, namely, smart windows.[1,2] The main challenge is to adapt the manufacturing method to the required application and hence to find a balance between electrode transmission and conduction. These parameters will vary depending on the manufacturing method used for the TE.[3]

In general, we can distinguish two types of TEs. In short, they can be called planar and patterned. In the former, the whole surface is covered by a continuous conductive material, e.g., indium tin oxide (ITO),[4,5] fluorine-doped tin oxide,[6] graphene,[7] a thin metal,[8] a polymer layer,[9] or other conductive films. The latter are transparent due to the very narrow width of the pattern, which can even be made of a nontransparent material; since the material only slightly covers the substrate surface, the entire electrode remains semitransparent.[10] Those patterns can take the shape of squares, circles, polygons, or other regular or irregular intersecting lines. They must intersect to ensure good contact with each other and thus the good conductivity of the whole pattern, which creates the electrode.

Regular shapes such as mesh-shaped patterns are very common in the context of transparent electrodes and can be manufactured using many different methods, usually with tunable line width and spacing.[11−13] Polygons, circles,[14,15] and other regular shapes always require predesign to plan the movement of the printer head, laser head, or other device used in the method or, in the case of photolithography, to make the mask. Regular shapes have the advantage easily predicted TE mechanisms of action due to the simple design that can be simulated. However, a disadvantage that may occur is the Moiré phenomenon induced by the metal grids, which has been observed in some TE applications.[16]

Irregular shapes that create TE are not that common and usually require specific manufacturing methods such as the biomimic template reported by Jia et al.[17] Additionally, irregularities are predominantly observed on the nanoscale, especially in methods utilizing nanowires. Silver nanowires are currently the most frequently reported nanomaterial.[18−20]

Meanwhile, achievements related to the production of TEs with irregular shapes on the macroscale are rarely reported. Such shapes require an unnecessary expenditure of energy and time to design a different pattern each time. It is challenging to obtain a shape with such a high degree of randomness, although such attempts have been made using the self-assembly process of Ag nanoparticles.[21,22] Those TEs achieved very good transmission and resistivity parameters. However, it is difficult to create a homogeneous surface with this method

Received: August 10, 2022
Accepted: October 7, 2022

because of differences in the layer morphology. Another idea for spontaneous shape formation is layer cracking. This technique was used by Rao et al. to obtain ITO-free organic solar cells,[23] Cui et al. in the application of a thermochromic device,[24] and Han et al. for the fabrication of a touch-screen device.[25] These irregular shapes were also studied and subjected to simulations by Kim et al.[26] A review summarizing the different types of transparent patterned conductors was also published by Gao et al.[27] The present challenge for electrodes with irregular shapes is to move individual stages to production-scale and make them commercially feasible.

In this work, we present a method that allows the production of TEs with irregular, unique shapes on the macroscale while simultaneously requiring minimal effort to produce an electrode of this shape. We are focusing on entirely new applications of TEs, which we would like to emphasize were not previously published in this context.

RESULTS AND DISCUSSION

Figure 1 shows a schematic diagram of the TE production procedure, starting with the preparation of the dispersion,

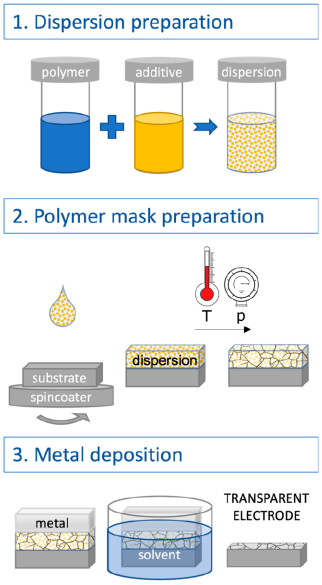

Figure 1. Scheme describing the procedure for manufacturing a transparent electrode using the cracking-induced technique.

continuing with the spin-coating and conditioning of the polymer mask, and ending with the deposition of the metal layer.

In the first step of the cracking-induced technique, which is called dispersion preparation in Figure 1, an appropriate polymer was chosen to constitute a matrix for a dispersion of nanoparticles that would later induce the cracking of that polymer. At the same time, this polymer should form a thin layer during spin-coating and should also be easily soluble for use as a disposable lift-off mask. All these requirements were met by the polyvinylpyrrolidone (PVP) powder with an average molecular weight of 10 000 that was purchased from Sigma-Aldrich. The concentration of PVP dissolved in ethanol was set at 0.5 g/mL. A vortex and a magnetic stirrer were used to help speed up the dissolution. As a nanodispersion, zinc oxide (ZnO) in ethanol was used because it was a readily available commercial reagent. It was bought from Sigma-Aldrich with 40 wt % nanoparticles and a particle size <130 nm. Due to the compatibility of the solvents of the two materials, it is easier to combine them because PVP is soluble in ethanol. To create a uniform polymer layer without agglomerates, this mixture was first homogenized for 6 min. This ensured a better dispersion of nanoparticles in the polymer and a longer suspension stability. The temperature during the homogenization process, measured with a thermometer immersed in the liquid, was 55 °C. The dispersion was stable for three days. After that time, the vortex was used to reunite the phases.

In the second step of the polymer mask preparation shown in Figure 1, 300 μL of the dispersion was spin-coated onto a transparent substrate at 4000 rpm for 40 s (POLOS). The layer thickness was measured on a Bruker Dektak contact profilometer. The sample was then placed onto hot plate and heated to 80 °C for 10 min to intentionally induce cracking. Higher temperatures up to 150 °C were also tested, but they did not caused any changes in the cracking process, proving that the evaporation temperature of the solvent (80 °C for ethanol) has a crucial impact. After that, the sample was placed under reduced pressure three times to intensify the shrinkage, which is a standard procedure to eliminate any moisture from a sample.

To examine the cracking process, mix ratios of PVP to ZnO were studied. Keeping a constant amount of PVP polymer matrix equal to 2 mL, the amount of added ZnO was gradually increased by 100 μL. All layers were prepared according to the procedure described, and the results are summarized in Figure 2.

In case of the addition of 100 μL of the nanodispersion, no cracking was observed. For an addition of 200 μL, some domains had started to be created, but the layer remained continuous. The 300 μL addition resulted in cracking, but the spaces between the resulting domains were not yet visible.

Volume addition of ZnO [μl]	Mix ratio PVP:ZnO	Layer thickness [μm]	Cracking	Optical microscopy photos (polymer layer on glass substrate)
100	20:1	5.9	-	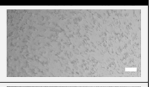
200	10:1	6.3	-	
300	6.7:1	5.3	+	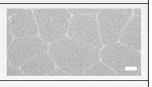
400	5:1	6.5	+	See Fig. 4 in this work

Figure 2. Results showing the effect of the amount of added ZnO on the induction of PVP polymer film cracking. The scale bar on the microscope pictures represents 20 μm.

https://doi.org/10.1021/acsomega.2c05131
ACS Omega XXXX, XXX, XXX−XXX

Finally, for the 400 μL addition, a satisfactory cracking effect was achieved because there were already visible spaces between the domains where the metallic material could enter during physical evaporation. Therefore, the PVP to ZnO ratio was set as 5:1.

In the final step (metal deposition in Figure 1), the prepared polymer mask was placed in a vacuum chamber to deposit the metallic layer in the MBraun evaporator. A 40 nm titanium adhesive layer was used under the 200 nm target silver layer. The resistive thermal evaporation system (for silver) and the electron beam (for titanium) were used with the following parameters: rate of 5 Å/s and pressure of 2×10^{-6} mbar. The metal was deposited all over the surface, including the spaces between the cracks. Since the PVP polymer is water-soluble, the substrate with the cracked polymer coating and the silver layer was immersed in water, which dissolved the PVP and caused the lift-off of the metallic layer. The remaining metallic part reproduced the shape of the cracks, creating a semi-transparent electrode. The well-cleaned sample was then dried with nitrogen and subjected to optical and electrical analysis.

The manufactured electrode is presented in Figure 3a and compared to the classical mesh-shaped semitransparent

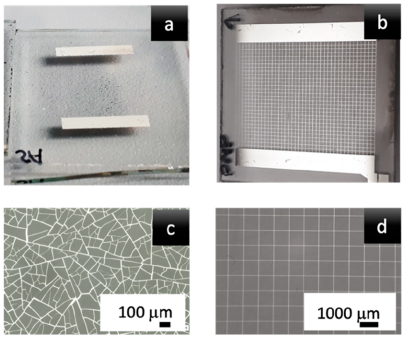

Figure 3. Comparison of (a) an electrode with a self-organized shape and (b) an electrode obtained by designing the mesh shape. (c and d) Photographs of the electrodes in panels a and b, respectively. Photographs were taken on an optical microscope.

electrode[13] (Figure 3b). The electrode obtained by inducing cracks in the polymer mask is characterized by unique shapes. Both types of electrodes are juxtaposed with each other in Figure 3 to show the shape differences.

Different substrates were examined to check for the occurrence of the fracture process. Three transparent materials were tested: sapphire, glass, and quartz (see Figure 4).

For each of the tested substrates, crack-induced electrodes were able to be manufactured. To compare the obtained results, the key parameters of the TEs, namely, their transparency and conductivity (resistivity), were measured.

In the case of transmission, pure substrates were examined first and then electrodes were made on these substrates. The initial transmission differs for each material. However, the changes in transmission before and after electrode insertion were almost the same, around 10−15% (Figure 5). The quartz from the Continental Trade Company performed the best in terms of optical and mechanical parameters while maintaining a reasonable price.

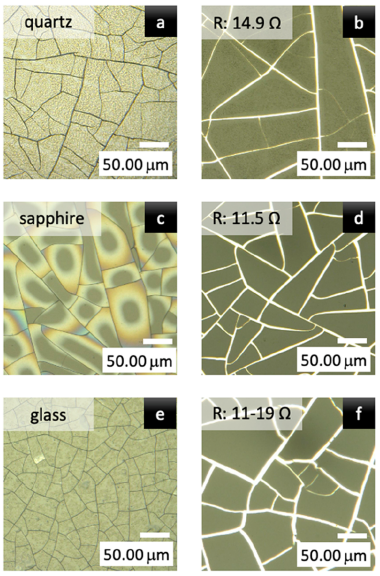

Figure 4. Optical microscope images of a polymer layer with the ZnO additive after heating at 80 °C on (a) quartz, (c) sapphire, and (e) glass substrates. Optical microscope images of the obtained semitransparent electrodes on the corresponding (b) quartz, (d) sapphire, and (f) glass substrates.

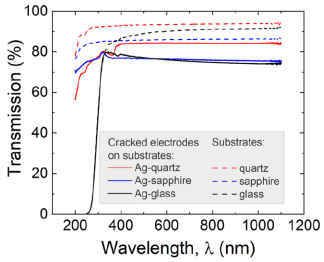

Figure 5. Transmission spectra of pure substrates (dashed lines) and substrates with deposited electrodes (solid lines). Differences in light transmission for quartz, sapphire, and glass are equal to 11.9%, 16.9%, and 11.1%, respectively. These differences can be attributed to the silver paths. For the measurement of the TE light transmission, a FILMETRICS F10-RT reflectometer was used.

From these results, it can be seen that the spectral range of TE transmission can be regulated by the substrate material. Moreover, this range is wider for all materials in comparison to that of ITO, a popular material for transparent electrodes.[4]

Resistance (R), the second crucial parameter of a TE, was measured using the two-terminal method[28−30] at a distance (L) of 11 mm. R ranged from 10 to 15 Ω, and these results were reproducible for various substrates. Using eq 1, the resistivity of the electrode (ρ) made on the glass substrate (with R = 15 Ω) was calculated to be 27×10^{-7} Ωm by considering the geometric sizes of the electrode (width W = 10

https://doi.org/10.1021/acsomega.2c05131
ACS Omega XXXX, XXX, XXX−XXX

mm) and the average estimated pattern thickness (t = 200 nm).

$$R = \rho\frac{L}{W\cdot t} \rightarrow \rho = R\frac{W\cdot t}{L} \quad (1)$$

The sheet resistance R_S for this electrode, as defined by eq 2,[29] is 13.65 Ω/sq.

$$R_s = \frac{\rho}{t} \quad (2)$$

In the case of sapphire, R_S = 10.45 Ω/sq; in the case of quartz, R_S = 13.55 Ω/sq. These results are compared with the sheet resistances of other TEs in Figure 6.[31,32]

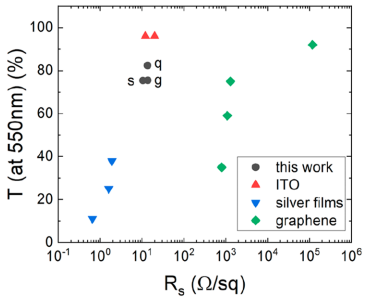

Figure 6. Transmittance (T) (550 nm) plotted as a function of the sheet resistance for graphene,[33] commercial indium tin oxide (ITO),[34,35] evaporated silver, and patterned silver described in this work (sapphire (s), quartz (q), and glass (g) substrates).

TEs with these unique, uneven patterns can be used as before in all TE applications, including contactless electroreflectance and surface photovoltage.[12] However, these wire-like TEs also gain a new, additional applications due to their individual character in a new area where properties such as transparency, conductivity, and uniqueness are needed. An example is transparent electromagnetic interference filters, which were investigated by Shen et al. using random-pattern metal-mesh.[36] Another interesting application of these TE could be prevention of the Moiré phenomenon so often present in the case of regular mesh-shaped TEs.[16] This distinctiveness can be used independently or with accompanying high transmission in applications we do not even know yet.

TEs of unique shapes can be scanned and compared over the whole surface but also can be analyzed using the intersections with only one horizontal line on the initial comparative stage; like in case of fingerprint description, only some characteristic types of minutiae are considered. Those solutions for identifying a particular TE can find applications in areas such as coding, security, anticounterfeiting, plagiarism protection, marking, and readability. The idea of the encryption mechanism is illustrated in Figure 7.

As shown in Figure 7, a lower degree of compaction occurs for smoother substrate surfaces and a higher degree of compaction occurs for more rough, porous surfaces. Based on the coding properties of TEs, there are other new areas of possible applications such as logistics, where barcodes are used to identify particular products.

The undeniable advantage of using electrodes for encryption is their uniqueness, which gives confidence that the code will not be broken because the process itself occurs spontaneously. There are many possibilities for encryption thanks to the ability to control the size of the surface, which is limited only by the devices that apply the layers (spin-coater and vacuum chamber), using two properties of TEs: electrical and optical. An example of an encoding mechanism could be a method for determining where a horizontal line is cut off (in the example presented, the line is located one-third of the height from the top of the photo) and then determining the intersection points. The points of intersection can be determined by an optical method such as that presented in the figure but can also be read by an electrical probe, which upon contact with the path will conduct and record the position of the path. However, in the case of encryption using such TEs, the problem may be the difficulty of recovering lost data or the things that can be encrypted in this way. It should be pointed out that each possible application should be preceded by the optimization of

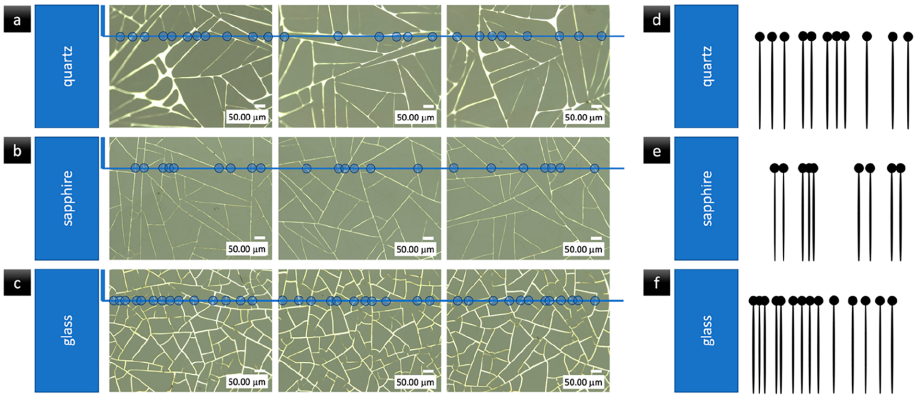

Figure 7. Optical images of transparent wire-like electrodes on the following substrates: (a) quartz, (b) sapphire, and (c) glass. (d–f) Illustration of the idea of coding the electrodes for each substrate; only the code for the first electrode of each material is presented.

https://doi.org/10.1021/acsomega.2c05131
ACS Omega XXXX, XXX, XXX−XXX

the TE for that application, e.g., increasing the durability of the electrode by applying protective layers for methods that may cause mechanical damage, protecting against temperature extremes when using TEs in variable conditions, or matching the size of the substrate to the microscope holder or encoding station.

It is worth emphasizing that these irregular shapes can be obtained by lithographic techniques; however, these techniques would require the production of a mask with a different shape every time, which is uneconomic. In addition, printing techniques will not be suitable for reproducing such irregular shapes because the problem of overlapping paths on the intersections occurs, which leads to a heterogeneous surface over the entire electrode. In this case, our method is favorable, as it offers the possibility of producing such multifunctional electrodes quickly and cheaply thanks to its simple mechanism of producing a mask with a unique shape.

CONCLUSIONS

In conclusion, we developed a novel technique for manufacturing TEs using standard materials. These electrodes are highly transparent (82.4%) in a broad spectral range, have transmission that can be regulated by the substrate selection, and possess low resistivity (27.3×10^{-7} Ωm). The method can be easily scaled up, since the structuring step is omitted. With these parameters, our TE is useful in well-known applications such as solar cells, touch panels, light-emitting diodes, transparent heaters, and others. Despite the fact that the electrode meets the requirements for existing applications because of its electrical and optical properties, it can also gain additional feature as a unique marker. We are fully convinced that TEs of irregular patterns can open up a completely new spectrum of application perspectives.

AUTHOR INFORMATION

Corresponding Author

Anna M. Melnychenko − *ŁUKASIEWICZ Research Network−PORT Polish Center for Technology Development, 54-066 Wrocław, Poland; Department of Semiconductor Materials Engineering, Faculty of Fundamental Problems of Technology, Wrocław University of Science and Technology, 50-370 Wrocław, Poland;* orcid.org/0000-0002-1537-2961; Email: anna.melnychenko@pwr.edu.pl

Author

Robert Kudrawiec − *ŁUKASIEWICZ Research Network−PORT Polish Center for Technology Development, 54-066 Wrocław, Poland; Department of Semiconductor Materials Engineering, Faculty of Fundamental Problems of Technology, Wrocław University of Science and Technology, 50-370 Wrocław, Poland;* orcid.org/0000-0003-2593-9172

Complete contact information is available at: https://pubs.acs.org/10.1021/acsomega.2c05131

Notes

The authors declare no competing financial interest.

ACKNOWLEDGMENTS

This work was supported by the National Science Center (NCN) of Poland through OPUS GRAND 2018/29/B/ST7/02135. We would like to thank Katarzyna Komorowska for a fruitful and insightful discussion.

REFERENCES

(1) Yang, J.; Bao, C.; Zhu, K.; Yu, T.; Xu, Q. High-Performance Transparent Conducting Metal Network Electrodes for Perovksite Photodetectors. *ACS Appl. Mater. Interfaces* **2018**, *10* (2), 1996−2003.

(2) View, Inc.*How Electrochromic Glass Works*. https://view.com/product/how-it-works (accessed 2022-05−21).

(3) Wang, T.; Lu, K.; Xu, Z.; Lin, Z.; Ning, H.; Qiu, T.; Yang, Z.; Zheng, H.; Yao, R.; Peng, J. Recent Developments in Flexible Transparent Electrode. *Crystals* **2021**, *11* (5), 511.

(4) Guillén, C.; Herrero, J. Comparison Study of ITO Thin Films Deposited by Sputtering at Room Temperature onto Polymer and Glass Substrates. *Thin Solid Films* **2005**, *480−481*, 129−132.

(5) Mazur, M.; Kaczmarek, D.; Domaradzki, J.; Wojcieszak, D.; Song, S.; Placido, F.Influence of Thickness on Transparency and Sheet Resistance of ITO Thin Films. In *Proceedings of the The Eighth International Conference on Advanced Semiconductor Devices and Microsystems*, Smolenice Castle, Slovakia, October 25−27, 2010; IEEE: New York, NY, 2010; pp 65−68. DOI: 10.1109/ASDAM.2010.5666348

(6) Kawashima, T.; Matsui, H.; Tanabe, N. New Transparent Conductive Films: FTO Coated ITO. *Thin Solid Films* **2003**, *445* (2), 241−244.

(7) Qing, F.; Zhang, Y.; Niu, Y.; Stehle, R.; Chen, Y.; Li, X. Towards Large-Scale Graphene Transfer. *Nanoscale* **2020**, *12* (20), 10890−10911.

(8) O'Connor, B.; Haughn, C.; An, K.-H.; Pipe, K. P.; Shtein, M. Transparent and Conductive Electrodes Based on Unpatterned, Thin Metal Films. *Appl. Phys. Lett.* **2008**, *93* (22), 223304.

(9) Nambiar, S.; Yeow, J. T. W. Conductive Polymer-Based Sensors for Biomedical Applications. *Biosens. Bioelectron.* **2011**, *26* (5), 1825−1832.

(10) Lu, X.; Zhang, Y.; Zheng, Z. Metal-Based Flexible Transparent Electrodes: Challenges and Recent Advances. *Advanced Electronic Materials* **2021**, *7* (5), 2001121.

(11) Moon, C.-J.; Kim, I.; Joo, S.-J.; Chung, W.-H.; Lee, T.-M.; Kim, H.-S. Flash Light Sintering of Ag Mesh Films for Printed Transparent Conducting Electrode. *Thin Solid Films* **2017**, *629*, 60−68.

(12) Ślusarz, A.; Kopaczek, J.; Dybała, F.; Wiatrowska, A.; Granek, F.; Kudrawiec, R. Contactless Electroreflectance Spectroscopy with a Semitransparent Capacitor Made of a Silver Mesh of Ultrathin Lines. *Measurement* **2021**, *169*, 108361.

(13) Ślusarz, A. M.; Komorowska, K.; Baraniecki, T.; Zelewski, S. J.; Kudrawiec, R. Transparent Metal Mesh Electrodes Microfabricated by Structuring Water-Soluble Polymer Resist via Laser Ablation. *ACS Sustainable Chem. Eng.* **2022**, *10*, 8196.

(14) Layani, M.; Gruchko, M.; Milo, O.; Balberg, I.; Azulay, D.; Magdassi, S. Transparent Conductive Coatings by Printing Coffee Ring Arrays Obtained at Room Temperature. *ACS Nano* **2009**, *3* (11), 3537−3542.

(15) Layani, M.; Berman, R.; Magdassi, S. Printing Holes by a Dewetting Solution Enables Formation of a Transparent Conductive Film. *ACS Appl. Mater. Interfaces* **2014**, *6* (21), 18668−18672.

(16) Shin, D.-K.; Park, J. Suppression of Moiré Phenomenon Induced by Metal Grids for Touch Screen Panels. *Journal of Display Technology* **2016**, *12*, 632−638.

(17) Jia, G.; Plentz, J.; Dellith, A.; Schmidt, C.; Dellith, J.; Schmidl, G.; Andrä, G. Biomimic Vein-Like Transparent Conducting Electrodes with Low Sheet Resistance and Metal Consumption. *Nano-Micro Lett.* **2020**, *12* (1), 19.

(18) He, X.; Duan, F.; Liu, J.; Lan, Q.; Wu, J.; Yang, C.; Yang, W.; Zeng, Q.; Wang, H. Transparent Electrode Based on Silver Nanowires and Polyimide for Film Heater and Flexible Solar Cell. *Materials* **2017**, *10* (12), 1362.

(19) Ma, C.; Gao, X.-M.; Bi, Y.-G.; Zhang, X.-L.; Yin, D.; Wen, X.-M.; Liu, Y.-F.; Feng, J.; Sun, H.-B. PFSA-Passivated Silver Nanowire

Transparent Electrodes for Highly Flexible Organic-Light-Emitting Devices with Improved Stability. *Org. Electron.* **2020**, *84*, 105727.
(20) Nam, S.; Song, M.; Kim, D.-H.; Cho, B.; Lee, H. M.; Kwon, J.-D.; Park, S.-G.; Nam, K.-S.; Jeong, Y.; Kwon, S.-H.; Park, Y. C.; Jin, S.-H.; Kang, J.-W.; Jo, S.; Kim, C. S. Ultrasmooth, Extremely Deformable and Shape Recoverable Ag Nanowire Embedded Transparent Electrode. *Sci. Rep* **2015**, *4* (1), 4788.
(21) Kim, M.-H.; Joh, H.; Hong, S.-H.; Oh, S. J. Coupled Ag Nanocrystal-Based Transparent Mesh Electrodes for Transparent and Flexible Electro-Magnetic Interference Shielding Films. *Curr. Appl. Phys.* **2019**, *19* (1), 8−13.
(22) Seo, K.-W.; Noh, Y.-J.; Na, S.-I.; Kim, H.-K. Random Mesh-like Ag Networks Prepared via Self-Assembled Ag Nanoparticles for ITO-Free Flexible Organic Solar Cells. *Sol. Energy Mater. Sol. Cells* **2016**, *155*, 51−59.
(23) Rao, K. D. M.; Hunger, C.; Gupta, R.; Kulkarni, G. U.; Thelakkat, M. Cracked Polymer Templated Metal Network as Transparent Conducting Electrode for ITO-Free Organic Solar Cells. *Phys. Chem. Chem. Phys.* **2014**, *16*, 15107−15110.
(24) Cui, M.; Zhang, X.; Rong, Q.; Nian, L.; Shui, L.; Zhou, G.; Li, N. High Conductivity and Transparency Metal Network Fabricated by Acrylic Colloidal Self-Cracking Template for Flexible Thermochromic Device. *Org. Electron.* **2020**, *83*, 105763.
(25) Han, B.; Pei, K.; Huang, Y.; Zhang, X.; Rong, Q.; Lin, Q.; Guo, Y.; Sun, T.; Guo, C.; Carnahan, D.; Giersig, M.; Wang, Y.; Gao, J.; Ren, Z.; Kempa, K. Uniform Self-Forming Metallic Network as a High-Performance Transparent Conductive Electrode. *Adv. Mater.* **2014**, *26* (6), 873−877.
(26) Kim, J.; Truskett, T. M. Geometric Model of Crack-Templated Networks for Transparent Conductive Films. *Appl. Phys. Lett.* **2022**, *120* (21), 211108.
(27) Gao, J.; Xian, Z.; Zhou, G.; Liu, J.-M.; Kempa, K. Nature-Inspired Metallic Networks for Transparent Electrodes. *Adv. Funct. Mater.* **2018**, *28* (24), 1705023.
(28) van de Groep, J.; Spinelli, P.; Polman, A. Transparent Conducting Silver Nanowire Networks. *Nano Lett.* **2012**, *12* (6), 3138−3144.
(29) Hu, L.; Hecht, D. S.; Grüner, G. Percolation in Transparent and Conducting Carbon Nanotube Networks. *Nano Lett.* **2004**, *4* (12), 2513−2517.
(30) Zhao, Y.-Y.; Zheng, M.-L.; Dong, X.-Z.; Jin, F.; Liu, J.; Ren, X.-L.; Duan, X.-M.; Zhao, Z. Tailored Silver Grid as Transparent Electrodes Directly Written by Femtosecond Laser. *Appl. Phys. Lett.* **2016**, *108*, 221104.
(31) Zhang, R.; Engholm, M. Recent Progress on the Fabrication and Properties of Silver Nanowire-Based Transparent Electrodes. *Nanomaterials* **2018**, *8* (8), 628.
(32) De, S.; Higgins, T. M.; Lyons, P. E.; Doherty, E. M.; Nirmalraj, P. N.; Blau, W. J.; Boland, J. J.; Coleman, J. N. Silver Nanowire Networks as Flexible, Transparent, Conducting Films: Extremely High DC to Optical Conductivity Ratios. *ACS Nano* **2009**, *3* (7), 1767−1774.
(33) De, S.; King, P. J.; Lyons, P. E.; Khan, U.; Coleman, J. N. Size Effects and the Problem with Percolation in Nanostructured Transparent Conductors. *ACS Nano* **2010**, *4* (12), 7064−7072.
(34) Chen, Z.; Li, W.; Li, R.; Zhang, Y.; Xu, G.; Cheng, H. Fabrication of Highly Transparent and Conductive Indium-Tin Oxide Thin Films with a High Figure of Merit via Solution Processing. *Langmuir* **2013**, *29* (45), 13836−13842.
(35) Mei-Zhen, G.; R, J.; De-Sheng, X.; R, F. W. Thickness Dependence of Resistivity and Optical Reflectance of ITO Films. *Chin. Phys. Lett.* **2008**, *25* (4), 1380−1383.
(36) Shen, S.; Chen, S.-Y.; Zhang, D.-Y.; Liu, Y.-H. High-Performance Composite Ag-Ni Mesh Based Flexible Transparent Conductive Film as Multifunctional Devices. *Opt. Express, OE* **2018**, *26* (21), 27545−27554.

https://doi.org/10.1021/acsomega.2c05131
ACS Omega XXXX, XXX, XXX−XXX

4.3 Porównanie przeźroczystych elektrod otrzymanych opracowanymi metodami

Każda z otrzymanych elektrod może znaleźć zastosowanie w różnorodnych obszarach ze względu na różnice w parametrach zarówno optycznych jak i elektrycznych. Ważne jest odpowiednie zaprojektowanie elektrody pod kątem zastosowań i dobranie właściwej metody jej wytworzenia. Istotnym czynnikiem jest dobór podłoża z uwzględnieniem jego wytrzymałości, parametrów elektrycznych (takich jak stała dielektryczna) czy optycznych (transmisja światła). W Tab. 2 znajduje się porównanie otrzymanych elektrod różnymi technikami.

Tabela 2. Porównanie przeźroczystych elektrod otrzymanych opracowanymi metodami.

Metoda wytwarzania przeźroczystych elektrod	DRUK - ULTRAPRECYZYJNA DEPOZYCJA [D1]	LASER LIFT-OFF [D2]	TRANSFER GRAFENU I LASEROWA STRUKTURYZACJA [D3]
Typ otrzymanej elektrody	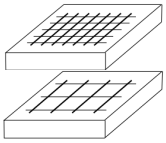	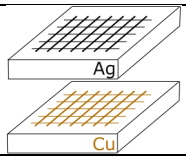	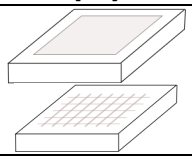
Materiał przewodzący	srebro	srebro, miedź i inne metale	grafen
Materiał podłoża i jego transmisja przy 500 nm	Szkło (93%)	Kwarc (93%)	Szafir (86,4%)
Zalety metody	łatwa możliwość kontroli rozstawu siatki, szybkość metody	szeroki wybór materiału elektrody, otrzymanie dowolnego kształtu w 2D (projekt w AutoCAD)	dobra jakość cienkiej warstwy przewodzącej o ciągłej powierzchni lub dowolnym kształcie w 2D
Wady metody	ograniczenie w wyborze materiału związane z każdorazowym otrzymaniem stabilnego składu tuszu	utrata znacznej ilości materiału podczas procesu „lift-off”	mała wytrzymałość na uszkodzenia
Rozdzielczość metody	1 μm	20 μm	20 μm
Regulacja transmisji	szerokość i rozstaw linii siatki, materiał podłoża	szerokość i rozstaw linii siatki, materiał podłoża	ilość warstw grafenu, szerokość i rozstaw linii siatki, materiał podłoża
Transmisja elektrody	88% rozstaw 400 μm 90% rozstaw 1000 μm na szkle	85% na kwarcu	86% na szafirze
Absorpcja warstwy przewodzącej	5% rozstaw 400 μm 3% rozstaw 1000 μm	8% Ag 8% Cu	0,4% siatka grafenowa 3% grafen

5. Wnioski

Praca w ramach doktoratu wdrożeniowego przyniosła efekty zarówno w jednostce zatrudniającej jaką jest Łukasiewicz – PORT jak i w jednostce naukowej, tj. Politechnice Wrocławskiej. Podczas pracy w Laboratoriach Katedry Inżynierii Materiałów Półprzewodnikowych na PWr zoptymalizowano uchwyt kondensatora z przeźroczystą elektrodą w układzie optycznym. W zależności od wykorzystywanej techniki pomiarowej służącej do charakteryzacji struktur półprzewodnikowych każdorazowo dobierano odpowiednią przeźroczystą elektrodę. W publikacji D1 otrzymano i przedstawiono wyniki badań, w których pomiar bezkontaktowego elektroodbicia przeprowadzono przy napięciu 100 V z wykorzystaniem elektrody drukowanej. W pracy D2 ten sam pomiar przeprowadzono z wykorzystaniem elektrody wykonanej techniką „laser lift-off" co dowodzi, że w przypadku pomiaru bezkontaktowego elektroodbicia z powodzeniem może być stosowana elektroda w kształcie siatki wykonana zarówno metodą druku jak i metodą „laser lift-off". Dzięki zastosowaniu elektrody grafenowej do pomiarów elektroodbicia w „miękkim kontakcie" przeprowadzono eksperyment przy napięciu rzędu kilku wolt. Było to możliwe, dzięki minimalizacji odległości elektrody od próbki. W efekcie opracowane zostało stanowisko do tego typu pomiarów. Wykorzystując ten sam uchwyt i elektrodę opracowano stanowisko pomiarowe do metody fotonapięcia powierzchniowego [D3]. Elektroda w kształcie siatki wykonana techniką „laser lift-off" może dodatkowo zostać użyta jako przeźroczysta grzałka w pomiarach termoodbicia – tutaj ważnym czynnikiem jest dobór materiału warstwy przewodzącej, który różnić się będzie właściwościami termicznymi (np. przewodnością cieplną). Pomiary takie zostały przeprowadzone i opisane w pracy [D2].

5.1 Wdrożenie wyników doktoratu

W Polskim Ośrodku Rozwoju Technologii wdrożono następujące metody otrzymywania przeźroczystych elektrod (Rys.9):

a) Druk z wykorzystaniem technologii ultraprecyzyjnej depozycji [D1]

Metoda ta wykorzystuje drukarkę firmy XTPL przeznaczoną do druku głównie tuszem srebrnym, ze względu na dobrze opracowany skład tego tuszu. Rozdzielczość metody zawiera się w przedziale od 1 μm do 100 μm i jest zależna od rozmiaru używanej dyszy. Możliwy jest druk na płaskich podłożach (2D), ale również nanoszenie ciągłej ścieżki na podłożach 2.5D, np. z małym stopniem pomiędzy dwiema warstwami. Ruch głowicy odbywa się w dwóch osiach przez co kształty dostępne w tej technologii są ograniczone do linii równoległych, linii przecinających się pod kątem prostym lub kropek.

b) „Laser lift-off" [D2]

Metoda ze względu na wieloetapowość procesu jest czasochłonna, jednak daje duże możliwości w zakresie dowolności otrzymanego kształtu. Na etapie strukturyzacji jednorazowej maski polimerowej może zostać zadany dowolny wzór ograniczony jedynie co do rozmiaru ścieżki (20 μm). Jest on odwzorowywany przez wiązkę laserową wywołującą ablację na powierzchni warstwy polimerowej. W kolejnym etapie nanoszona jest docelowa warstwa (metaliczna). Możliwe jest otrzymanie dowolnego materiału, który nanoszony jest w napylarce próżniowej np. Ag, Cu, Au, Al, Pt, Ti itd. Przy zachowaniu odpowiedniej grubości warstwy dla danego materiału możliwe jest przeprowadzenie kolejnego etapu. Po

rozpuszczeniu warstwy polimerowej wybrane fragmenty warstwy metalicznej unoszą się (ang. lift-off) i odrywają od powierzchni podłoża w efekcie czego otrzymywany jest wzór wcześniej zapisany przez laser. Oprócz możliwości otrzymania kształtu siatki ta metoda oferuje wykonanie bardziej skomplikowanych kształtów, w tym okręgów, łuków i innych ze względu na precyzyjny system laserowy stosowany w metodzie.

c) „Crack-templated lift-off" [D4]

Kolejna metoda również wykorzystuje technikę „lift-off". Jednak tutaj etap strukturyzacji laserowej jest zastąpiony przez zjawisko pękania. Warstwa polimerowa umieszczona w odpowiednich warunkach pęka samoczynnie. Następnie nanoszona jest dowolna warstwa metaliczna w napylarce próżniowej, a na końcu rozpuszczana jest warstwa polimerowa tak jak w poprzedniej metodzie. W efekcie otrzymuje się półprzeźroczystą, metaliczną elektrodę o nieregularnym i niepowtarzalnym kształcie. Metoda ta może znaleźć zastosowanie w obszarze zabezpieczeń poprzez unikalny wzór niedający się powtórzyć w kolejnym procesie.

d) Synteza i transfer grafenu [D3]

Metoda syntezy grafenu odbywająca się na foli miedzianej pozwala na otrzymanie wystarczająco dużych powierzchni tego materiału, by możliwy był jego transfer na podłoże w celu otrzymania przeźroczystej elektrody. Dzięki zastosowaniu tej metody możliwe jest użycie dowolnego materiału jako podłoża tj. szafir, kwarc, szkło i inne. Otrzymane warstwy są dobrej jakości, a ich ilość może się wahać od jednej do nawet pięciu.

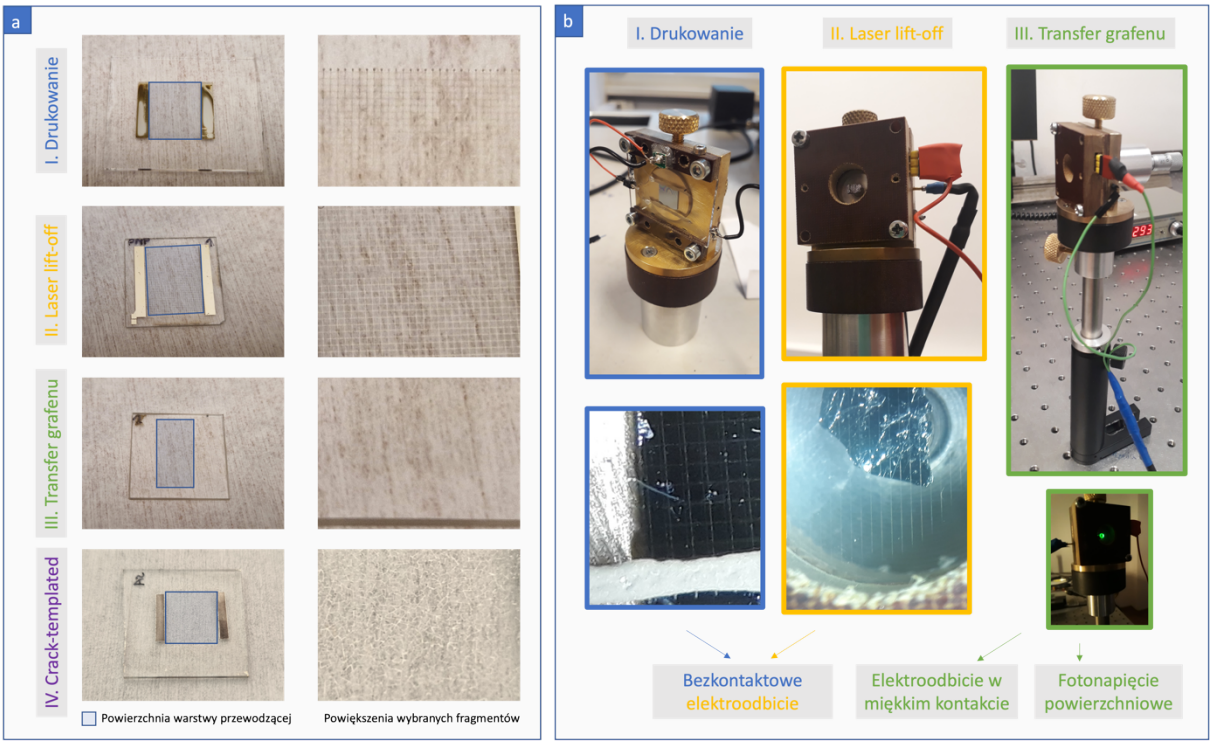

Rysunek 9. a) Elektrody przeźroczyste wykonane różnymi metodami. W lewej kolumnie pokazano otrzymane elektrody na zdjęciu oraz zaznaczono obszar warstwy przewodzącej. W prawej kolumnie pokazano powiększenia wybranych części powierzchni przewodzących. b) Uchwyty z przeźroczystymi elektrodami wykonanymi różnymi technikami przystowane do pomiarów spektroskopii struktur półprzewodnikowych.

Obok metody druku cienkich ścieżek wdrożono od podstaw dwie nowe techniki dotychczas niestosowane w Laboratorium Technologii Materiałowych: metodę „laser lift-off" oraz „crack-templated lift-off". Pierwsza metoda otwiera szeroki wachlarz zastosowań, dzięki możliwości otrzymywania cienkich ścieżek o skomplikowanych kształtach. Druga metoda stwarza obiecujące możliwości aplikacyjne dzięki samorzutnie powstającemu wzorowi o nieregularnym i niepowtarzalnym kształcie. Natomiast metoda syntezy i transferu grafenu na podłoża szafirowe pozwala na otrzymanie uniwersalnej przeźroczystej elektrody wysokiej jakości, dzięki warstwie przewodzącej o grubości na poziomie atomowym do zastosowań w bardziej wymagających warunkach np. badaniach w nanoskali.

Wykonane różnymi metodami przeźroczyste elektrody zostały wykorzystane z powodzeniem w pomiarach spektroskopii struktur półprzewodnikowych, jednak perspektywy zastosowań przeźroczystych elektrod wykraczają poza te przedstawione w niniejszej dysertacji.

Bibliografia

Prace tworzące cykl publikacji:

[D1] **A. Ślusarz**, J. Kopaczek, F. Dybała, A. Wiatrowska, F. Granek, R. Kudrawiec, Contactless electroreflectance spectroscopy with a semitransparent capacitor made of a silver mesh of ultrathin lines, Measurement. 169 (2021) 108361. https://doi.org/10.1016/j.measurement.2020.108361.

[D2] **A.M. Ślusarz**, K. Komorowska, T. Baraniecki, S.J. Zelewski, R. Kudrawiec, Transparent Metal Mesh Electrodes Microfabricated by Structuring Water-Soluble Polymer Resist via Laser Ablation, ACS Sustainable Chem. Eng. 10 (2022) 8196–8205. https://doi.org/10.1021/acssuschemeng.2c01835.

[D3] **A.M. Melnychenko**, S.J. Zelewski, D. Hlushchenko, K. Lis, A. Bachmatiuk, R. Kudrawiec, Electro-Modulation and Surface Photovoltage Spectroscopy with Semi-Transparent Graphene Electrodes. Available at SSRN: https://ssrn.com/abstract=4134845 or http://dx.doi.org/10.2139/ssrn.4134845

[D4] **A.M. Melnychenko**, R. Kudrawiec, Crack-Templated Wire-Like Semitransparent Electrodes with Unique Irregular Patterns, ACS Omega. (2022) https://doi.org/10.1021/acsomega.2c05131.

[1] N.V. Tkachenko, Optical Spectroscopy: Methods and Instrumentations, Elsevier, 2006.

[2] R. Kudrawiec, J. Misiewicz, Optical Modulation Spectroscopy, in: A. Patane, N. Balkan (Eds.), Semicond. Res., Springer Berlin Heidelberg, Berlin, Heidelberg, 2012: pp. 95–124. https://doi.org/10.1007/978-3-642-23351-7_4.

[3] F.H. Pollak, Modulation Spectroscopy As A Technique For Semiconductor Characterization, in: Opt. Charact. Tech. Semicond. Technol., SPIE, 1981: pp. 142–156. https://doi.org/10.1117/12.931700.

[4] N. Bottka, D.K. Gaskill, R.S. Sillmon, R. Henry, R. Glosser, Modulation spectroscopy as a tool for electronic material characterization, J. Electron. Mater. 17 (1988) 161–170. https://doi.org/10.1007/BF02652147.

[5] P. YU, M. Cardona, Fundamentals of Semiconductors: Physics and Materials Properties, 4th ed. 2010 edition, Springer, Berlin ; New York, 2010.

[6] R. Kudrawiec, W. Walukiewicz, Electromodulation spectroscopy of highly mismatched alloys, J. Appl. Phys. 126 (2019) 141102. https://doi.org/10.1063/1.5111965.

[7] R. Kudrawiec, P. Sitarek, J. Misiewicz, S.R. Bank, H.B. Yuen, M.A. Wistey, J.S. Harris, Interference effects in electromodulation spectroscopy applied to GaAs-based structures: A comparison of photoreflectance and contactless electroreflectance, Appl. Phys. Lett. 86 (2005) 091115. https://doi.org/10.1063/1.1873052.

[8] J. Misiewicz, P. Sitarek, G. Sęk, R. Kudrawiec, Semiconductor heterostructures and device structures investigated by photoreflectance spectroscopy, Mater. Sci.-Pol. 21 (2003) 263–320.

[9] B.O. Seraphin, ELECTROREFLECTANCE IN SURFACE PHYSICS, J. Phys. Colloq. 31 (1970) C1-134. https://doi.org/10.1051/jphyscol:1970121.

[10] S. Datta, S. Ghosh, B.M. Arora, Electroreflectance and surface photovoltage spectroscopies of semiconductor structures using an indium–tin–oxide-coated glass electrode in soft contact mode, Rev. Sci. Instrum. 72 (2001) 177–183. https://doi.org/10.1063/1.1332114.

[11] X. Yin, F.H. Pollak, Novel contactless mode of electroreflectance, Appl. Phys. Lett. 59

(1991) 2305–2307. https://doi.org/10.1063/1.106051.
[12] J. Misiewicz, R. Kudrawiec, Contactless electroreflectance spectroscopy of optical transitions in low dimensional semiconductor structures, Opto-Electron. Rev. 20 (2012) 101–119. https://doi.org/10.2478/s11772-012-0022-1.
[13] C.N. Berglund, Temperature-Modulated Optical Absorption in Semiconductors, J. Appl. Phys. 37 (1966) 3019–3023. https://doi.org/10.1063/1.1703156.
[14] E. Matatagui, A.G. Thompson, M. Cardona, Thermoreflectance in Semiconductors, Phys. Rev. 176 (1968) 950–960. https://doi.org/10.1103/PhysRev.176.950.
[15] C.-H. Ho, H.-W. Lee, Z.-H. Cheng, Practical thermoreflectance design for optical characterization of layer semiconductors, Rev. Sci. Instrum. 75 (2004) 1098–1102. https://doi.org/10.1063/1.1667255.
[16] L. Kronik, Y. Shapira, Surface photovoltage phenomena: theory, experiment, and applications, Surf. Sci. Rep. 37 (1999) 1–206. https://doi.org/10.1016/S0167-5729(99)00002-3.
[17] N. Cui, Y. Song, C.-H. Tan, K. Zhang, X. Yang, S. Dong, B. Xie, F. Huang, Stretchable transparent electrodes for conformable wearable organic photovoltaic devices, Npj Flex. Electron. 5 (2021) 1–8. https://doi.org/10.1038/s41528-021-00127-7.
[18] H.B. Lee, W.-Y. Jin, M.M. Ovhal, N. Kumar, J.-W. Kang, Flexible transparent conducting electrodes based on metal meshes for organic optoelectronic device applications: a review, J. Mater. Chem. C. 7 (2019) 1087–1110. https://doi.org/10.1039/C8TC04423F.
[19] T. Wang, K. Lu, Z. Xu, Z. Lin, H. Ning, T. Qiu, Z. Yang, H. Zheng, R. Yao, J. Peng, Recent Developments in Flexible Transparent Electrode, Crystals. 11 (2021) 511. https://doi.org/10.3390/cryst11050511.
[20] D. Zhang, A. Alami, W. Choy, Recent Progress on Emerging Transparent Metallic Electrodes for Flexible Organic and Perovskite Photovoltaics, Sol. RRL. (2021). https://doi.org/10.1002/solr.202100830.
[21] X. Feng, L. Wang, Y.Y.S. Huang, Y. Luo, J. Ba, H.H. Shi, Y. Pei, S. Zhang, Z. Zhang, X. Jia, B. Lu, Cost-Effective Fabrication of Uniformly Aligned Silver Nanowire Microgrid-Based Transparent Electrodes with Higher than 99% Transmittance, ACS Appl. Mater. Interfaces. 14 (2022) 39199–39210. https://doi.org/10.1021/acsami.2c09672.
[22] K.-W. Seo, Y.-J. Noh, S.-I. Na, H.-K. Kim, Random mesh-like Ag networks prepared via self-assembled Ag nanoparticles for ITO-free flexible organic solar cells, Sol. Energy Mater. Sol. Cells. 155 (2016) 51–59. https://doi.org/10.1016/j.solmat.2016.04.056.
[23] X. He, F. Duan, J. Liu, Q. Lan, J. Wu, C. Yang, W. Yang, Q. Zeng, H. Wang, Transparent Electrode Based on Silver Nanowires and Polyimide for Film Heater and Flexible Solar Cell, Materials. 10 (2017) 1362. https://doi.org/10.3390/ma10121362.
[24] X. Meng, Y. Xu, Q. Wang, X. Yang, J. Guo, X. Hu, L. Tan, Y. Chen, Silver Mesh Electrodes via Electroless Deposition-Coupled Inkjet-Printing Mask Technology for Flexible Polymer Solar Cells, Langmuir. 35 (2019) 9713–9720. https://doi.org/10.1021/acs.langmuir.9b00846.
[25] T. Gao, B. Wang, B. Ding, J. Lee, P.W. Leu, Uniform and Ordered Copper Nanomeshes by Microsphere Lithography for Transparent Electrodes, Nano Lett. 14 (2014) 2105–2110. https://doi.org/10.1021/nl5003075.
[26] H. Kwon, J. Hong, S. Yong Nam, H. Ho Choi, X. Li, Y. Jin Jeong, S. Hyun Kim, Overview of recent progress in electrohydrodynamic jet printing in practical printed electronics: focus on the variety of printable materials for each component, Mater. Adv. 2 (2021) 5593–5615. https://doi.org/10.1039/D1MA00463H.
[27] Z. Zhang, W. Zhu, Controllable fabrication of a flexible transparent metallic grid

conductor based on the coffee ring effect, J. Mater. Chem. C. 2 (2014) 9587–9591. https://doi.org/10.1039/C4TC01908C.
[28] M. Chen, R.C. Haddon, R. Yan, E. Bekyarova, Advances in transferring chemical vapour deposition graphene: a review, Mater. Horiz. 4 (2017) 1054–1063. https://doi.org/10.1039/C7MH00485K.
[29] H.C. Lee, W.-W. Liu, S.-P. Chai, A.R. Mohamed, A. Aziz, C.-S. Khe, N.M.S. Hidayah, U. Hashim, Review of the synthesis, transfer, characterization and growth mechanisms of single and multilayer graphene, RSC Adv. 7 (2017) 15644–15693. https://doi.org/10.1039/C7RA00392G.
[30] R. Qin, M. Hu, N. Zhang, Z. Guo, Z. Yan, J. Li, J. Liu, G. Shan, J. Yang, Flexible Fabrication of Flexible Electronics: A General Laser Ablation Strategy for Robust Large-Area Copper-Based Electronics, Adv. Electron. Mater. 5 (2019) 1900365. https://doi.org/10.1002/aelm.201900365.
[31] S. Nam, M. Song, D.-H. Kim, B. Cho, H.M. Lee, J.-D. Kwon, S.-G. Park, K.-S. Nam, Y. Jeong, S.-H. Kwon, Y.C. Park, S.-H. Jin, J.-W. Kang, S. Jo, C.S. Kim, Ultrasmooth, extremely deformable and shape recoverable Ag nanowire embedded transparent electrode, Sci. Rep. 4 (2014) 4788. https://doi.org/10.1038/srep04788.
[32] C. Ma, X.-M. Gao, Y.-G. Bi, X.-L. Zhang, D. Yin, X.-M. Wen, Y.-F. Liu, J. Feng, H.-B. Sun, PFSA-passivated silver nanowire transparent electrodes for highly flexible organic-light-emitting devices with improved stability, Org. Electron. 84 (2020) 105727. https://doi.org/10.1016/j.orgel.2020.105727.
[33] B. Han, K. Pei, Y. Huang, X. Zhang, Q. Rong, Q. Lin, Y. Guo, T. Sun, C. Guo, D. Carnahan, M. Giersig, Y. Wang, J. Gao, Z. Ren, K. Kempa, Uniform Self-Forming Metallic Network as a High-Performance Transparent Conductive Electrode, Adv. Mater. 26 (2014) 873–877. https://doi.org/10.1002/adma.201302950.
[34] J. Gao, Z. Xian, G. Zhou, J.-M. Liu, K. Kempa, Nature-Inspired Metallic Networks for Transparent Electrodes, Adv. Funct. Mater. 28 (2018) 1705023. https://doi.org/10.1002/adfm.201705023.
[35] M. Cui, X. Zhang, Q. Rong, L. Nian, L. Shui, G. Zhou, N. Li, High conductivity and transparency metal network fabricated by acrylic colloidal self-cracking template for flexible thermochromic device, Org. Electron. 83 (2020) 105763. https://doi.org/10.1016/j.orgel.2020.105763.
[36] G. Jia, J. Plentz, A. Dellith, C. Schmidt, J. Dellith, G. Schmidl, G. Andrä, Biomimic Vein-Like Transparent Conducting Electrodes with Low Sheet Resistance and Metal Consumption, Nano-Micro Lett. 12 (2020) 19. https://doi.org/10.1007/s40820-019-0359-9.
[37] Y. González, A. Abelenda, O. de Melo, C. Calvo-Mola, L. García-Pelayo, B.J. García, M. Sánchez, Automated system for surface photovoltage spectroscopy, Rev. Sci. Instrum. 92 (2021) 013104. https://doi.org/10.1063/5.0035179.
[38] A.K. Geim, Graphene: Status and Prospects, Science. 324 (2009) 1530–1534. https://doi.org/10.1126/science.1158877.
[39] A.A. Balandin, S. Ghosh, W. Bao, I. Calizo, D. Teweldebrhan, F. Miao, C.N. Lau, Superior Thermal Conductivity of Single-Layer Graphene, Nano Lett. 8 (2008) 902–907. https://doi.org/10.1021/nl0731872.
[40] T.V. Khai, D.S. Kwak, Y.J. Kwon, H.Y. Cho, T.N. Huan, H. Chung, H. Ham, C. Lee, N.V. Dan, N.T. Tung, H.W. Kim, Direct production of highly conductive graphene with a low oxygen content by a microwave-assisted solvothermal method, Chem. Eng. J. 232 (2013) 346–355. https://doi.org/10.1016/j.cej.2013.07.123.

[41] A.K. Geim, K.S. Novoselov, The rise of graphene, Nat. Mater. 6 (2007) 183–191. https://doi.org/10.1038/nmat1849.
[42] S.W. Tong, K.P. Loh, 3.22 - Graphene Properties and Application, in: V.K. Sarin (Ed.), Compr. Hard Mater., Elsevier, Oxford, 2014: pp. 565–583. https://doi.org/10.1016/B978-0-08-096527-7.00059-3.
[43] Ultraprecyzyjna depozycja, XTPL Ultraprecyzyjne Druk. Nanomater. (n.d.). https://xtpl.com/pl/technologia/ultraprecyzyjna-depozycja/ (accessed October 14, 2022).